Modelling of the heating and evaporation of fuel droplets

Tarsisius Kristyadi

Ph.D. **2007**

PDF created with.32 263.04 TD ( ) 468 121.44 TD -0.084 Tc (P) Tj-0.024 32 263.04 TD7.FD.j/eatcr Pm ri

Modelling of the heating and evaporation of fuel droplets

Tarsisius Kristyadi

A thesis submitted in partial fulfilment of the requirements of the University of Brighton for the degree of Doctor of Philosophy

October 2007

School of Engineering
University of Brighton

PDF created with pdfFactory Pro trial version www.pdffactory.com

COPYRIGHT

Attention is drawn to the fact that copyright of this thesis rests with its author. This copy of the thesis has been supplied on condition that anyone who consults it is understood to recognise that its copyright rests with its author and that no quotation from the thesis and no information derived from it may be published without the prior written consent of the author.

This thesis may be made available for consultation within the University Library and may be photocopied or lent to other libraries for the purposes of consultation.

PDF created with pdfFactory Pro trial version www.pdffactory.com

ABSTRACT

The results of a comparative analysis of liquid and gas phase models for fuel droplets heating and evaporation, suitable for implementation into computational fluid dynamics (CFD) codes, are presented. Among liquid phase models, the analysis is focused on the model based on the assumption that the liquid thermal conductivity is infinitely large, and the so called effective thermal conductivity model. Seven gas phase models are compared. These are six semi-theoretical models, based on various assumptions, and a model based solely on the approximation to experimental data. It is pointed out that the gas phase model, taking into account the finite thickness of the thermal boundary layer around the droplet, predicts the evaporation time closest to the one based on the approximation to experimental data.

The values of the absorption coefficients of gasoline fuel (BP Pump Grade 95 RON ULG), 2,2,4-trimethylpentane $(CH_3)_2CHCH_2C(CH_3)_3$ (iso-octane) and 3-pentanone $CH_3CH_2COCH_2(CH_3)_3$ have been measured experimentally in the range of wavelengths between 0.2 m and 4 m. The values of the average absorption efficiency factor for all fuels have been approximated by a power function aR_d^b, where R_d is the droplet radius. a and b in turn have been approximated by piecewise quadratic functions of the radiation temperature, with the coefficients calculated separately in the ranges 2 - 5 m, 5 - 50 m, 50 - 100 m and 100 - 200 m for all fuels. This new approximation is shown to be more accurate compared with the case when a and b are approximated by quadratic functions or fourth power polynomials of the radiation temperature, with the coefficients calculated in the full range of 2 - 200 m.

Results of experimental studies of heating and evaporation of monodisperse ethanol an6 Tc (a) Tj0 Tc (p)4 Tc (n) Tj2.76 Tc ( ) Tj0. (c) Tj0.0 tonodis

LIST OF FIGURES

L

LIST OF TABLES

DECLARATION

I hereby certify that this thesis is my own work except where otherwise indicated. I have identified my sources of information, and in particular have put in quotation marks and identified the origins of any passages that have been quoted word for word.

Signed: Date:

PDF created with pdfFactory Pro trial version www.pdffactory.com

NOMENCLATURE

a	coefficient introduced in Equation (2.1.28) (m^{-b}), acceleration in Equation (6.2.12)
$a_{''}$	liquid fuel absorption coefficient (1/m)
$a_{0,1,2,3,4}$	coefficients introduced in Equf f e005.94 12.72 re h W (1) Tj0.3 Tc (,) Tj-0.12 Tc (2)

k_p	rate coefficient of branching reaction in Shell autoignition model
k_q	rate coefficient of branching reaction in Shell autoignition model
k_t	rate coefficient of branching reaction in Shell autoignition model
k_{br}	coefficient on Equation (6.2.22)
k_{fr}	coefficient on Equation (6.2.22)
L	specific heat of evaporation (J/kg)
Le	Lewis number: $k_g/(c_{pg}\$_g D)$
m	mass (kg), molar concentration (mole/m^3)
$\dot{m}$	evaporation rate (kg/s)
m''	complex index of refraction: $n_\#$-i$k_\#$
M	molar mass (kg/kmol), species
n	index of refraction (does not depend on λ)
n''	index of refraction (depends on #)
n_0	1.46
Nu	Nusselt number
p	pressure (Pa), parameter introduced in Equation (2.3.14)
p_n	coefficients introduced in Equation (2.1.22) (K/s)
$p''(R)$	spectral distribution of radiative power density (W/(m^3 μm))
$P(R)$	radiative term in Equation (2.1.21) (K/s)
P_{total}	total amount of radiation absorbed in a droplet (K/s)
Pe	Peclet number
Pr	Prandtl number
q	parameter introduced in Equation (2.3.14)
$\dot{q}$	heat flux (W/m^2)
Q	intermediate agent
Q_a	efficiency factor of absorption
Q_K	the total heat release rate defined in Equation (2.3.21) (W)
Q_L	heat loss through the boundary walls defined by Equation (2.3.22) (W)
R	distance from the droplet centre (m)
R_g	gas constant (J/(kg K))
R_u	universal gas constant (J/(kmol K))
R_{eq}	radius of equilibrium Equation (6.2.9) (m)
R^*	radical
RH	hydrocarbon fuel
Re	[illegible]

$w_{\lambda}(R)$	normalised absorbed spectral power density of radiation
W	molecular weight (kg/mole)
We	Weber number
x_1,x_2,x_3,x_4	kinetic rate parameters on Shell autoignition model defined in Equations (2.3.15)-(2.3.18)
X	molar fraction
x_{λ}	size parameter: $2\pi R_d/\lambda$
y_1,y_2,y_3,y_4	kinetic rate parameters on Shell autoignition model defined in Equations (2.3.15)-(2.3.18)
Y	mass fraction
y	dimensionless parameter on Equation (6.2.3)
z	parameter introduced in Equation (2.2.24)
Z	Dimensionless number defined as : $\sqrt{We_l / Re_l}$

Greek symbols

α	angle between the two beams
β	wedge angle
β_c	coefficients introduced in Equation (2.1.12)
β_m	evaporation or condensation coefficient
δm_{RBQ}	total change in mass of R*, B and Q over time step (kg/s)
ε	emissivity
ε/k_B	parameter used in Equation (C5) (K)
f	frequency (1/s)
g	coefficient of autoignition model introduced in Equation (2.3.14)
$\bar{g}$	parameter introduced in Equation (2.1.37)
$\eta_{T,M}$	film thickness (m)
θ_R	radiative temperature (K)
Φ	parameter introduced in Equation (2.5.2)
ψ_{ij}	function introduced in Equation (C3)
ω	$k_l/(c_l\rho_l R_d^2)$ (1/s)
ω_{η}	index of absorption
λ	wavelength (m or μm)
λ_m	3.4 μm
λ_n	eigen values obtained from the solution of Equation (2.1.6)
λ_{st}	evaporation rate constant in Equation (2.2.2)
Λ_0	function introduced in Equation (2.1.28)
ξ	parameter introduced in Equation (2.1.8)
π	parameter introduced in Equation (2.2.52)
Φ	phase shift
μ	dynamic viscosity (kg/(m s))
μ_*	$\sqrt{1-(1/n(R/R_d))^2}$
μ_c	$\sqrt{1-(1/n^2)}$
$\theta_0(t)$	$(hT_g(t)R_d/k_l)$ (K)
ν	kinematic viscosity (m^2/s)
ρ	parameter introduced in Equation (2.1.9)
σ	parameter introduced in Equation (2.1.38)
χ	parameter introduced in Equation (2.3.24)

PDF9.84 0 TD5170.36 Tc (/F4 12 Tf-361.44 -100.8 TD -018 Tc (.) Tj0.120.12 Tc (d) Tj-792 Tc (E) tTj0.0316

ρ	density (kg/m^3)
σ	Stefan–Boltzmann constant (W/(m^{2}K^4))
σ_s	interfacial surface tension (N/m)
τ_e	evaporation time (s)
$\Phi_\#$	$a_\# R$
Φ_0	$a_\# R_d$
φ	k_{eff}/k_l (see Equation (2.1.11))
Ω	collision integral, frequency (1/s)
ω	frequency (1/s)
Λ	wavelength (m)
t_{bu}	breakup time (s)

Subscripts

b	boiling
abs	absorbed
amb	ambient
c	centre or convection
cr	critical
d	droplet
eff	effective
eq	equilibrium
ext	external
f	film surrounding droplets or fuel
F	fuel vapour
g	gas
inj	injection
iso	isolated
l	liquid
lg	from liquid to gas
m	type of species in the liquid phase
mix	mixture
0	initial or non-evaporating
p	constant pressure, pump
R	radiation
ref	reference
s	surface
S	Stokes
sv	saturated fuel vapour
t	time dependent
u	universal
v	fuel vapour
- 0	inner side of the droplet surface
+0	outer side of the droplet surface
(	infinitely far from the droplet surface

Superscripts

—	average
~	normalised

PDF created with pdfFactory Pro trial version www.pdffactory.com

1. INTRODUCTION

1.1 Background

Diesel engines are widely used due to their high efficiency and cost effectiveness. This has increased the demand for higher output, lower noise and emission performance from these engines. In meeting these demand igd rt

the results of implementation of this scheme for non-coupled solutions and a simple gas phase model showed that it is more accurate and computer efficient than the scheme based on a numerical solution of the heat conduction equation inside droplets (Sazhin et al., 2005a). It remained uncertain whether this conclusion is valid for more realistic cases (coupled solutions) and other gas phase models.

A simplified yet accurate model describing the thermal radiation absorption in semi-transparent Diesel fuel droplets was developed by Dombrovsky et al. (2001) and Sazhin et al. (2004a). In this model, detailed Mie

5. The comparison of the prediction of the new customised version of the KIVA-2 CFD code with available in-house experimental data.

1.3 Structure of the thesis

The thesis comprises the following main parts. The literature review on spray modelling and experimental studies with a view of applications to Diesel engines is presented in Chapter 2. A comparative analysis of droplet heating and evaporation models is given in Chapter 3. In Chapter 4, further development of the droplet radiative heating model is presented. The experimental validation of the model of droplet heating and evaporation is presented and discussed in Chapter 5. The result of implementation of the model into the KIVA-2 CFD code and the application of the new customised version of this code to the analysis of the processes in Diesel engines is discussed in Chapter 6. The conclusions drawn from this thesis and recommendations for further work are presented in Chapter 7. The appendices contain additional information relating to various part of the thesis.

PDF created with pdfFactory Pro trial version www.pdffactory.com

2. LITERATURE REVIEW

During the Diesel cycle, the air at close-to-atmospheric pressure and temperature is inducted to the combustion chamber and then compressed to a pressure of about 4 MPa and temperature of about 800 K during the compression stroke (Heywood, 1988). Liquid fuel is injected by the fuel injection system into the engine cylinder at the end of the compression stroke. The fuel atomises into small droplets and penetrates into the combustion chamber. Fuel injection pressures in the range from 20 to 170 MPa are used, depending on engine size and type of combustion system employed (Heywood, 1988). Then, the liquid fuel is heated and evaporates and fuel vapour mixes with the high-temperature high-pressure air. Since the air temperature and pressure are above the fuel's ignition point, spontaneous ignition (autoignition) of portions of the already-mixed fuel vapour and air occurs.

Chap

where R_d is the droplet radius, $\$_l$ and c_l are the liquid density and specific heat capacity respectively, T

models can be based on the solution of the heat conduction equation inside the droplet which can be written as (Luik0176 Tc (e) Tj0.84 Tc 76 Tc (c) Tj0.13821i

Chapter 2: Liter

Chapter 2: Literature Review

($Pe_l = Re_l Pr_l$), it has been approximated by the following expression (Abramzon and Sirignano, 1989):

$$1\ 86 \quad 0\ 86\ \tanh\left[2.225\log_{10}\left(\quad _1 / \nu 30\right)\right]$$

to be proportional to $Re^{1/2}Pr^{1/3}$ (Fuchs, 1959). Thus the general formula for *Nu* can be TF

results involving metals and water. *Nu* predicted by Equation (2.1.17) is reasonably close to *Nu* predicted by Equation (2.1.14).

2.1.2 Radiative heating

2.1.2.1 Early models

The theory of radiative exchange between particulates and gas has been developed by a number of authors (e.g. Siegel and Howell, 1992; Modest, 1993). The simplest model for radiative heating of droplets could be based on the assumption that droplets are opaque grey spheres characterised by the surface emissivity *e* (Sazhin et al., 2000). In this case, the heat flux into the droplets can be described by the following expression:

$$|q| = h\left(T_{g\infty} - T_s\right) + se\left(q_R^4 - T_s^4\right), \qquad (2.1.18)$$

where σ is the Stefan-Boltzmann constant and q_R is the so called radiative temperature. For optically thick gas q_R can be identified with the ambient temperature T_g. For optically tui yasit ca ye m

$$P_{\text{total}} = 4p \int_0^{R_d} P(R) R^2 dR \qquad (2.1.20)$$

is the total amount of thermal radiation absorbed in a droplet, P_{total} is measured in K/s.

In the case of finite thermal conductivity and effective thermal conductivity models (Groups 3 and 4), the heat conduction equation for semi transparent droplets in the presence of thermal radiation can be written as:

$$c_l r_l \frac{\partial T}{\partial t} = k_l \left(\frac{\partial^2 T}{\partial R^2} + \frac{2}{R} \frac{\partial T}{\partial R} \right) + c_l r_l P(R), \qquad (2.1.21)$$

where ***P(R)*** accounts for the radiative heating of droplets, measured in K/s. This equation can be solved subject to the same boundary condition (2.1.4) as before.

Analytical solution of Equation (2.1.21) is a straightforward generalisation of solution (2.1.5) and can be written as (Sazhin et al., 2004b):

$$T(R,t) = \frac{R_d}{R} \sum_{n=1}^{\infty} \left\{ \frac{p_n}{k l_n^2} + \exp\left[-k l_n^2 t\right] \left(q_n - \frac{p_n}{k l_n^2} \right) - \frac{\sin l_n}{\|v_n\|^2 l_n^2} m_o(0) \exp\left[-k l_n^2 t\right] - \frac{\sin l_n}{\|v_n\|^2 l_n^2} \int_0^t \frac{dm_0(t)}{dt} \exp\left[-k l_n^2 (t-t)\right] dt \right\} \sin l_n \left(\frac{R}{R_d} \right) + T_g(t), \qquad (2.1.22)$$

where

$$p_n = \frac{1}{R_d^2 \|v_n\|^2} \int_0^{R_d} RP(R) \sin\left(l_n \left(\frac{R}{R_d} \right) \right) dR. \qquad (2.1.23)$$

The value of thermal radiation power can be calculated based on the equation:

$$P(R) = \frac{1}{r_l c_l} \int_0^{\infty} p_l(R) dl, \qquad (2.1.24)$$

where $p_l(R)$ is the distribution of thermal radiation power density absorbed inside the droplet. The value of $p_l(R)$ can be calculated based on the Mie theory, but these calculations are very complicated and are beyond the scope of this review. Various approximations for ***P(R)*** will be considered in the next section.

PDF created with pdfFactory Pro trial version www.pdffactory.com

2.1.2.2.1 Radiative heating of the whole droplets

In most

$$\frac{}{} = \frac{4}{(\quad +1)} \left\{ 1 - \left[\frac{\left[\int_{1}^{2} \frac{\exp\left(- \frac{8}{\quad} \right)}{[\exp(\quad / (\quad)) - 1]} \right]}{\left[\int_{1}^{2} \frac{}{^{5}[\exp(\quad _{2} / (\quad _{\text{ext}})) - 1]} \right]} \right] \right\}$$

fuels (boiled and un-boiled BP Ford reference Diesel fuel, boiled low sulphur ESSO AF1313 Diesel fuel), for droplet radii in the range 2 μm ≤ R_d ≤ 200 μm and external temperature in the range 500 K ≤ T_{ext} ≤ 3000 K. The boiling simulated the ageing process of fuels. From these analyses it can be concluded that Approximation (2.1.28) with a and b defined by Equations (2.1.29) is applicable for all four types of fuel in the range 2 μm ≤ R_d ≤ 200 μm and 1000 K ≤ T_{ext} ≤ 3000 K, although it becomes less accurate for droplets with radii greater than 50 μm. For 500 K ≤ T_{ext} ≤ 3000 K Equations (2.1.29) appeared to be poor for all types of fuel under consideration. To achieve better accuracy, Sazhin et al., (2004a) suggested the following approximations:

$$\left.\begin{aligned} a &= a_0 + a_1\left(\frac{T_{ext}}{1000}\right) + a_2\left(\frac{T_{ext}}{1000}\right)^2 + a_3\left(\frac{T_{ext}}{1000}\right)^3 + a_4\left(\frac{T_{ext}}{1000}\right)^4 \\ b &= b_0 + b_1\left(\frac{T_{ext}}{1000}\right) + b_2\left(\frac{T_{ext}}{1000}\right)^2 + b_3\left(\frac{T_{ext}}{1000}\right)^3 + b_4\left(\frac{T_{ext}}{1000}\right)^4 \end{aligned}\right\}. \qquad (2.1.30)$$

The values of a_0, a_1, a_2, a_3, a_4, b_0, b_1, b_2, b_3 and b_4, depend on the type of Diesel fuel used. For un-boiled low sulphur ESSO AF 1313 Diesel fuel in the range of 5μ

where $I_l^{0(\mathrm{ext})}$ is the intensity of external thermal radiation, P_{total} is defined by Equation (2.1.20)

Presentation of the results for differential absorption of thermal radiation is simplified if the following normalised function is introduced (Dombrovsky and Sazhin, 2003b):

$$w(R) = \frac{p_l(R)}{\left[\frac{3}{R_{\mathrm{d}}^3}\int_0^{R_d} p_l(R)R^2 dR\right]}, \tag{2.1.32}$$

where $p_\lambda(R)$ is the spectral radiation power absorbed per unit volume.

In this case, the value of thermal radiation power absorbed per unit volume inside the droplet can be calculated based on the following equation (Dombrovsky and Sazhin, 2003b):

$$P(R) = \int_0^{\infty} p_l(R)dl = \frac{0.75}{r_1 c_1 R_d}\int_0^{\infty} Q_a w(R) I_l^{0(\mathrm{ext})} dl\ . \tag{2.1.33}$$

If the external thermal radiation is that of a black body at temperature T_{ext} then $I_l^{0(\mathrm{ext})} = 4pB_l(T_{\mathrm{ext}})$ and Equation (2.1.33) can be written as:

$$(\ ) = \frac{3}{r_1 \rho_{\mathrm{l}}\ \mathrm{d}}\int_0^{\infty}\ _{\mathrm{a}}(\ )\ \ (\ _{\mathrm{ext}})\ l$$

where $\bar{g} = (1.5/t_0)^2 - (0.6/n)^2$, $t_0 = a_l R_d$, $m_c = \sqrt{1-\left(\frac{1}{n}\right)^2}$, $m_* = \sqrt{1-\left(\frac{1}{n(R/R_d)}\right)^2}$,

$$\Theta(x) = \begin{cases} 0 & \text{when } x < 0 \\ 1 & \text{when } x \geq 0 \end{cases}$$

and

$$w(R) = \frac{x^2 t_0^3}{3} \frac{\exp[-x(t_0 - t)]}{t_0(xt_0 - 2) + (2/x)[1 - \exp(-xt_0)]}, \tag{2.1.37}$$

where $x = 2/(1+m_c)$. Equation (2.1.36) was used when $t_0 < \sqrt{2.5}$. Otherwise Equation (2.1.37) was used. The generalisation of this model to the case of asymmetrically illuminated droplet was reported by Dombrovsky and Sazhin (2004).

From above consideration, there are two different approaches to modelling the effects of thermal radiation on heating and evaporation of droplets. If the distribution of thermal radiation absorption inside droplets is needed, the term of ***P(R)*** in Equation (2.1.21) as defined by Equation (2.1.34) is used. If the distribution of thermal radiation absorption inside droplet is ignored then a much simpler approach can be used as

suggested in [76]. Tc ( ) Tnjj-0.18912 4c (e) Tc (p) Tj-0.42912 TTc (i) Tj0.02544 18912 4c (e) Tc (p) Tj-

processes. The heat required for evaporation is transferred to the droplet surface

2.2.1 Classical D^2-law

The classical D^2- law was formulated in the 1950s by Godsave and Spalding (e.g. Lefebvre, 1989; Sirignano, 1999). It was derived for an isolated, single component droplet, burning in a quiescent, oxidizing environment. The term D^2-law indicates that the square of the droplet diameter decreases linearly with time. For constant droplet surface temperature the evaporation rate $\#_{st}$ is introduced as the surface regression rate defined as:

$$l_{st} = -\frac{dD^2}{dt}. \tag{2.2.2}$$

In order to obtain the evolution of droplet diameter, Equation (2.2.2) is integrated with the initial condition $D(t=0)= D_0$ (Lefebvre, 1989):

$$D^2(t) = D_0^2 - l_{st} t. \tag{2.2.3}$$

The result is the well-known D^2-law, stating that the square of the droplet diameter decreases linearly with time during droplet evaporation. In addition to the evaporation rate, another important parameter in droplet evaporation is the life time of the droplet, also called evaporation time $\&_e$, which can be determined from Equation (2.2.3) with $D(t=t_e)=0$:

$$t_e = \frac{D_0^2}{l_{st}}. \tag{2.2.4}$$

The applicability of the D^2-law is limited since it is based the assumption that droplet temperature is constan2.e

$$_{fs} = \exp\left[\; _{f} - \frac{x_f}{T_s - 43} \right]$$

gives the following expression for $\dot{m}_d$:

$$\dot{m}_d = -4\pi R_d D_g \rho_{total} \ln(1+B_M). \quad (2.2.15)$$

This model is widely use for stationary evaporating droplets. Remembering the definition of h_m we can write:

$$\dot{m}_d = 4\pi R_d^2 h_m (\rho_{vs} - \rho_{v\infty}). \quad (2.2.16)$$

Combining Equations (2.2.15) and (2.2.16) we obtained the following expression for *Sh* (Lefebvre, 1989):

$$Sh = \frac{2\ln(1+B_M)}{B_M}. \quad (2.2.17)$$

Equation (2.2.17) can be presented in a more general form:

$$Sh = Sh_0 \frac{\ln(1+B_M)}{B_M}, \quad (2.2.18)$$

where Sh_0 =2 for stationary droplets.

Similarly, the following expression for the Nusselt number was obtained (Lefebvre, 1989):

$$Nu = Nu_0 \frac{\ln(1+B_M)}{B_M}, \quad (2.2.19)$$

where Nu_0 is the Nusselt number for non-evaporating droplets (Nu_0=2 for stationary droplets).

An alternative expression for *Nu* can be found taking into account the effect of vapour superheating (raising of fuel vapour temperature from T_s to T_g). The energy balance equation for a droplet taking into account this effect can be written as (Sirignano, 1978):

— (s) d (s) | d|

$$4\pi k_g \frac{dT}{c_{pv}(T-T_s)+L(T_s)-(|\dot{q}_d|/\dot{m}_d)} = -\frac{\dot{m}_d\, dR}{R^2}. \quad (2.2.21)$$

Introducing the Spalding heat transfer number B_T (Abramzon & Sirignano, 1989):

$$B_T = \frac{c_{pv}(T_g - T_s)}{L(T_s)-(|\dot{q}_d|/\dot{m}_d)} \quad (2.2.22)$$

and integrating both parts of Equation (2.2.21) from T=T_s to T=T_g and from tm

$$Nu = \frac{2\ln(1+B_T)}{B_T}. \tag{2.2.28}$$

The Sherwood number for evaporating moving droplets depends on *Re* and *Sc*. The well known correlation for Sh_0 can be presented as (Bird et al., 2002):

$$Sh_0 = 2 + 0.6\,Re_d^{1/2}\,Sc_d^{1/3}. \tag{2.2.29}$$

For evaporating moving droplets the expression for the Nusselt number and the Sherwood number can be presented as:

$$Sh = \frac{\ln(1+B_M)}{B_M}\left(2 + 0.6\,Re_d^{1/2}\,Sc_d^{1/3}\right) \tag{2.2.30}$$

$$Nu = \frac{\ln(1+B_T)}{B_T}\left(2 + 0.6\,Re_d^{1/2}\,Pr_d^{1/3}\right). \tag{2.2.31}$$

The factor 0.6 in the equations above can be replaced by 0.552. Hence, Correlations (2.2.30) and (2.2.31) become (Abramzon and Sirignano, 1989):

$$Sh = \frac{\ln(1+B_M)}{B_M}\left(2 + 0.552\,Re_d^{1/2}\,Sc_d^{1/3}\right) \tag{2.2.32}$$

$$Nu = \frac{\ln(1+B_T)}{B_T}\left(2 + 0.552\,Re_d^{1/2}\,Pr_d^{1/3}\right). \tag{2.2.33}$$

Alternatively, remembering Equation (2.1.15), we can write (Abramzon and Sirignano, 1989):

$$Nu = \frac{\ln(1+B_T)}{B_T}\left(1 + (1 + Re_d\,Pr_d)^{1/3}\,f(Re_d)\right) \tag{2.2.34}$$

$$Sh = \frac{\ln(1+B_M)}{B_M}\left(1 + (1 + Re_d\,Sc_d)^{1/3}\,f(Re_d)\right). \tag{2.2.35}$$

Abramzon and Sirignano (1989) refined the classical model above by taking into account the effect of convective transport caused by the droplet motion relative to the gas by introducing so called ‘film’ theory. The film theory assumes that the resistance to heat or mass exchange between a surface and a gas flow may be modelled by introducing the concept of gas h Tj0.13824 Tc (e) Tj-0.48 Tc (y) Tj0.8824 Tc (a) Tj-0088 Tc (t) Tj0.12 T

1989):

$$\frac{2}{{}_{0}\quad 2}$$

In practical implementations into CFD codes the actual Sherwood number (*Sh*) and Nusselt number (*Nu*) need to be used. These parameters can be found from the following equations:

$$Nu = Nu^* \frac{\ln(1+B_T)}{B_T} \tag{2.2.44}$$

$$Sh = Sh^* \frac{\ln(1+B_M)}{B_M}. \tag{2.2.45}$$

Taking into account film theory, the correlations for *Nu* and *Sh* should be modified and Equations (2.2.30)-(2.2.35) become:

$$Sh = 2\frac{\ln(1+B_M)}{B_M}\left[1+0.3\frac{Sc_d^{1/3}\,Re_d^{1/2}}{F(B_M)}\right] \tag{2.2.46}$$

$$Nu = 2\frac{\ln(1+B_T)}{B_T}\left[1+0.3\frac{Pr_d^{1/3}\,Re_d^{1/2}}{F(B_T)}\right] \tag{2.2.47}$$

$$Sh = 2\frac{\ln(1+B_M)}{B_M}\left[1+0.276\frac{Sc_d^{1/3}\,Re_d^{1/2}}{F(B_M)}\right] \tag{2.2.48}$$

$$= 2\frac{\ln(1+\ _T)}{\ _T}\left[1+0\ 276\frac{\ _d^{1\ 3}\,Re_d^{1\ 2}}{F(B_T)}\right]$$ *Tc (.12 Tc (.12 8 15.64M.v: 0625( ) B) Tj11.56..84 TD (B) Tj-5*

C

Model 0	$Sh = \frac{\ln(1+B_M)}{B_M}\left(2+0.6\,Re_d^{1/2}\,Sc_d^{1/3}\right)$ $Nu = \frac{\ln(1+B_M)}{B_M}\left(2+0.6\,Re_d^{1/2}\,Pr_d^{1/3}\right)$
Model 1	$Sh = \frac{\ln(1+B_M)}{B_M}\left(2+0.6\,Re_d^{1/2}\,Sc_d^{1/3}\right)$ $Nu = \frac{\ln(1+B_T)}{B_T}\left(2+0.6\,Re_d^{1/2}\,Pr_d^{1/3}\right)$
Model 2	$Sh = 2\frac{\ln(1+B_M)}{B_M}\left[1+0.3\frac{Sc_d^{1/3}\,Re_d^{1/2}}{F(B_M)}\right]$ $= \frac{(\quad+\quad)}{\quad}\left[\quad+\quad\frac{\quad}{(\quad_T)}\right]$

2.3 Autoignition modelling

Autoignition of Diesel sprays is usually described in terms of ignition delay and ignition sites location. Although the autoignition may be considered as a continuous process (Dec and Espey, 1998) it is widely accepted that autoignition is the beginning of the thermal explosion that follows the physical processes (mixing of fuel with ambient gas) and chemical reactions leading to the onset of a flame (Aggarwal, 1998). Modelling of the autoignition is essential for predicting the initiation of combustion in Diesel engines (Griffiths and Barnard, 1995). Two main parameters characterize the autoignition process: the initial temperature at which the autoignition can develop and the time delay before the start of autoignition (Brady, 1996). Detailed kinetic mechanism of the autoignition process is very complicated as it includes many chemical reactions and species. The chemical part of the autoignition process can be dbcliicaj0 Tc (d) Tj0.12 Tc ( )

Termination

$R^* \rightarrow out$	Rate coefficient $f_2 k_p$	(2.3.7)
$2R^* \rightarrow out$	Rate coefficient $f_2 k_p$,	(2.3.8)

where *RH* represents hydrocarbon fuel (C_nH_{2m}), *R** is radical, *B* is the branching agent, *Q* is the intermediate agent and *P* is the product, consisting of H_2O, CO a andO,ch intermdia

The coefficient γ determines the burned products mixture via $[CO]/[CO_2] = g/(1-g)$

The rate constants in Equations (2.3.9) – (2.3.13) are defined by the following expressions (Halstead et al.,1977; Schäpertöns and Lee,1985):

be based only on the contribution of the chemical reaction. Equation (2.3.20) is simplified to (Sazhin et al., 1999):

$$\frac{dT}{dt} = \frac{1}{c_v n_{tot}} k_p q V [R^*] \tag{2.3.23}$$

The development of the Shell model followed two main directions. The first direction is focused on the modifications of the coefficients without changing the overall structure by adjusting the kinetic rates to fit experimental data (Schäpertöns and Lee, 1985; Theobald, 1986). The second direction is focused on modifying the equations to better reflect the underlying chemistry and this leads to change in the overall structure of model.

Sazhin et al. (1999) suggested a new mathematical formulation for the Shell model. This is partil 2

Tj -0.10176 T2.28 (o) 2.04 Tj 0.mi.u1bu

ei u.88 -19.2 TD -0.669 Tj -0.10176 T tmm ulau ma Tce (T56 Tc (s) Tj1.j0.) Tj-0.0Tj-0.21 ao i u.88 -19

eo04 T76 .

$$g_B \quad mA_{f1} \exp\left(-\frac{E_{f1}}{R_u \; T_0 \; \frac{mq}{C_v[N]}}\right) \left([O_2]_0 \quad pm\right)^{x1} \left([RH]_0 \quad\right)^{y1}$$

$$mA_{f2} \exp\left(\frac{E_{f2}}{R_u \; T_0 \; \frac{mq}{C_v[N]}}\right)\Bigg|_0 [Q].$$

inhibited if the temperature increases higher than 1100 K or very sharp temperature rise ($>10^7$) K/s occurs. The authors showed that the autoignition chemical delay for Diesel fuel is much less than physical delay due to droplet transit time, atomisation, heating, evaporation and mixing for droplet radii. This justifies the application of less accurate than detail kinetic mechanism, but more s( ) Tj76 Tc (e) Tj0.6 Tc ( ) T3 Tc (e) Tj0 (i) Tj-0.42912 Tc (

turbulence model and a modified version of this model (sub-grid scale model). Spray break-up is modelled using the Taylor Analogy Break-up (TAB) model based on the analogy between an oscillating and distorting droplet and a spring mass system.

The change in droplet radius due to vaporisation is described by hydrodynamic model with the following equation (Amsden et al., 1989):

$$\frac{dR}{dt} = \frac{r_g D_g}{2 r_l R_d} B_M Sh \tag{2.4.1}$$

where Sh is described in Equation (2.2.30). This equation is equivalent to Equation (2.2.15). The rate of droplet temperature change is determined by the energy balance equation in such a way that the energy supplied to the droplet either increases the droplet temperature or supplies heat for its vaporisation. These are described by the following equation (Amsden et al., 1989):

$$-\dot{m}_d L + r_l c_l \frac{4}{3} p R_d^2 \frac{dT}{dt} = 4 p R_d^2 \frac{Nu k_g}{2 R_d} (T_g - T_s), \tag{2.4.2}$$

where the Nusselt number is described in Equation (2.2.31) with B_T replaced by B_M (similarly to Model 0). The latter equation takes into account the effect of vapour superheating.

Several versions of this code have been developed by Los Alamos National Laboratory. These are KIVA, KIVA-2, KIVA-3 and KIVA-3V. KIVA-2 is an improved version of KIVA that has better computational efficiency, numerical accuracy and physical sub-models. It is more user friendly and versatile than KIVA (Amsden et al., 1989). KIVA-3 is an extension of KIVA-2. It uses the same numerical solution procedure, and solves the same set of equations. KIVA-3 is applicable to laminar or turbulent flows, subsonic or supersonic flows and single-phase or dispersed two-phase flows. In contrast to KIVA-2, KIVA-3 uses a block structured mesh with connectivity defined through indirect addressing. KIVA-3V is an extended version of KIVA-3, can model any number of vertical valves in the cylinder head. Other new features developed in KIVA-3V are particle based liquid wall film model, improved sorting subroutine, mixing-controlled turbulent combustion model and an optional RNG k-. turbulence model (Amsden, 1997).

PDF created with pdfFactory Pro

2.5 Experimental studies

Experimental studies

configuration of a PDA system is showed in figure 2.5.1 below.

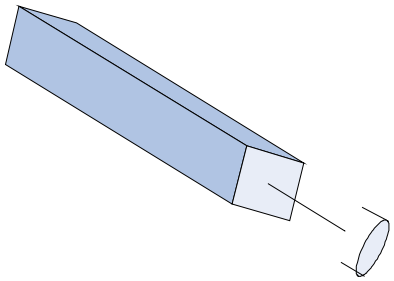

Photomultiplier

Chapter 2: Literatu

account the semi-transparency of the droplets, but can ignore the spatial variations of radiation absorption inside the droplets. Models of radiative heating in Diesel engines have been suggested by a number authors (Dombrovsky, 2000; Dombrovsky et al., 2001; Dombrovsky and Sazhin, 2003c; Sazhin et al., 2004a). However, further analysis of these models and their applications are needed.

Various methods used to investigate spray and combustion characterisation in Diesel engine experimentally have been reviewed.

PDF created with pdfFactory Pro trial version www.pdffactory.com

3. COMPARATIVE ANALYSIS OF THE MODELS FOR FUEL DROPLET HEATING AND EVAPORATION

As mentioned in Chapter 2, the importance of the development of accurate and computer efficient models, describing fuel droplet heating and evaporation in engineering and environmental appTj0.46416 Tc (t) Tj-0.49584 Tc (i) Tj0.12 Tc (on32.Tj0.0837

issues. The performance of the new model, developed by Sazhin et al. (2005a,b), will be investigated taking into account the coupling of liquid and gas phases, and using various models for the gas phase. The m tgaaagmh.

reach almost 15%. If we assume that Model 6 is the most accurate one, as the one based merely on experimental data, then we can conclude that the most accurate semi-theoretical models are Models 3 and 4, and the least accurate is Model 0 used by Sazhin et al. (2005b). Interestingly, the prediction of Model 3 is closer to the prediction of Model 6 than the prediction of Model 4, although Model 4 is expected to be more accurate than Model 3.

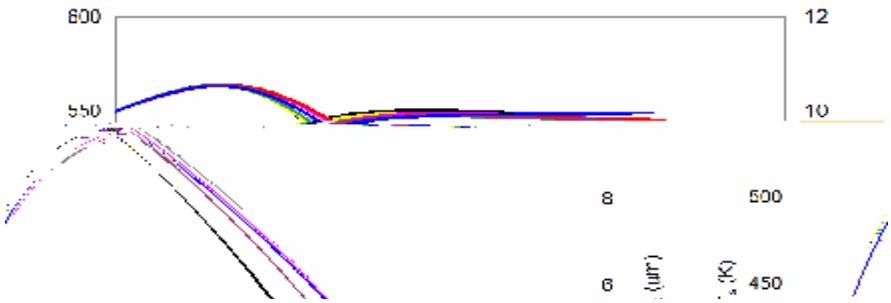

Figure 3.1.1 Plots of T_s and R_d versus time for the initial gas temperature T_{g0} = 880 K, gas pressure P_{g0} = 3 MPa, initial droplet temperature T_{d0} = 300 K, initial droplet radius R_{d0} = 10 m and velocity v_{d0} = 102 m/s. The overall volume of injected liquid fuel was taken to be 1.74·10-13

one predicted by Model 6. In contrast to the case shown in Figure 3.1.1, however, the evaporation times predicted by Models 3 and 6 are noticeably different. The difference in Models 3 and 4 lies in the values of $F(B_M)$ and $F(B_T)$ (see Equations (2.2.50) and (2.2.51)). The contribution of the terms containing these functions in Equations (2.2.50) and (2.2.51) is proportional to $\sqrt{Re_d}$. Hence the accuracy of calculating these terms is more important in the case of the droplet with the initial velocity 10 m/s (Figure 3.1.2) than in the case of the droplet with the initial velocity 1 m/s (Figure 3.1.2).

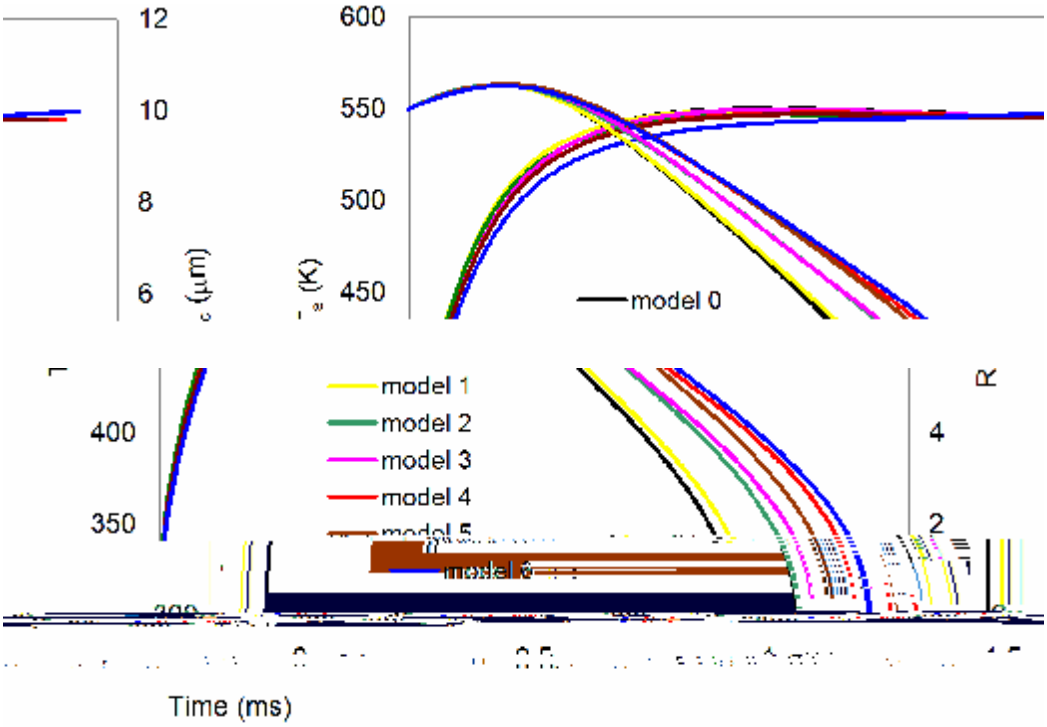

Figure 3.1.2 The same as Figure 3.1.1 but for the initial droplet velocity equal to 10 m/s

In Figures 3.1.3 and 3.1.4 the same plots as in Figures 3.1.1 and 3.1.2 are shown, but for the droplets with the initial radii equal to 50 m. The same closeness between the plots for R_d predicted by Models 4 and 6 as in Figures 3.1.1 and 3.1.2, can be clearly seen in Figures 3.1.3 and 3.1.4. Note that in the case of Figures 3.1.3 and 3.1.4, the values of $\sqrt{Re_d}$ are $\sqrt{5}$ larger than in the case of Figures 3.1.1 and 3.1.2. Hence the contribution of the terms $F(B_M)$ and $F(B_T)$ is expected to be more important in the cases shown in Figures 3.1.3 and 3.1.4 than in the cases shown in Figures 3.1.1 and 3.1.2. t

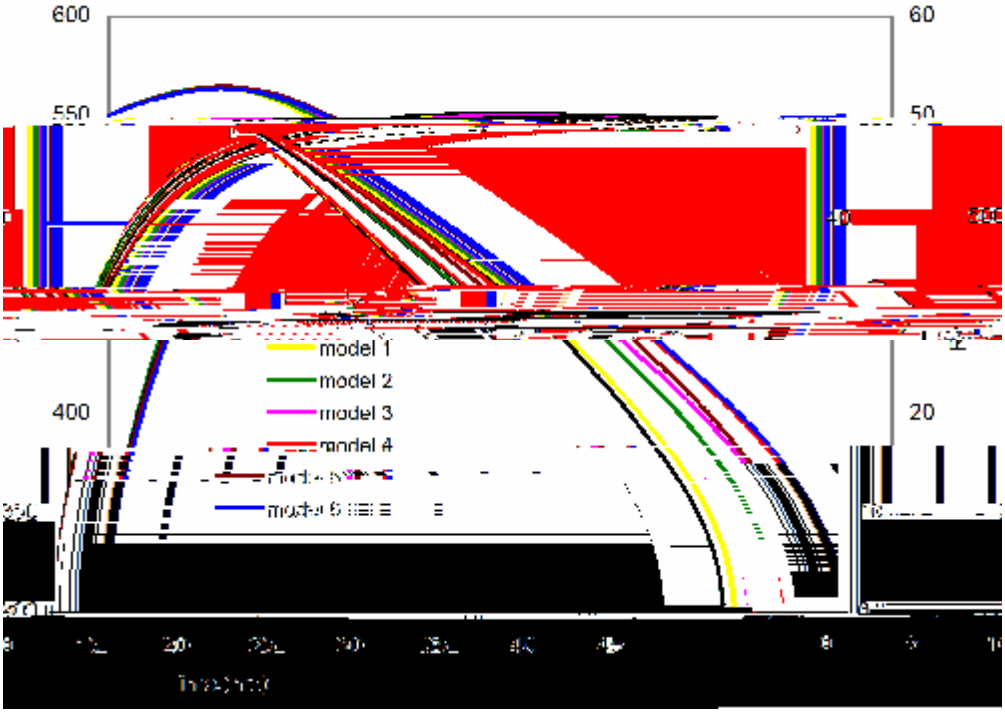

Figure 3.1.3 The same as Figure 3.1.1 but for the initial droplet radius equalovq l

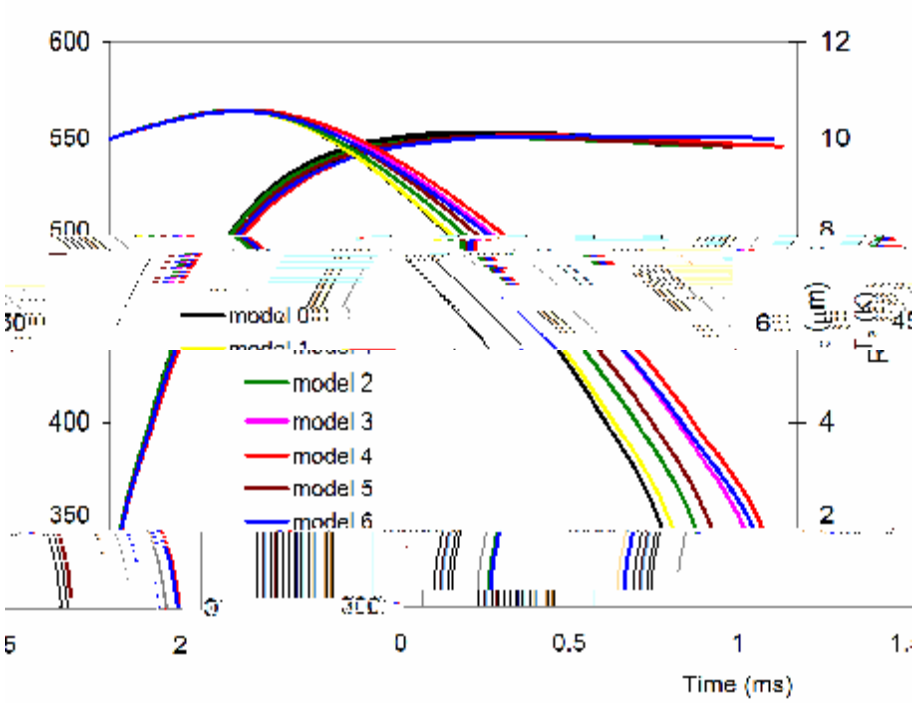

Figure 3.1.5 The same as Figure 3.1.1 but taking into account the effects of thermal radiation assuming that T_{ext} = 2000 K

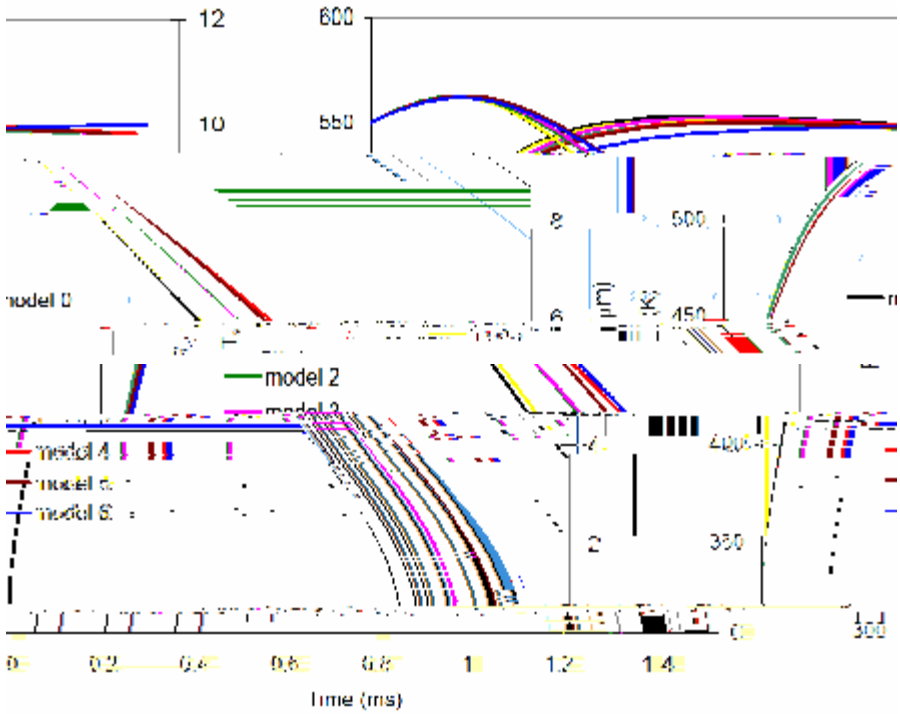

Figure 3.1.6 The same as Figure 3.1.2 but taking into account the effects of thermal radiation assuming that T_{ext} = 2000 K

PDF created with pdfFactory Pro trial version www.pdffactory.com

approximately proportionally to $R_d^{2.6}$ (see Equation (2.1.38) in which b **3** 0.50

In Figures 3.1.7 and 3.1.8 the same plots as in Figures 3.1.5 and 3.1.6 are sho

The same closeness between the predictions of Models 4 and 6 was observed when the pressure was reduced to 2 MPa. Also this result remained the same when the data for n-dodecane molecules reported by Hirschfelder et al. (1967) rather than by Paredes et al. (2000) were used, or the reference temperature and fuel vapour mass fraction in Model 6 were calculated similarly (totaoe cateeea dtass h2rt ( )t) j 0 . 2 2 4 1 6 TT c (t) Tj c (l) T j 0

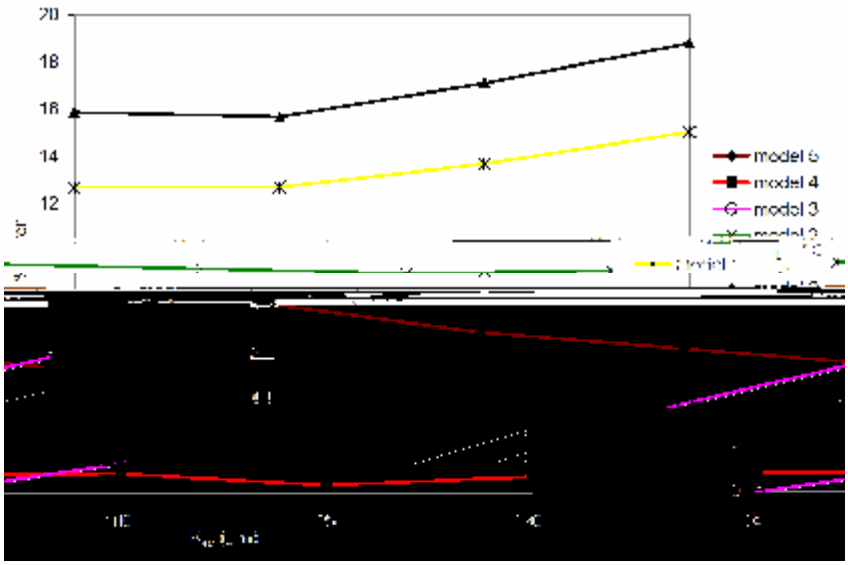

Figure 3.1.10 The same as Figure 3.1.9 but for the initial droplet velocity 10 m/s

The main advantage of Model 4 compae h111111 s 1 e24.36 Tc (h) Tj- Tc (i) Tj-0

based on the analytical solution of the heat conduction equation and its numerical solution, predict practically the same results in a wide range of parameters typical for Diesel engines. In both cases the time step was taken as 0.001 ms. For the numerical solution of the heat conduction equation inside the droplets, 100 cells along the radius were used.

The evaporation time predicted by both these algorithms was close to the evaporation time predicted by the model, based on the assumption of no temperature gradient inside the droplets (ITC model or liquid phase Model 2). However, a noticeable difference in temperatures was observed at the initial stage of droplet heating and evaporation. This is illustrated in Figure 3.2.1 for the droplets with the initial radius equal to 10 m and initial velocity 1 m/s injected into the gas with the same parameters as in the case shown in Figure 3.1.1.

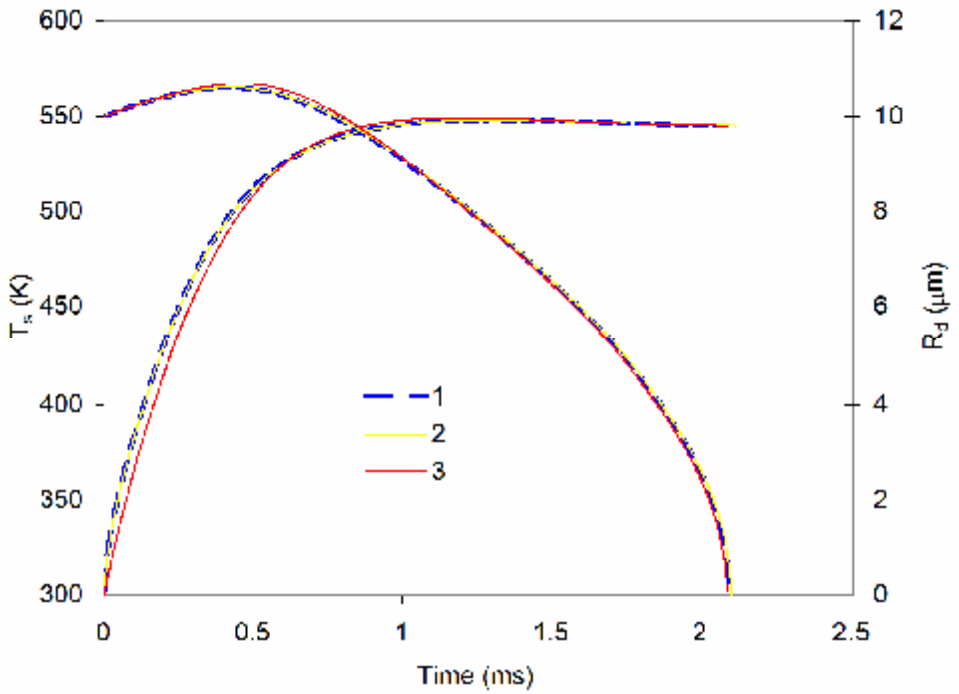

Figure 3.2.1 The same as Figure 3.1.1 but using three liquid phase numerical algorithms: the algorithm based on the analytical solution of the heat conduction equation inside the droplet (1), the algorithm based on the numerical solution of the heat conduction equation inside the droplet (2), the algorithm based on the assumption that the thermal conductivity inside droplets is infinitely large (3)

PDF created with pdfFactory Pro trial version www.pdffactory.com

Chapter 3: Comparative analysis of the models for fuel droplet heating and evaporati

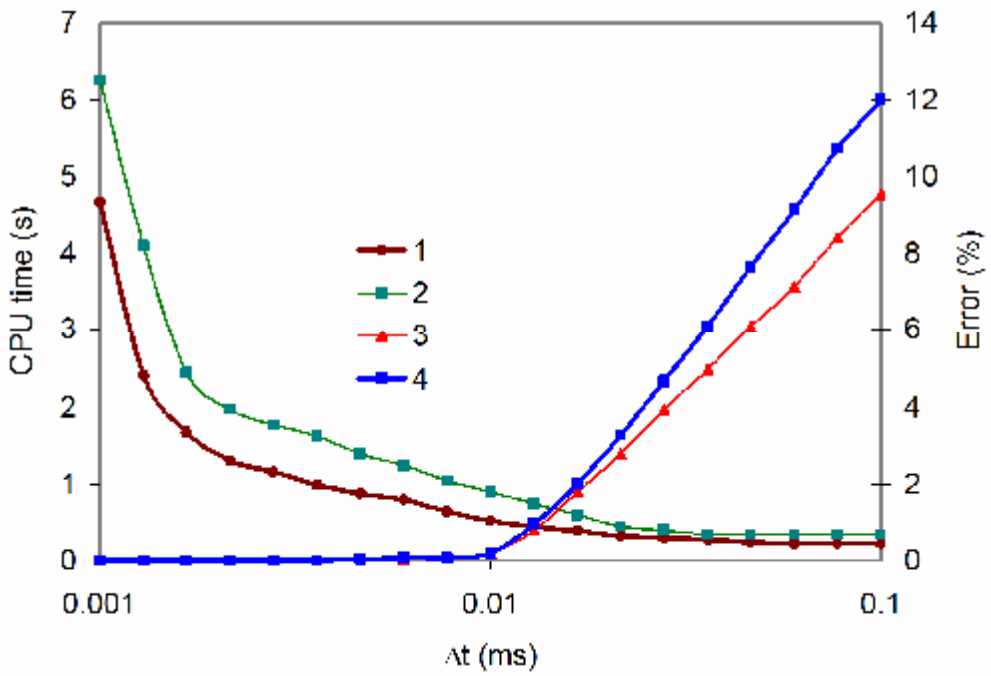

Figure 3.2.2 Plots of error and CPU times of the calculations of the evlorti ti

evaporation process was measured starting with droplet diameter equal to 72 m. The results of measurements were presented in the form of a plot of $(R_d/R_{d0})^2$ versus time t and are shown in Figure 3.3.1. In the same figure, the time evolution of this variable, predicted by algorithms described in Chapter 2, are presented. The calculations were performed using the effective thermal conductivity (ETC) model for the liquid phase and Model 4 for the gas phase (Curve 1), ETC model for the liquid phase and Model 0 for the gas phase with the same values of parameters as used by Sazhin et al. (2005b) (Curve 2), infinite thermal conductivity (ITC) model for the liquid phase and Model 4 for the gas phase (Curve 3), ETC model for the liquid phase and Model 4 for the gas phase, using the parameters reported by Hirschfelder et al. (1967) for tetradecane molecules (used for calculation of the binary diffusion coefficient) (Curve 4). The parameters reported by Paredes et al. (2000) for tetradecane molecules were used for Curves 1-3. The physical properties of tetradecane, used in the calculations, are given in Appendix A. The effect of thermal radiation was taken into account assuming that the radiation temperature is equal to the gas temperature.

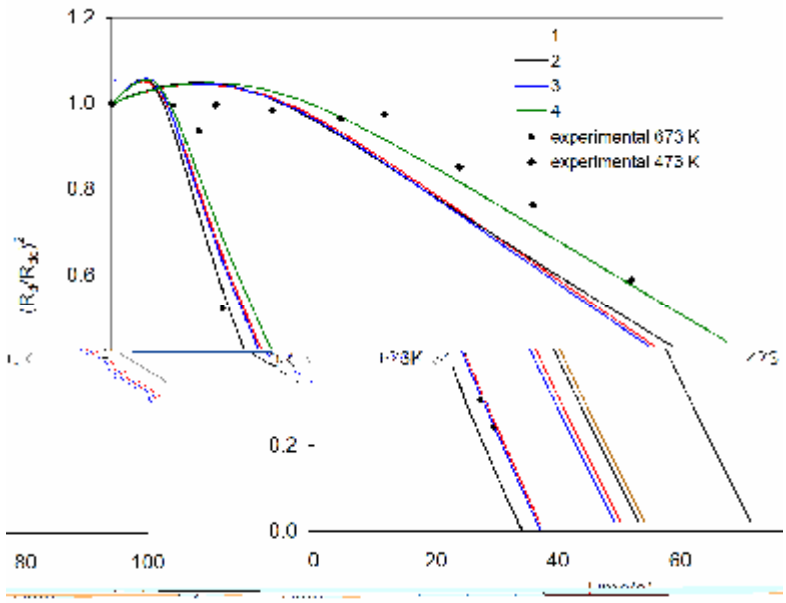

Figure 3.3.1 The values of $(R_d/R_{d0})^2$ for evaporating tetradecane droplets versus time, as measured by Belardini et al. (1992), and the results of calculations based on algorithms described in Chapter 2. The values of the initial gas temperatures are indicated near the curves

PDF created with pdfFactory Pro trial version www.pdffactory.com

Chapter 3r

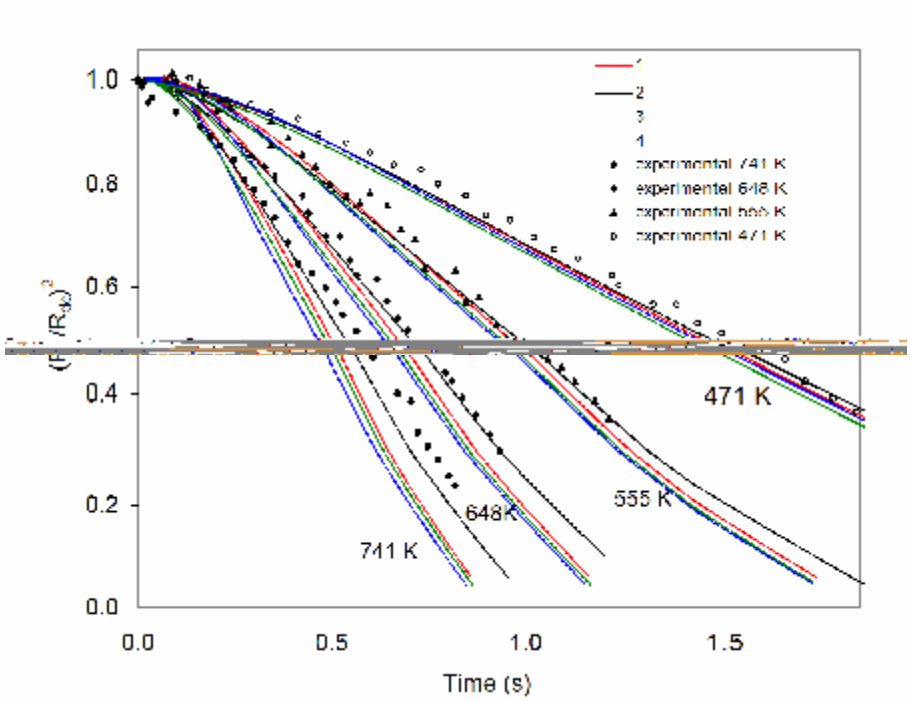

Figure 3.3.2 The values of $(R_d/R_{d0})^2$ for evaporating n-heptane droplets versus time for the initial pressure of 0.1 MPa, as measured by Nomura et al. (1996), and the results of calculations for the same combination of liquid and gas models as in Figure 3.3.1. The values of the initial gas temperatures are indicated near the curves

Plots of droplet surface temperature T_s versus t for the same parameters as in Figure 3.3.2 are shown in Figures 3.3.3 and 3.3.4. As can be seen in Figure 3.3.4, at the very initial stage of droplet heating and evaporation, the values of T_s are relatively insensitive towards the choice of gas phase model (Curves 1, 2 and 4 are rather close), but depend strongly on the choice of the liquid phase model (cf. Curves 1 and 3). The values of T_s predicted by the ITC model are much less than those predicted by the ETC model at the very initial stage of droplet heating regardless of the choice of the gas phase model.

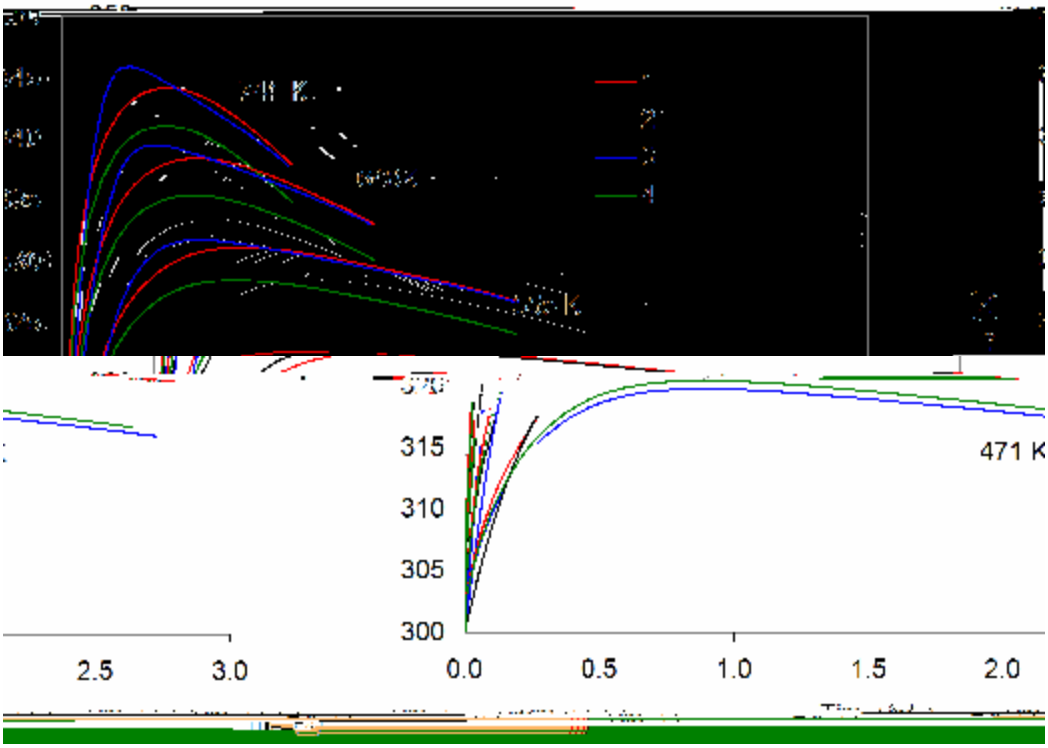

Figure 3.3.3 The plots of T_s versus time for the same values of parameters as in Figure 3.3.2, calculated using the same liquid and gas phase models as in this figure

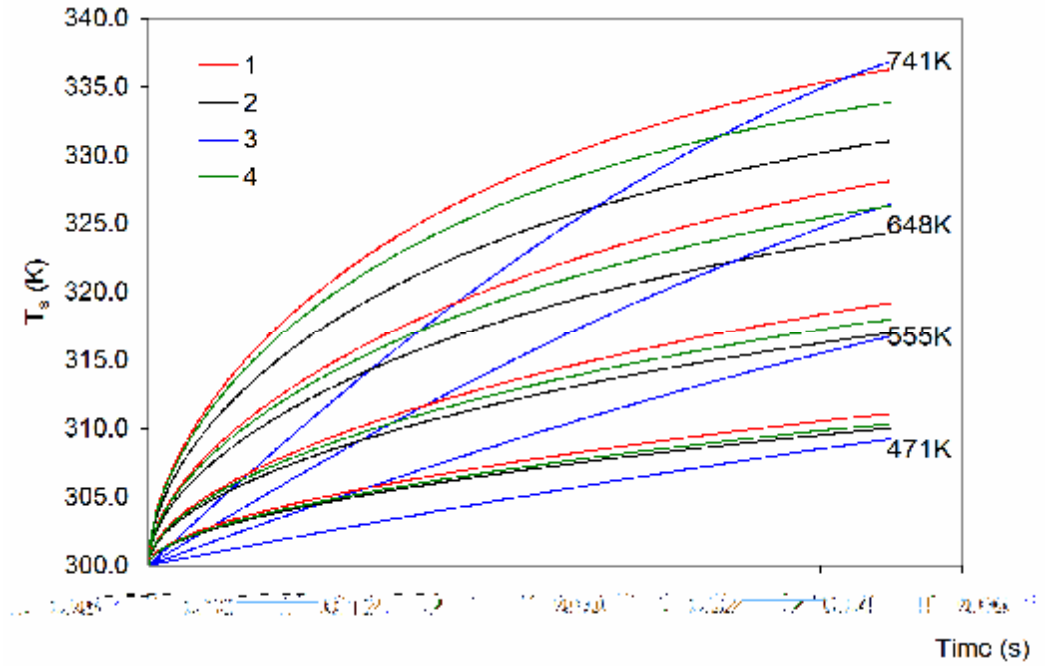

Figure 3.3.4 Zoomed part of Figure 3.3.3 referring to the very initial stage of evaporation

PDF created with p Tc (r) Tj-0.2phFactory Pro trial version www.pdffactory.com

At intermediate times both liquid and gas phase models affect the values of T_s (see Figure 3.3.3). During longer times the effects of liquid phase model on the values of T_s are negligible in most cases, and the predicted values of this temperature depend mainly on the choice of the gas phase model (see Figure 3.3.2).

predictions of gas phase Model 4. The effect of the binary diffusion coefficient on the values of R_d is relatively small in this case, as shown in Figure 3.3.2. In agreement with the results reported by Sazhin et al. (2005b), the ETC model predicts marginally more accurate results compared with the ITC one, similar to the case of lower pressure (see Figure 3.3.2). The comparison of the experimental results and the predictions of the models for the initial gas pressure 1 MPa and various initial gas temperatures is shown in Figure 3.3.6. The conclusions, which are obtained from the observation of this figure, are essentially the same as those which follow from Figure 3.3.5. The corresponding plots of T_s versus t have properties similar to those shown in Figures 3.3.3 and 3.3.4 for pressure 0.1 MPa.

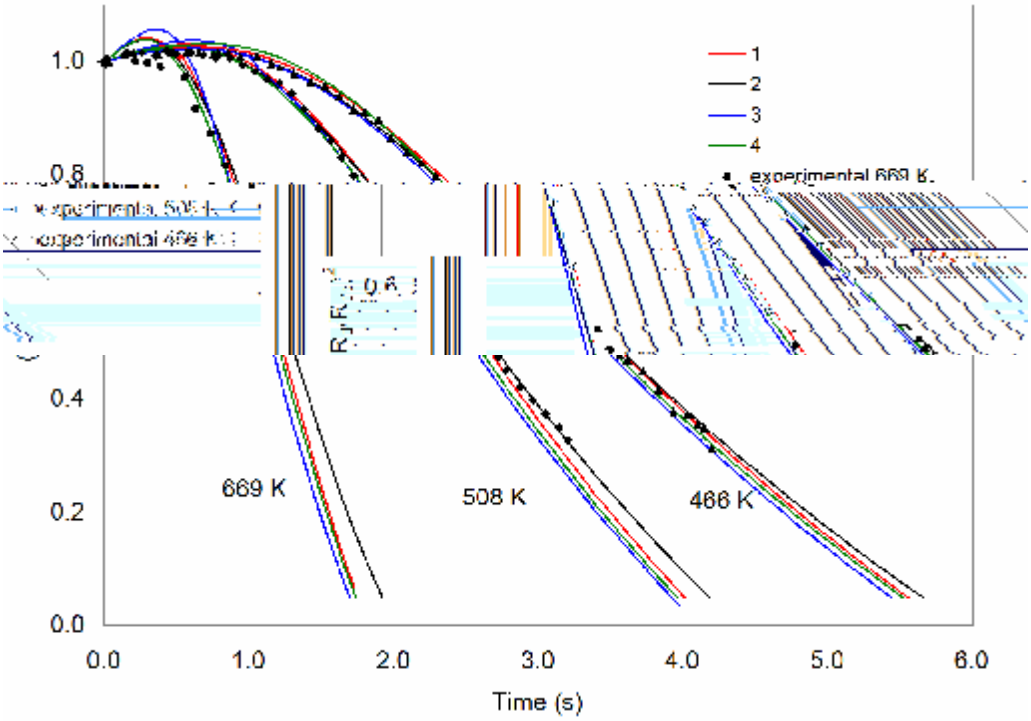

Figure 3.3.6 The same as in Figure 3.3.2 but for the initial gas pressure of 0.1 MPa

To summarise the results presented in this section, the comparison between the predictions of the models and experimental data reported by Belardini et al. (1992) and Nomura et al. (1996), is rather inconclusive. Namely, these data cannot support any of the gas phase models under consideration. The

PDF created with pdfFactory Pro trial version www.pdffactory.com

effect of liquid phase models is relatively small in the general case, and it leads to marginally better agreement between the predictions of the models and experimental data.

3.4 Effects of droplet break-up and autoignition

The models and experimental results considered so far did not take into account the effects of autoignition of fuel vapour/ air mixture, and the effects of droplet break-up. In this section both these effects are taken into account. As in Sazhin et al. (2005b), the S20832 Tc (c) Tj0.70416.3 Tc ( ) Tj0.03168 Tc (a(.) Tj0.3 Tc ( )0.20832 T

modelling of the ignition delay. Note that the agreement between the predictions of the ETC model with experimental data for initial gas temperatures greater than about 650 K, shown in this figure, cannot be interpreted as the experimental validation of the model, due to the uncertainty of the parameters of the Shell model.

The rest of this section will focus on the investigation of the effects of various liquid and gas models on droplet heating and evaporation, and the ignition of fuel vapour/ air mixture in a monodisperse spray, taking into account the droplet break-up effect. The effect of thermal radiation is ignored. The fuel is approximated by n-dodecane (see Appendix A). Gas and liquid parameters are the same as in the cases shown in Figures 3.1.1 – 3.1.8 and 3.2.1- 3.2.2. The autoignition process is assumed to be completed when the fuel vapour/ air temperature reached 1100 K.

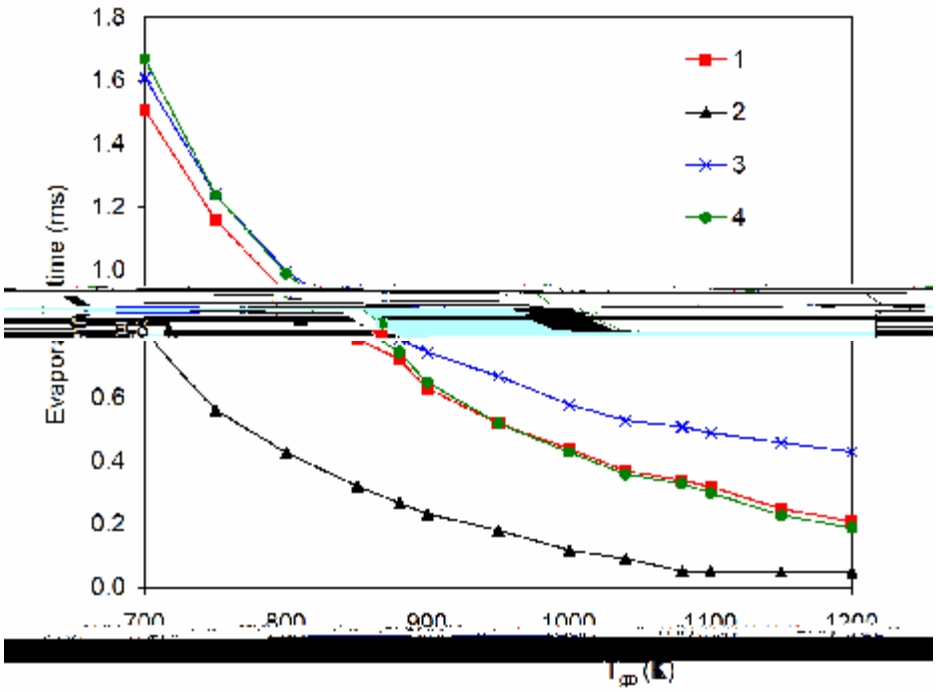

Figure 3.4.2 The values of the evaporation time versus initial gas temperature calculated based on the same combination of liquid and gas models as in the cases shown in Figures 3.3.1-3.3.6 and 3.4.1. Bag and stripping droplet break-ups were taken into account. The initial droplet diameter and velocity are taken equal to 50 m and 50 m/s respectively. Symbols indicate the values of gas temperatures for which the evaporation times were calculated

PDF created with pdfFactory Pro trial version www.pdffactory.com

Figure 3.4.2 illustrates the effect of various gas and liquid models on droplet evaporation time at various initial gas temperatures in the presence of break-up, but without taking into account chemical reactions in the gas phase. The initial droplet diameter and velocity are assumed equal to 50 m and 50 m/s respectively. Symbols in the figure indicate the values of the initial gas temperatures for which calculations of the evaporation time were performed. As one can see from Figure 3.4.2, in the presence of break-up, the contribution of gas and liquid models to the values of evaporation time are of the same order of magnitude. This situation is different from the one presented in Figures 3.1.1 – 3.1.8 where it was shown that in the absence of break-up the contribution of the liquid phase models to the evaporation time is negligible. In all cases shown in Figure 3.4.2, taking into account the effects of finite thermal conductivity in droplets and recirculation in them, leads to a prediction of shorter evaporation times in agreement with the results reported by Sazhin et al. (2005b). At small initial gas temperatures (less than about 900 K) this predicted increase in the evaporation time on n 0.08376 Tc (r) Tj0.03168 Tc (e) Tj-0.06d Tj-0.49584 Tc (iTj-0.25

reported by Sazhin et al. (2005b). The effect of the binary diffusion coefficient on the total ignition delay is visible but not dominant.

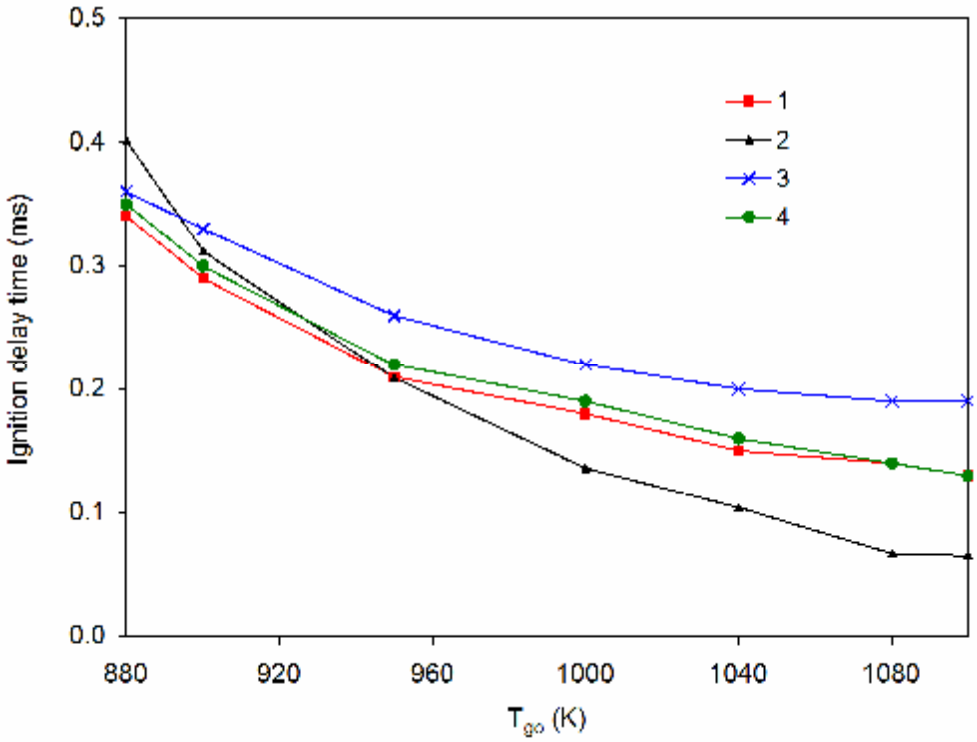

Figure 3.4.3 The plots of the total ignition delay versus the initial gas temperature T_{g0} in the presence of the break-up for the same droplets as used in Figure 3.4.2, calculated based on the same models as in the cases shown in Figures 3.3.1-3.3.6 and Figures 3.4.1-3.4.2. The Shell autoignieo111 Tj -0.40.12 Tc (d) Tj 33 iFest eeT Tc (s) Tj99

Chapter 3: Compate

Chapter 3: Comparative analysis of the models for f

4. APPROXIMATE ANALYSIS OF THERMAL RADIATION ABSORPTION IN FUEL DROPLETS

As mentioned in Chapter 2, more advanced models for radiation absorption in Diesel fuel droplets have been developed by Dombrovsky (2004), Dombrovsky and Sazhin (2003c, 2004). These take into account the distribution of absorption inside droplets. None of these models, however, seem to be suitable for implementation into CFD codes due to excessive CPU requirements (Sazhin, 2006; Sazhin et al., 2004a, 2005a; Abramzon and Sazhin, 2005, 2006). Therefore in practical applications, implementing the distribution of radiation absorption insi f sadra g.56 Tc ( )

Chapter 4: Approximate analysis of thermal radiation a

Results of the calculation of the indices of absorption for all three fuels, based on the measurements of the corresponding absorption coefficient, are presented in Figure 4.1.1. On the same figure, the previously reported plots by Sazhin et al. (2004a) of ***!*** versus ″ for Diesel fuel are reproduced. About 2300 individual measurements were used for presenting each of these plots.

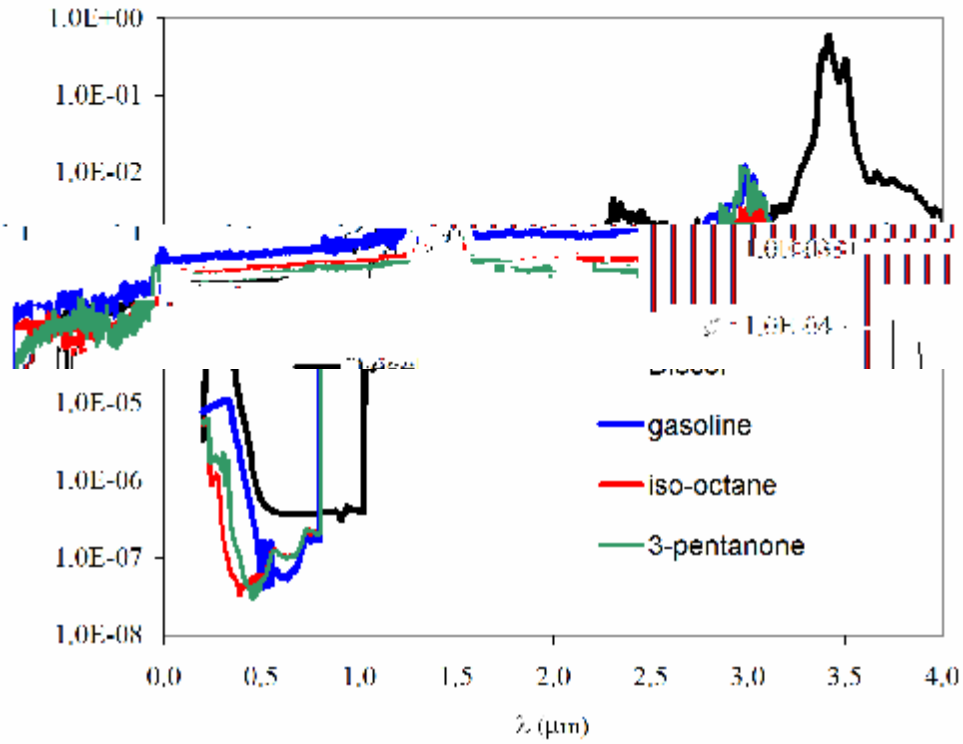

Figure 4.1.1 Indices of absorption of four types of fuel: low sulphur ESSO AF1313 Diesel fuel, gasoline fuel (BP Pump Grade 95 RON ULG), 2,2,4-trimethylpentane (iso-octane) and 3-pentanone versus wavelength *l*. The results for Diesel fuel are reproduced from Sazhin et al. (2004a)

As can be seen in Figure 4.1.1, the dependence of ***!*** on the type of fuel is noticeable, and there are a number of similarities between the plots. For all fuels, the region of semi-transparency in the range 0.5 m < ″ < 1 m is evident. The index of absorption increases by approximately 3 orders of magnitude when ″ increases from 0.5 m to 1.5 m. At the same time, some noticeable differences between the

PDF created with pdfFactory Pro trial version www.pdffactory.com

indices of absorption of the fuels can be identified. For example, the peak of absorption of Diesel fuel at " **3** 3.4 m is much more pronounced than the corresponding peaks of absorption of the other fuels. Also the value of " when this peak is observed is shifted from 3.4 m for Diesel fuel to approximately 3.0 m for other fuels. Strong peaks at around 3.5 m are related to C-H stretch vibrations of non-aromatic molecules, occurring in the range of 3.3 m - 3.5 m. Less intense peaks at around 3.0 m are most likely due to the presence of aromatic hydrocarbons, in which C-H stretch vibrations from benzene rings are expected. This is supported by the absorbance at around 0.25 m which is characteristic of the %-% electron transitions in the aromatic benzene ring. Aromatic hydrocarbons are added to gasoline to increase its octane number. The differences in the optical properties of the fuels shown in Figure 4.1.1 are expected to produce 4 different values of the average absorption efficiency factors of fuel droplets.

Index of refraction measurements were conducted using the ABBE 60 direct reading refractometer at room temperature. This index was measured by turning a dual prism combination through an angle, which is proportional to the refractive index of liquid placed between the two prisms. The light source was white. It was emitted from a tungsten lamp. The angle of light emerging from the combination of prisms was measured using a telescope that moved over a calibrated refractive index scale. The telescope was focused on the edge of the light beam, which showed up as a dark edge in the field of view. The values of refractive indices for the three fuels were: gasoline (n = 1.394 ± 0.001); iso-octane (n = 1.389 ± 0.001) and 3- pentanone (n = 1.390± 0.001). The measurement of the index of refraction for Diesel fuel was n = 1.460 with similar error except in the region of strong absorption (" **3** 3.4 m) (Dombrovsky et al., 2003). The relatively weak dependence of n on " for Diesel fuel has only a minor effect on the efficiency factor of absorption of this fuel (Dombrovsky et al., 2003). Therefore, this dependence can be ignored when this factor is calculated for Diesel fuel (Sazhin et al., 2004a). We assume that this conclusion re

s

minmi son

4.2 Average efficiency fac0464 Tc (l) Tj32 Tc (f)62 TD 0 Tc (74) TjETQ q 314.64 98.88 0.48 12.48 re h

from a strong absorption band in the 6.8 m – 7.5 m region. In the case of $)_R$ = 1000 K, $)_R$ = 2000 K and $)_R$ = 3000 K, the maximal contribution from the later range is estimated to be 3.8%, 0.9% and <0.3% respectively (Silverstein et. al., 2005). This is well below the errors shown in Figure 4.2.1. Hence, the application of data presented in Figure 4.1.1 for calculation of $\overline{Q}_a$ based on Equation (2.1.27) can be justified.

Following Dombrovsky et al. (2001) and Sazhin et al. (2004a) the results of the calculation of $\overline{Q}_a$ based on Equation (2.1.27) are approximated by the following expression (see Equation (2.1.28)):

$$\Lambda = aR_d^b$$

where

$$a = \sum_{i=0}^{N} a_i \left(\frac{q_R}{1000} \right)^i \tag{4.2.1}$$

$$b = \sum_{i=0}^{N} b_i \left(\frac{q_R}{1000} \right)^i \tag{4.2.2}$$

$)_R$ is in K, R_d is in m, a_i is in $m^{5b}K^{5i}$/F6 10.8 Tf4.yTj-0.-912 Tc (i) Tj0 Tc (44.8 0 .04 Tf13.68 0 TD (a) Tj/F5 7.2 Tf5.52 -1.2 TD (i) Tj/F5 11.04 Tf1.92 1

C

Coefficients \ Fuel	Diesel (low sulphur ESSO AF1313)	Gasoline (BP 95 RON ULG)	2,2,4 -Trimethylpentane	3-Pentanone
a_0	0.143452	0.074546	0.035479	0.045995
a_1	-0.016510	-0.049511	-0.034435	-0.047760
a_2	-0.058531	0.023057	0.023033	0.029250
a_3	0.027674	-0.006836	-0.007777	-0.009075
a_4	-0.003661	0.000829	0.000964	0.001065
b_0	0.482037	0.406702	0.429499	0.327158
b_1	-0.249135	0.334640	0.625147	0.686807
b_2	0.286669	-0.208455	-0.462004	-0.463508
b_3	-0.094873	0.068515	0.152989	0.147149
b_4	0.010658	-0.008410	-0.018322	-0.017281

be of use in practical engineering applications, including computational fluid dynamics (CFD) codes.

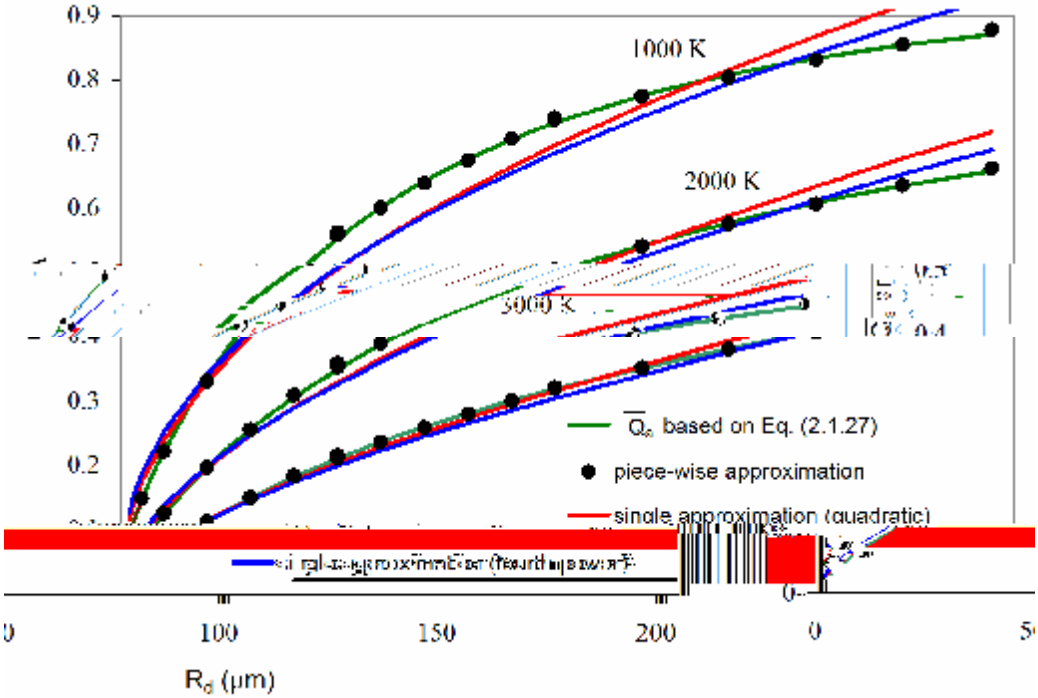

Figure 4.3.1 Plots of $\overline{Q}_a$ and its three approximations Λversus droplet radius for Diesel fuel. Three radiation temperature: 1000 K, 2000 K and 3000 K (indicated near curves) were considered. Green solid curve refer to $\overline{Q}_a$ as calculated from Equation (2.1.27). Black dots refer to piecewise approximation for ", as calculated from Equation (2.1.28). Red solid curved refer to a single quadratic approximation for ". Blue solid curves refer to a single fourth power approximation for "

The same conclusion was drawn for gasoline (Figure 4.3.2), iso-octane (Figure 4.3.3) and 3-pentanone (Figure 4.3.4). Note that the temperature effect on $\overline{Q}_a$ is greatest for Diesel fuel. The maximum values of $\overline{Q}_a$ are greater for Diesel and gasoline fuels than for iso-octane and 3-pentanone. For all fuels, the values of $\overline{Q}_a$ decrease with increasing external temperature in agreement with the results reported earlier by Dombrovsky (2001) and Sazhin et al. (2004a).

PDF created with pdfFactory Pro trial version www.pdffactory.com

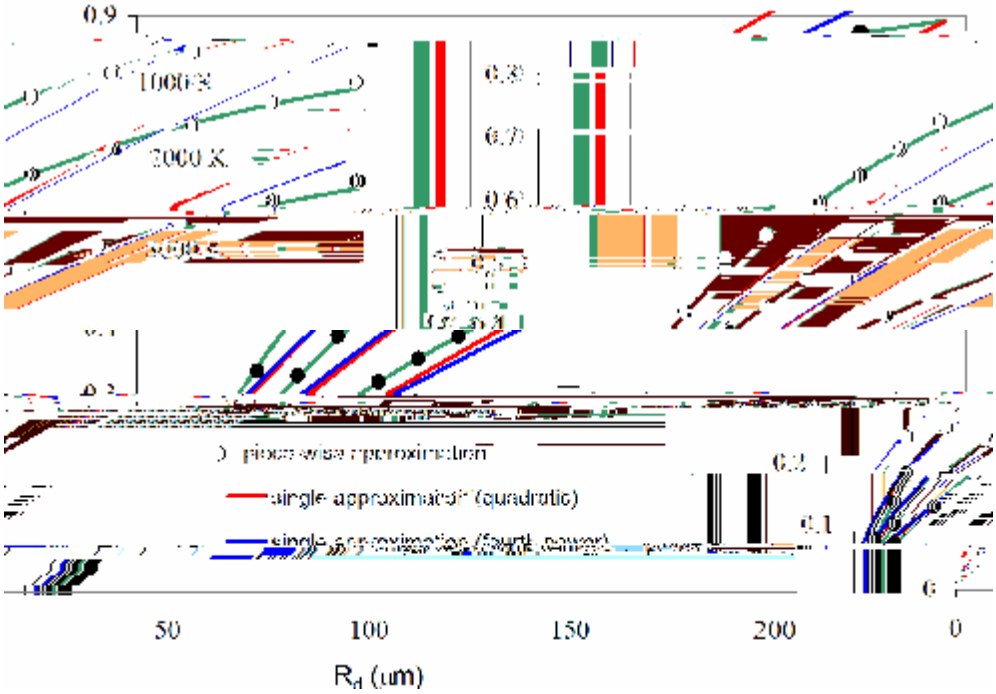

Figure 4.3.2 The same as Figure 4.4.1 but for gasoline fuel

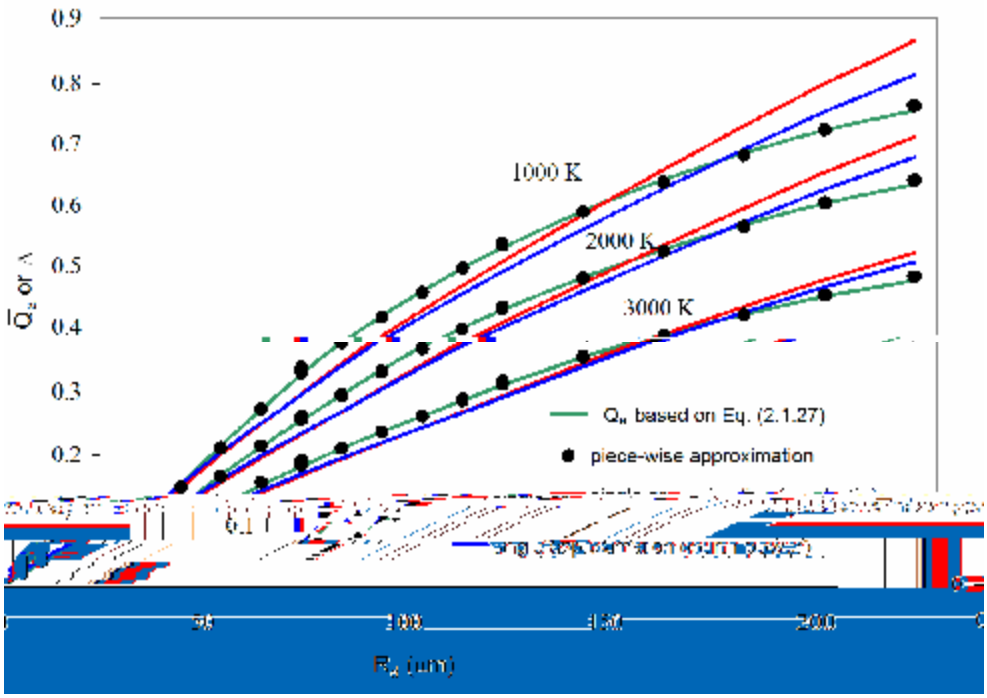

Figure 4.3.3 The same as Figure 4.3.1 but for iso-octane

PDF created with pdfFactory Pro trial version www.pdffactory.com

(2006). The droplet was irradiated homogeneously from all directions by external thermal radiation from a source at temperatures in the range from 1000 K to 3000 K.

This is a rather idealised case, as in Diesel engines the droplets are likely to be irradiated from one side only (Flynn et al., 1999) (a detailed mathematical analysis of this case is presented by Dombrovsky and Sazhin (2004)). To take into account the effect of asymmetrical irradiation of droplets, the actual power absorbed by droplets could be halved, compared with the case of homogeneous irradiation. Alternatively, this effect can be accounted for by the corresponding adjustment of the radiation temperature. The integral effect of symmetrical radiative heating of droplets by the source at temperature $)_R$ is approximately equivalent to the effect of asymmetrical droplet heating by a source at temperature $)_{R(eff)} = 2^{1/4})_R = 1.19)_R$. As pointed out in (Sazhin et al., 2005a; Abramzon and Sazhin, 2005, 2006) the effect of non-homogeneous, but spherically symmetrical, distribution of the radiative heating inside a droplet is insignificant when the radiative heating of droplets takes place simultaneously with convective heating. We anticipate that this conclusion is valid in the case of asymmetrical droplet radiative heating.

The effect of thermal radiation was taken into account using the new model based on the piecewise approximation of the coefficients a and b in Equation (2.1.28) (see Table 4.1) for T_{ext} = 1000 K, 2000 K and 3000 K, and the model based on the single quadratic approximations of these coefficients (see Table 4.3) for T_{ext} = 3000 K. The predictions of the model based on the single fourth power approximations are expected to lie between the predictions of these two models. The liquid and gas phase models used in the analysis are summarised in Chapter 2. The solutions in both these phases are fully coupled (see Chapter 3).

monotonically increases until it reaches the wet bulb temperature. When the effect of thermal radiation is taken into account, the surface temperature reaches a maximum value before it reduces to the same wet bulb temperature. This effect was discussed in detail by Abramzon and Sazhin (2006).

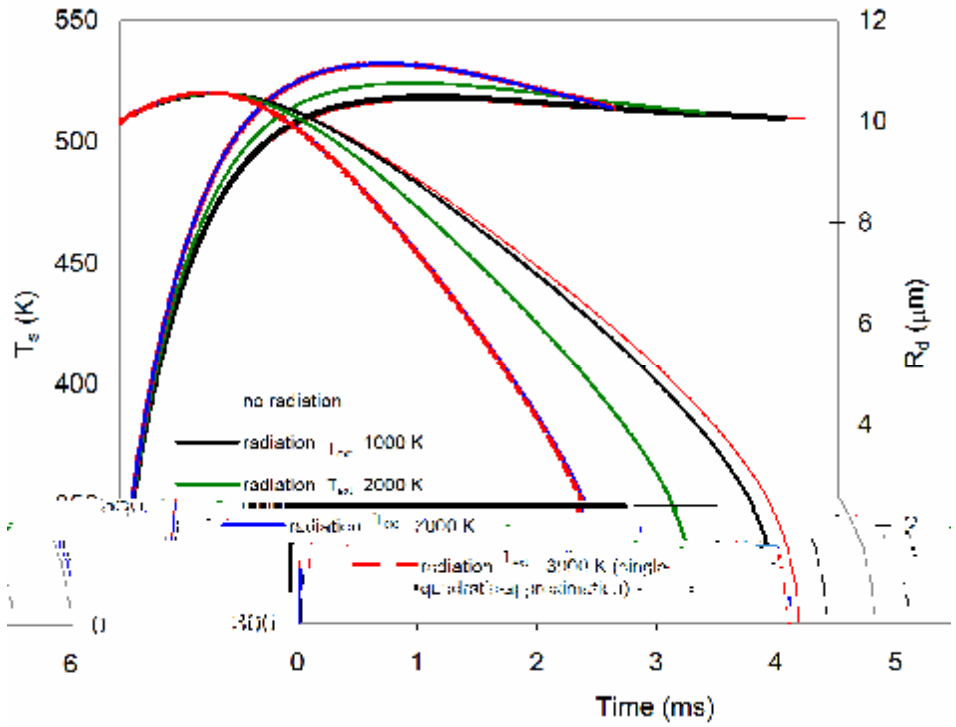

F0.13824 Tc (a) Tj-0.186 Tc (29088 TcTc (a) Tj513824 Tc (a) Tj-0.186 (a) Tj-0.186 Tc (290824 Tc (c (

The plots calculated using the model based on the piecewise approximation of the coefficients a and b in Equation (2.1.28) and the model based on the single quadratic approximations of these coefficients are nearly coincident for T_{ext} = 3000 K. These curves are expected to be even closer for lower external temperatures. This happens despite the fact that the values of the average absorption efficiency factors predicted by these models are visibly different (see Figure 4.3.1). Thus, in many practical applications, including modelling of heating and evaporation of droplets, the high accuracy of the approximation of the average absorption efficiency factor, provided by the model based on a piecewise approximation of the coefficients a and b, is not always required. However, since the computer requirements of the implementation of this new model are all but the same as those of the model based on the single quadratic approximations of these coefficients, the application of the new model is recommended in all cases.

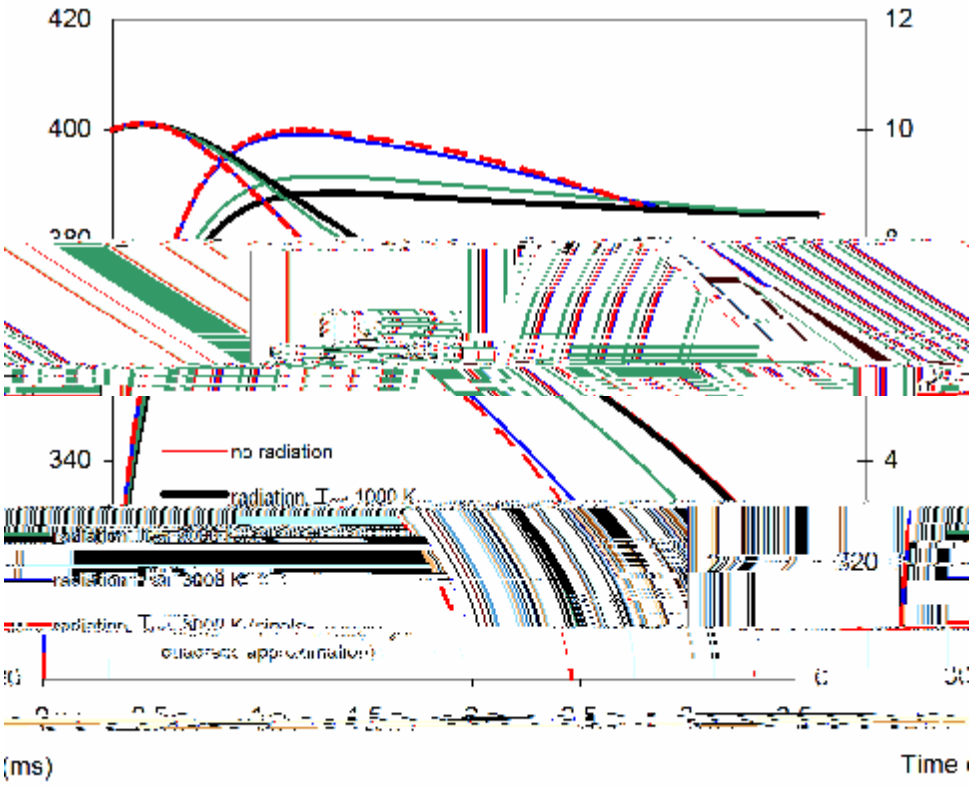

Figure 4.4.2 The same as Figure 4.4.1 but for gasoline fuel, injected into a gas volume equal to 620 mm^3

PDF created with pdfFactory Pro trial version www.pdffactory.com

Plots similar to those shown in Figure 4.4.1, but for gasoline fuel are presented in Figure 4.4.2. The physical properties of the gasoline fuel used in our study are shown in Appendix 2. In contrast to Diesel fuel, gasoline fuel is injected into a gas volume of 620 mm^3. The volume was calculated under the assumption that gasoline fuel can be approximated as $C_{7.9}H_{17.8}$. In this case, provided that all gasoline fuel is evaporated without combusting, the fuel vapour/ air mixture is expected to become close to stoichiometric, as in the case of Diesel fuel. The general shapes of the curves shown in Figures 4.4.1 and 4.4.2 are rather similar, except that the difference between the curves calculated using the model based on the piecewise approximation of the coefficients *a* and *b* in Equation (2.1.28) and the model based on the single quadratic approximations of these coefficients, is more pronounced in the case of Figure 4.4.2 than Figure 4.4.1. This justifies the application of the new model in the case of gasoline.

n d t f r p .1.1 Tc (h) TjT Tj0 Tc (n) Tj-0.10176 Tc (e) Tj-0.050

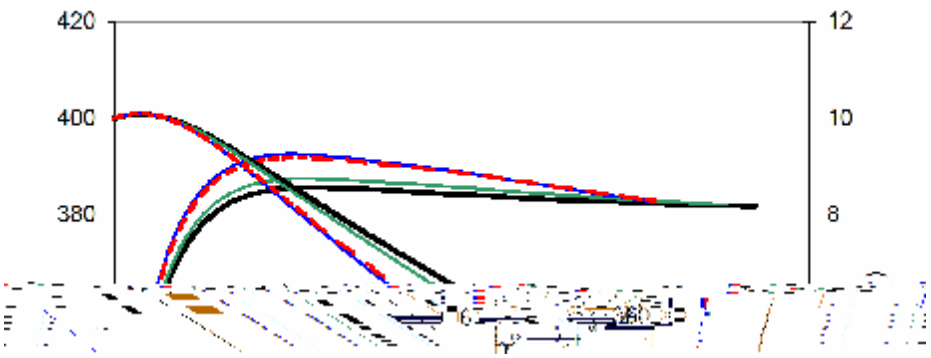

The iso-octane and 3-pentanone cases are presented in Figures 4.4.3 and 4.4.4 respectively. The physical properties of iso-octane and 3-pentanone are shown in Appendix A. These fuels were injected into gas volumes of 625 mm^3 and 712 mm^3 respectively. C t

Returning to our problem of finding an approximation for the absorption efficiency factor we can say that the relatively weak dependence of droplet heating and evaporation on the accuracy of this approximation gives us an additional argument in favour of using an approximate formula (2.1.25) instead of the detailed Mie calculations of the distribution of thermal radiative absorption inside droplets. In contrast to the model described in this chapter, the implementation of the model, based on Mie calculations, into CFD codes would be infeasible.

4.5 Conclusions to Chapter 4

The values of absorption coefficients of gasoline fuel (BP Pump Grade 95 RON ULG), 2,2,4-trimethylpentane (iso-octane) and 3-pentanone have been measured experimentally in the range of wavelengths 0.2 m – 4 mm Ultra(vio)lejhE1046T0 D-0.2T( )j

radius. Coefficients a and b are approximated by piecewise quadratic functions of the radiation temperature, with the coefficients calculated separately in the ranges of radii 2 m – 5 m, 5 m – 50 m, 50 m – 100 m and 100 m – 200 m for all fuels. This new approximation has been shown to be more accurate when compared with the case when a and b are approximated by quadratic functions or fourth power polynomials of the radiation temperature, with the coefficients calculated over the entire range 2 m – 200 m suggested by Sazhin et. al. (2004a). This difference in the approximations of a and b, howe0.429..24 Tc .Tj-0.24 Tc (h) Tj-0.10176 Tc (e) Tj0.12 Tc ( ) Tj-01.32 Tc (

5. MONODISPERSE DROPLETS HEATING AND EVAPORATION: EXPERIMENTAL STUDY AND MODELLING

So far our analysis has been focused on single isolated droplets. In practical situations, however, many droplets are present in a spray and the average distance between them can be less than a few droplet diameters. A typical droplet therefore will not behave as an isolated droplet, rather than as part of droplet arrays that take into account droplet to droplet interaction phenomena. These interaction phenomena are particularly important near the fuel injection devices, where the droplet concentration is high.

The importance of sprays in various engineering and environmental applications is well known (Sirignano, 1999). Heating, evaporation and coa

Chapter 5: Monodisperse droplets heating and evaporation: experimental stud

Chapter 5: Monodisperse droplets heating and evaporation: experimental study and modellin

thermocouple, decreased from 550°C at the injection point to about 100°C at z=60 mm (Figure 5.1.1a,b).

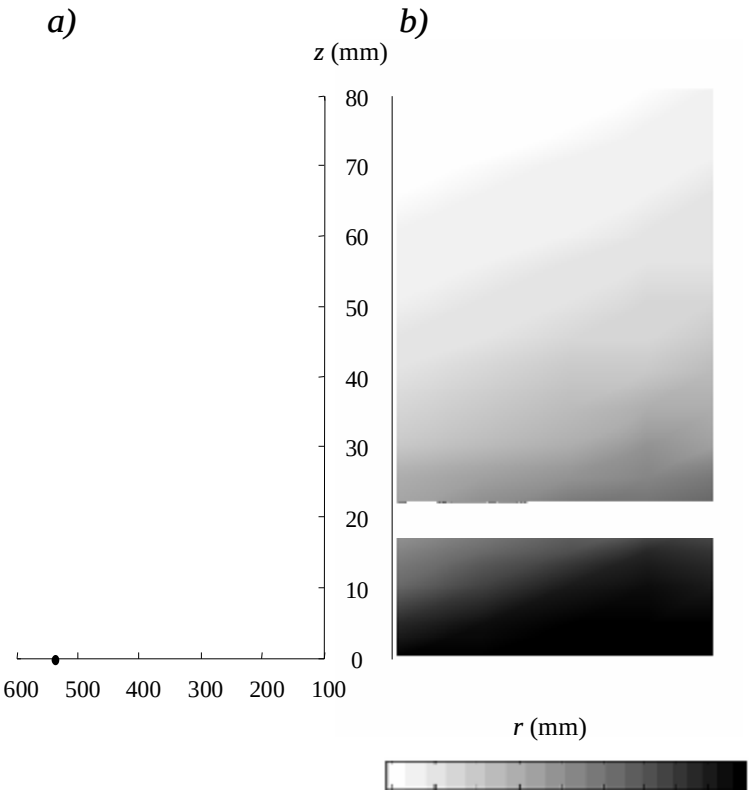

Chapter 5: Monodi

Chapter 5: Monodisperse droplets heating and evaporar

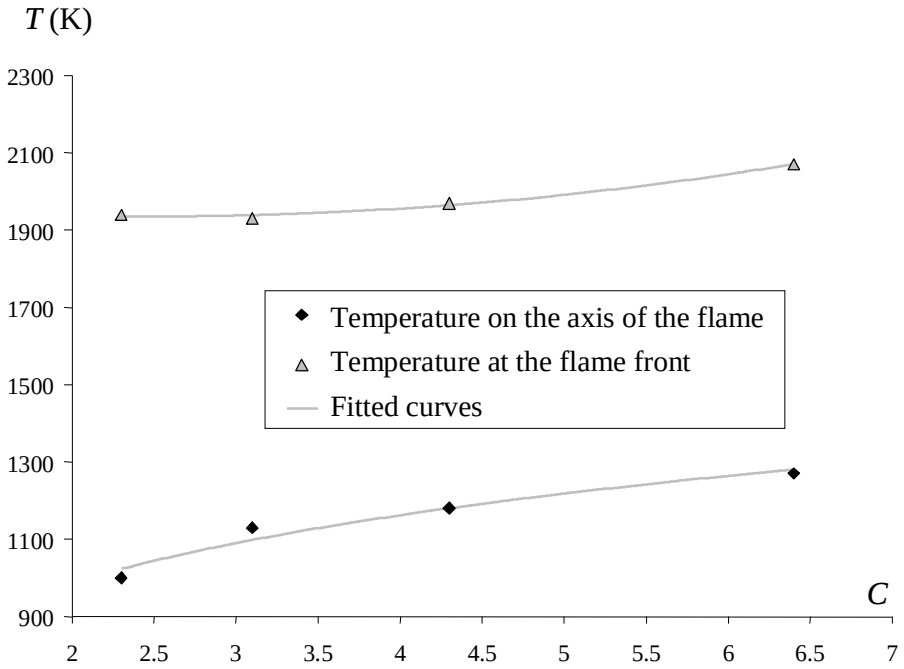

Figure 5.1.3 Temperature in the flame as a function of the distance parameter

5.1.3 Velocity and size measurements

Phase Doppler Anemometry (PDA) in the refraction mode was used to measure droplet velocities and diameters at various distances from the injector. The main problem with the size measurements arises from the trajectory ambiguity. When the droplet size is of the order or larger than the laser beam, the Doppler signal may be altered by unwanted scattering modes which may lead to an error of measurements. The risk of error is very high in the case of linear monodispersed droplet streams since the trajectory of the droplets is very stable and the droplets are rather large compared to the width of the laser beam in the probe volume. To reduce as much as possible the trajectory effects, the position of the stream axis in the probe volume can be adjusted so that the contribution of the refractive mode is strengthened compared to the reflection mode in the direction of the receiving optics. A calibration of the PDA is required to achieve accurate size measurements. Both the positioning of the droplet streams and the calibration process were performed as described by Castanet et al. (2005). The discrepancy is about 1µm for droplet diameters around 100µm. The droplet velocity is measured concomitantly by processing the Doppler frequency of the bursts at ± 1%. Size measurements are

PDF created with pdfFactory Pro trial version www.pdffactory.com

performed only for combusting droplets, since the size reduction of droplets evaporating within the hot air plume is too small to be captured with a sufficient accuracy by this technique.

5.1.4 Two-colour laser induced fluorescence ther/Tj-0.03168 Tcla

Ithmedhm(m) Tj 0.04684 Tc ((i)) Tj 0.500.12 Tc (n) Tj 0.0348.3 Tc (,) Tj -0.2362462 Tc (i) Tj 0.2316244 Tc (f) Tj4.38 T

since only the droplet velocity is measured. Regarding the collection optics, in the focus plane of the collection front lens, the image of the core of the optical fibre extends roughly over 200 µm (this image is however slightly reduced in the presence of a droplet within the probe due to the refraction processes at the air-liquid interface).

Regions located near the droplet surface may have a rather limited contribution to the fluorescence signal depending on the optical arrangement, the size and the trajectory of the droplets. This comes essentially from the Gaussian distribution of the energy in the laser beams and the refraction at the droplet surface as explained in Maqua et al. (2006). This effect can safely be ignored in the case of droplets significantly smaller than the probe volume. Regarding the probe volume size in the case of the purely evaporating droplets, this implies that the measured temperature is more likely to be close to the temperature at the droplet centre instead of the volume averaged temperature when the droplet diameter becomes larger than 150µm.

Note that the droplet detection is based on the initial determination of the - 0hresholds for each spectral band (Lavieille et al., 2001). Each Threi84 Tc (i)cTjan a (

radiative properties. It was shown that the predicted temperatures and pressures in the presence and absence of thermal radiation differ by not more than about 2% in most case, even if the radiation temperature was assumed to be equal to the maximal temperature in the flame (this is true only when gas is totally transparent to thermal radiation). Since this error can be tolerated in our analysis, we believe that the effect of thermal radiation can be ignored as the first step in the modelling of the process.

This model has been further developed to capture the effect of finite distance parameter. In the case of droplet streams, Castanet et al. (2002) suggested the following correction to take into account the finite distance parameter C (ratio of the distance between droplets and their diameters)

$$\frac{Nu}{Nu_{iso}} = \frac{Sh}{Sh_{iso}} = h(C), \tag{5.2.1}$$

where

$h(C) = \tanh(0.36C - 0.82)$ and $C > 3$.

Hence the Nusselt number and Sherwood number can be written as:

$$Sh = 2h(C)\frac{\ln(1+B_M)}{B_M}\left[1 + \frac{(1+Sc_d\,Re_d)^{1/3} f(Re) - 1}{2F(B_M)}\right] \tag{5.2.2}$$

$$Nu = 2h(C)\frac{\ln(1+B_T)}{B_T}\left[1 + \frac{(1+Pr_d\,Re_d)^{1/3} f(Re) - 1}{2F(B_T)}\right]. \tag{5.2.3}$$

To evaluate the Reynolds number Re_d in calculation of Sherwood number and Nusselt number, the droplet velocity relative tv / a o / y 0.22416 Tc (t) Tj

Chapter 5: Monodisperse droplets heating and evaporation: experimental study and modellin

observed time dependence of droplet relative velocities has been approximated by Equation (5.3.3).

$$v_d(m/s) = 0.00294t^2 - 0.1383t + 9.154 \quad (5.3.3)$$

$$T(^oC) = 0.0264t^4 - 1.2121t^3 + 21.113t^2 - 167.75t + 630.86 \quad (5.3.4)$$

The Nusselt and Sherwood numbers were calculated similarly to the first experiment. The plots referring to the second experiment are shown in Figure 5.3.2. As in the case of Figure 5.3.1, temperatures at the surface and centre of the droplets, and droplet average temperatures differ considerably from one another, especially at the initial stage of droplet heating and evaporation.

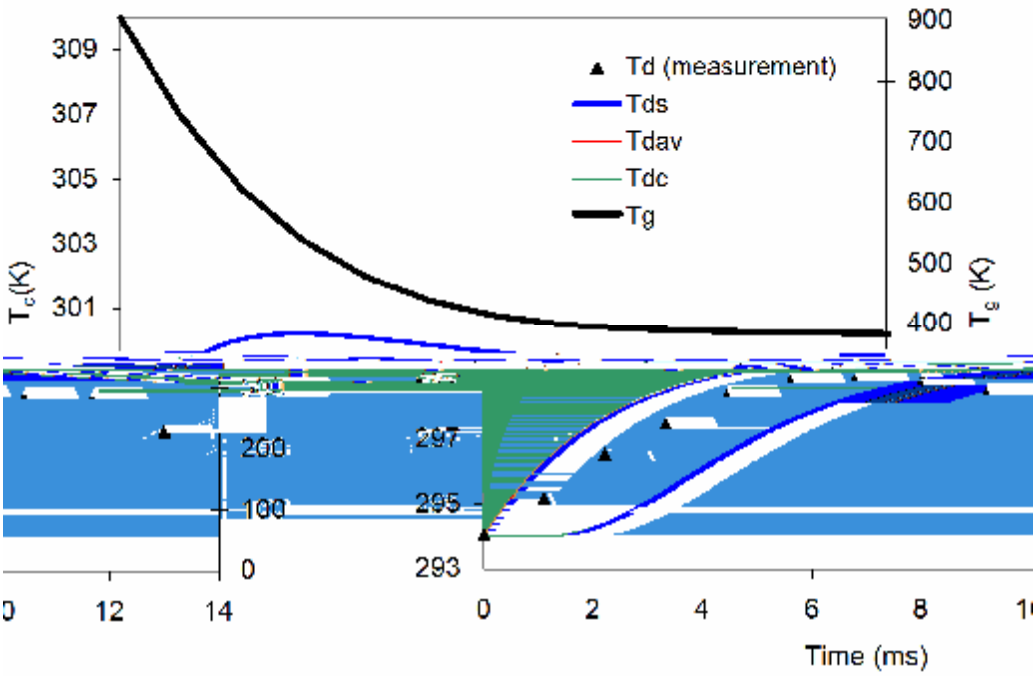

Figure 5.3.2 Plot of ethanol droplet temperature T_d, measured experimentally (solid triangles) and predicted by the model (T_{ds} droplet temperatures at the surface of the droplet, T_{dav} average droplet temperature, and T_{dc} droplet temperature at the centre of the droplet) and gas temperature T_g for the initial conditions R_{do}= 118.65 μm, T_{do}=294 K, C=3.97

PDF created with pdfFactory Pro

The best agreement with experimental data in the case shown in Figure 5.3.2 is observed not for droplet average temperature but for the temperature between the average temperature and the temperature at the centre of the droplet. This can be related to the fact that the measurement volume in this case is noticeably less than the droplet volume. As in the case shown in Figure 5.3.1, the maximum droplet temperature, observed experimentally and predicted by the model is related to a decrease in gas temperature. This maximum for the second experiment is observed at later times (about 6 ms).

In the third experiment, acetone droplets with initial radii 63.2 m, initial temperature 300 K and the initial distance parameter C=7.56 were considered. The approximations of the observed time dependence of the droplet relative velocities and ambient gas temperature are given by asj0.0837satar1-0c (s)r Tc (j0dT (s)r T1x1.j0.08376 Tc (r

Chapter 5: MonodiC

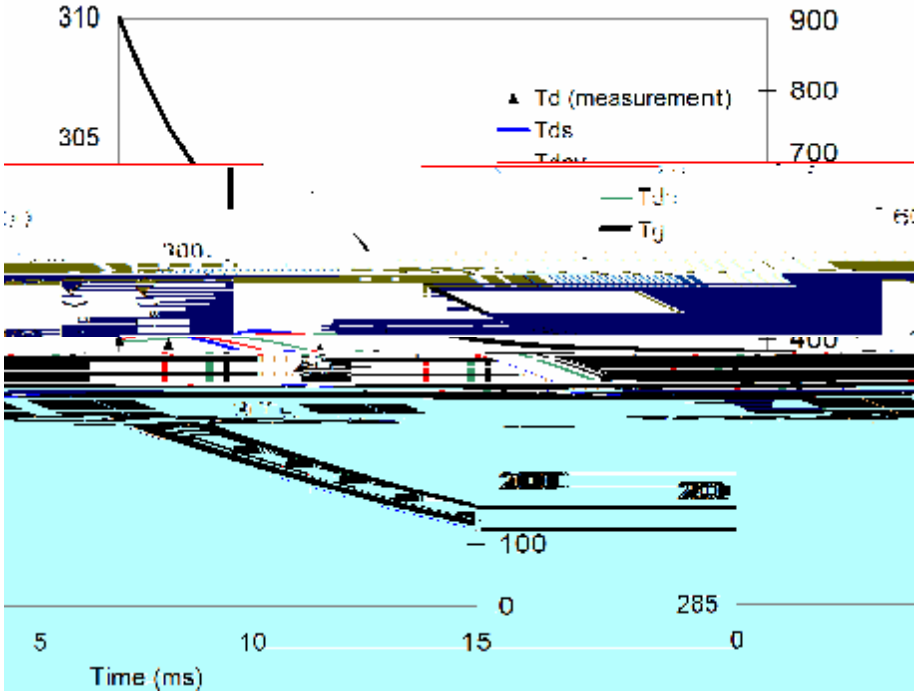

Figure 5.3.4 Plot of acetf

ambient temperature is assumed to be constant and its value is obtained from Figure 5.1.3 for the given initial distance parameter *C*. As in the cases considered in Section 5.3.1, droplet velocities were not calculated, but measured.

In the first experiment, ethanol droplets with initial radii 52.25 m, initial temperatures 309 K and the initial distance parameter *C*= 3.4 were considered. The average gas temperature at the location of the droplets was 1140 K. and the droplet velocity evolves as described by:

$$v_d(m/s) = -0.0021t^3 + 0.0332t^2 - 0.3221t + 6.9956 \qquad (5.3.9)$$

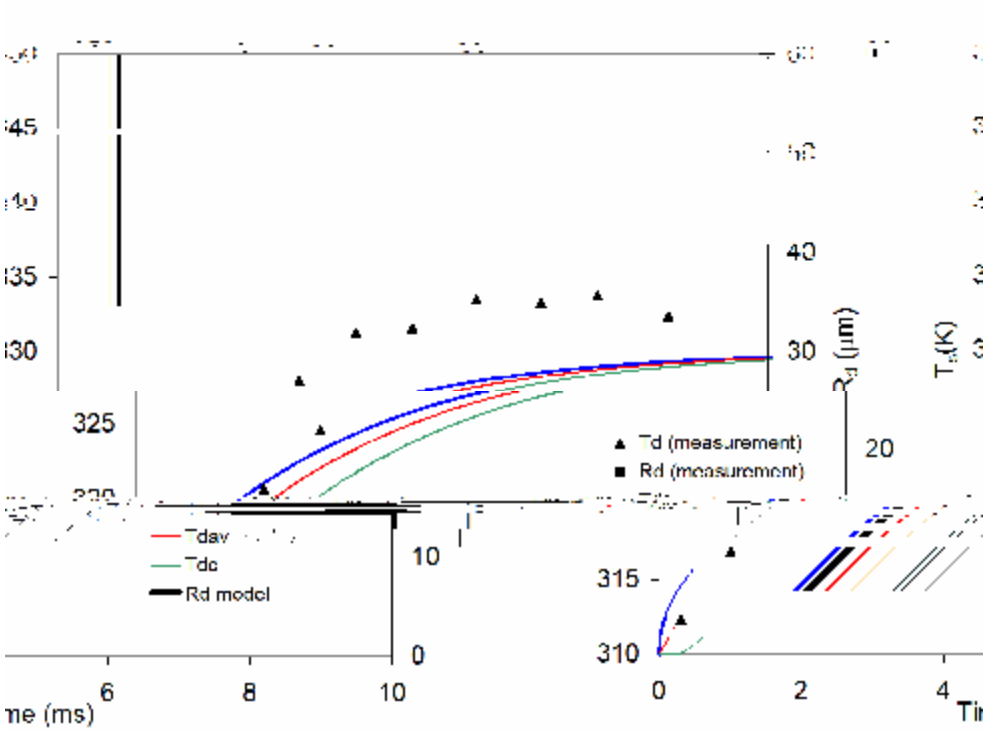

Figure 5.3.5 Plot of ethanol droplet temperature T_d radius R_d, measured experimentally (solid triangles and squares) and predicted by the model (T_{ds} droplet temperatures at the surface of the droplet, T_{dav} average droplet temperature, and T_{dc} droplet temperature at the centre of the droplet) and droplet radii R_d for gas average d T_{dc} d(Tj180Tj0.2 Tc () Tj-0.3.98

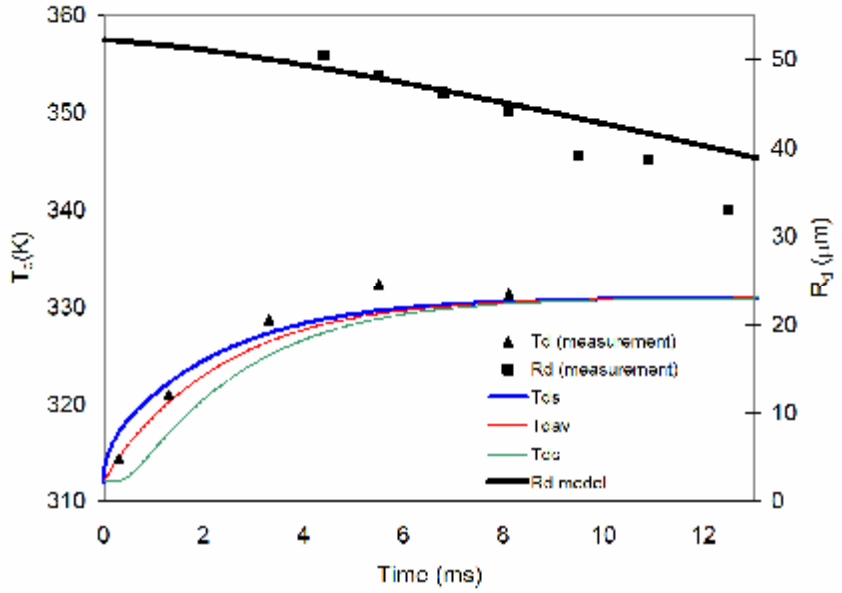

Figure 5.3.7 The same as Figure 5.3.5 but for gas average temperature T_g equal to 1270 K and for the initial conditions R_{do}= 52.25 μm, T_{do}=309 K, C=10.5

In the fourth experiments, ethanol droplets with the initial radii 55.2 μm and n

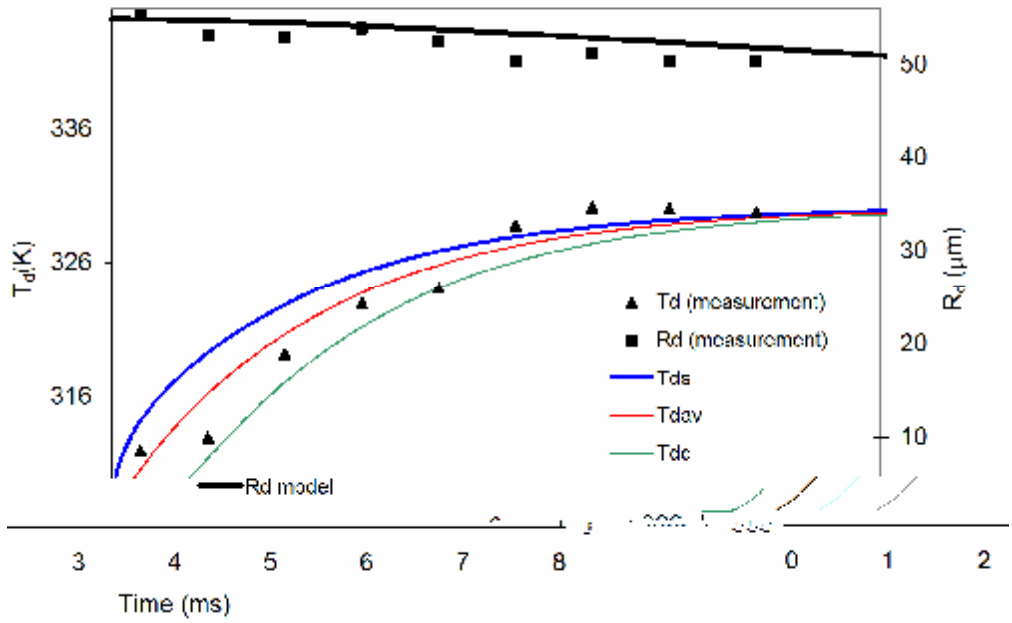

Figure 5.3.8 The same as Figure 5.3.5 but for gas average temperature T_g equal to 1150 K and for the initial conditions R_{do}= 55.2 μm, T_{do}=312 K, C=4.4

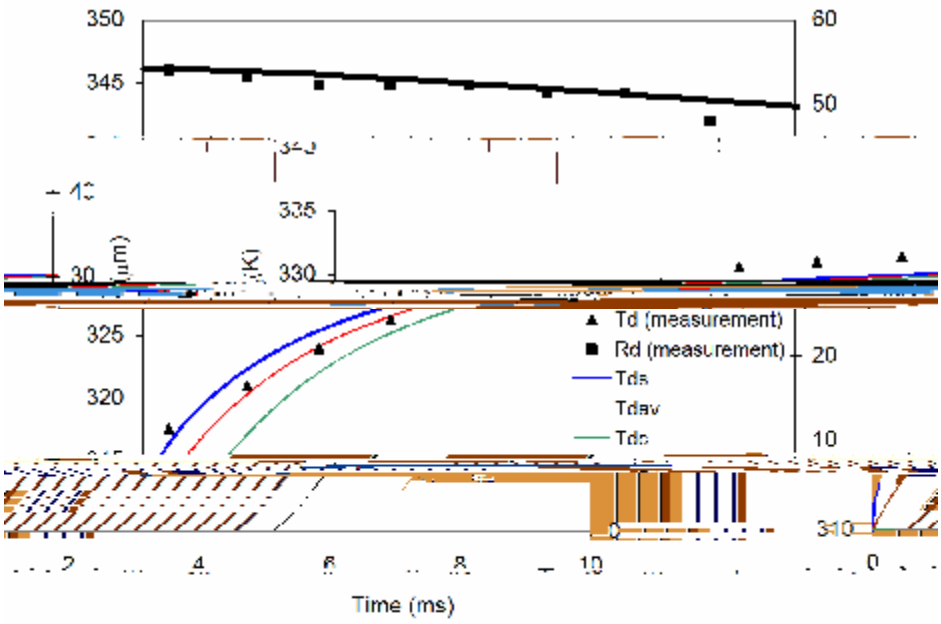

Figure 5.3.9 The same as Figure 5.3.5 but for gas average temperature T_g equal to 1150 K and for the initial conditions R_{do} = 54.0 μm, T_{do} =318 K, C=4

PDF created with pdfFactory Pro trial version www.pdffactory.com

5.4 Conclusions to Chapter 5

Heating and evaporation of monodisperse ethanol and acetone droplets has been studied in two regimes: pure heating and evaporation of droplets in a flow of air of prescribed temperature, and droplet heating and evaporation in flame produced by previously injected combusting droplets. Two colour laser induced fluorescence thermometry has been used for the estimate of droplet temperatures, while their sizes and velocities have been characterized by Phase Doppler Anemometry. In the flames, CARS technique has made it possible to estimate the gas temperature. The experiments have been performed for various distances between droplets and various initial droplet radii and velocities. The experimental data have been compared with the results of modelling, based on given gas temperatures, and Nusselt and Sherwood numbers calculated using measured values of droplet relative velocities. When estimating the latter numbers the finite distance between droplets was taken into account. The model has been based on the assumption that droplets are spherically symmetric with a radial distribution of temperature inside droplets is taken into account. This model considers the recirculation inside droplets via the introduction ohs erodeseTj0.12 T
rso

e e (e) Tj-0.12 Tc - Tc (s) Tj Tc (eTj0.12 Tc (o49584 Tc (i) Tj0.36 Tc (o) Tj0.22416 Tc 1.2-0.20832 Tc (0.224
l(i) Tj0.36 Tc (oj Tj0.22416 Tc (t)j8376 Ty (r) Tjj0.22416 Tc (t) Tj0.08306792 Tc) Tj0.36 Tc (d) Tjj-0.49y6 Tc Tj0.0
1.4-0.25584-0.22416 Tc (t) Tj0.36 Tc (h) Tj-0.17208 Tc (s) Tj-0.25 Tc (i) Tj0.36 Tc (

6. THE IMPLEMENTATION OF THE NEW MODELS INTO THE KIVA-2 CFD CODE

The effects of temperature gradient inside droplets, described by the ETC liquid phase model based on the analytical solution of the heat conduction Equation (2.1.5), on the heating, evaporation and ignition of Diesel fuel droplets were discussed in Chapter 3. This analysis was based on the zero dimensional code that takes into account the coupling between liquid and gas phases, droplet breakup and uses the Shell autoignition model. In this code all values of gas parameters (velocity, temperature, fuel vapour concentration) were assumed to be homogeneous.

This chapter is focused on the implementation of the ETC model and the

Tj-0.25584 Tc (i)gnitma ETtton168 Tc (a) Tj-04.78 Tc ( ) Tj0.22Tc (m) Tj0.12 Tj0.36 Tc (o) Tj2 T56 Tc (
Tj-0.2.08376 Tc (C) Tj0.78 Tc ( ) Tj-0.03168 Tc (e) Tj0.3 Tc K (e) Tj0.08376 TI Tj-0.2558V Tc (e) Tj0.3

cylinder Ricardo Proteus test engine which was converted to two-stroke cycle. The engine had a bore of 135 mm, a stroke of 150 mm and a displacement of 2.2 litres. The Proteus rig was coupled to a DC dynamometer via reduction belts (6:1). An optical chamber 80 mm in length and 50 mm in diameter was fitted on the cylinder head to investigate the spray development. This allowed a fuel spray to be injected vertically without any impingement on the walls or the windows. A second generation Bosch common rail fuel injection system was used to generate the high pressure required to maintain injection pressure ranging from 60 to 160 MPa. The fuel pump was driven externally via an electrical motor running at 1400 rpm to maintain the required high pressure in the fuel rail with minimum fluctuation (Crua, 2002).

The main parameters which were studied using this setup were spray penetration and autoignition delay. To investigate the spray visualisation a Kodak

Ek apparatus HS 1000 Tc (A93 Tc ( ) Tj 0.1416 Tc 27168 Tc (a) Tj0 T0.20832 Tc (e) Tjj-0.49584 T .25584 T

The test cases chosen for the analysis were based on the measurements of sprays under r

6.2 Spray models in the KIVA-2 CFD code

6.2.1 Droplet breakup models

6.2.1.1 TAB model

The Taylor Analogy Breakup (TAB) model is based on the analogy between an oscillating and distorting droplet and a spring mass system (O'Rourke and Amsden, 1987). In this model the droplet motion is governed by a linier differential equation for a forced, damped harmonic oscillator. The ext

the experimental data. O'Rourke and Amsden (1987) suggested that the values of C_F, C_k and C_d are 1/3, 8 and 5 respectively.

6.2.1.2 Conventional WAVE model

The model is based on the first-order theory of stability analysis (Kelvin-Helmholtz instability) of a stationary, round liquid jet immersed into a quiescent and incompressible gas (Reitz, 1987). The theory considers a cylindrical liquid jet issuing from a circular orifice of radius a into a stationary, incompressible infinitely large gas medium. The atomisation is the result of aerodynamic interaction between the liquid and gas that induces unstable wave growth on the liquid jet surface.

The model determines how and when droplets breakup by calculating the wavelength of the fastest growing disturbances on the surface of a liquid jet due to aerodynamic instabilities. The model assumes that aerodynamic forces at a liquid-gas interface and the resulting surface waves are responsible for atomisation. The rate of change of the droplet radius and the resulting child droplet size are related to the frequency (Ω) and wavelength (Λ) of the fastest growing surface wave, determined by the following expressions:

$$\Lambda = \frac{9.02 R_{\mathrm{d}} \left(1 + 0.45\sqrt{Z}\right)\left(1 + 0.4T^{0.7}\right)}{\left(1 + 0.865 We^{1.67}\right)^{0.6}} \tag{6.2.7}$$

$$\Omega = \frac{0.34 + 0.385 We^{1.5}}{\left(1+Z\right)\left(1+1.4T^{0.6}\right)}\sqrt{\frac{s}{r_1 R_{\mathrm{d}}^3}} \tag{6.2.8}$$

where We is Weber number for gas. The Ohnesorge number Z is defined as .12 Tc (g) Tj-0.2083

ra umb0.06 T6.24 0 TD 2.1- Tj05.2 TD (3168 0.-0.36 Tl m145.2 264.72 l1D (+.-0.36 0.2 264.487208 T80Tj/F) Tj0.3
(e) Ti2.22 Tc ( ) Ti0.25584Ti0.36 Tc (d) Ti2.2.16 Tc ( ) Ti-0.12 Tc (n) Ti0.12 Tc (n) Ti.3584 Tc (mb) Ti0.012 7 Tc (e

$$\begin{cases} \\ \quad (\quad | \quad | \quad) \\ \quad (\quad) \end{cases}$$

$$o\Delta \qquad - \qquad 2\varepsilon\nu TT$$

6.2.1.3 Modified WAVE model

A modified WAVE breakup model was suggested by Martynov et al. (2007). This model takes into account the e s 8Tj01.74 Tc ( ) Tjfc (() TTj (i) Tj0. T() TTj (i) Tj0. Tc (

wa

monte

mb3 b

mof

model 0), $Pr = \frac{m_{\text{air}}(T_{ref})c_{\text{air}}(T_{ref})}{k_{\text{air}}(T_{ref})}$, $k_{\text{air}}(T_{ref}) = \frac{K_1 T_{ref}^{3/2}}{T_{ref} + K_2}$, $m_{\text{air}} = \frac{A_1 T_{ref}^{3/2}}{T_{ref} + A_2}$,

K_1=252 g cm/(s^{3}K$^{3/2}$), K_2=200 K, A_1 =1.457E-5 g/(s.cm K$^{1/2}$), $A_2$3/20 K,

experimental data (see Chapter 3). This model is based on Equations (2.2.50) and (2.2.51) and is called Model 4 in our analysis. It will be used in calculations based on the KIVA-2 code.

6.2.3 Ignition model

The ignition process in the conventional KIVA-2 code is described in terms of the chemical reactions in a system which are generally symbolised as (Amsden et al.,1989):

$$\sum_m a_{mr} X_m \quad \rightleftharpoons \quad \sum_m b_{mr} X_m \,, \tag{6.2.19}$$

where X_m represents one mole of species m and a_{mr} and b_{mr} are integral stoichiometric coefficients for reaction r. The stoichiometric coefficients must satisfy the following equation:

$$\sum_m (a_{mr} - b_{mr}) W_m = 0 \,, \tag{6.2.20}$$

so that mass is conserved in the chemical reaction. Chemical reactions are divided into two classes: those that proceed kinetically and those that are assumed to be in equilibrium.

In the KIVA-2 CFD code the kinetic reaction is presented in CHEM subroutine. Kinetic reaction r proceeds at a rate $\dot{w}_r$ given by Amsden et al. (1989):

$$\dot{w}_r = k_{fr} \prod_m (r_m / W_m) a'_{mr} - k_{br} \prod_m (r_m / W_m) b'_{mr} \tag{6.2.21}$$

Here, the reaction orders a'_{mr} and b'_{mr} need not to be to equal to a_{mr} and b_{mr}, so that empirical reaction orders can be used. The coefficients k_{fr} and k_{br} are assumed to be of a generalised Arrhenius form (Amsden et al., 1989):

$k \quad A\ T\ \ exp(\ \ E_{\text{a}} / T)$

9ee9ee99. Te (:) Tj ET 2h

6.3 Numerical simulation

In this section a brief description of the implementation of various liquid and gas phase models of droplet heating and evaporation into the customised version of the KIVA-2 CFD code is presented. The ETC and ITC liquid models based on the analytical solution and gas Models 0 and 4, described in Chapter 2, were implemented in the KIVA-2 CFD code via the EVAP subroutine. These replaced the Spalding model in the original KIVA-2. The effects of various breakup models were investigated using the TAB model, the conventional and modified WAVE models. These models were implemented in the BREAK subroutine. To investigate the effect of the ETC model on the autoignition delay time, the customised version of the Shell autoignition model was implemented in the CHEM subroutine to replatinraiaaHai

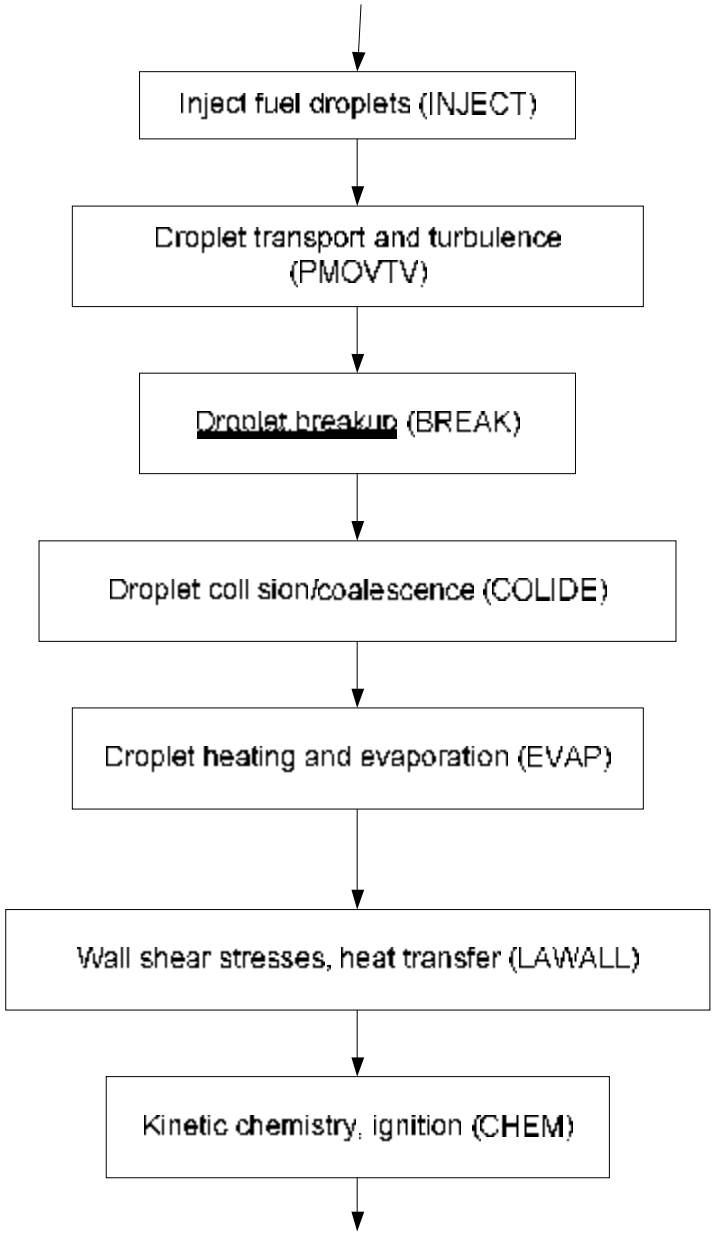

Figure 6.3.1 Block diagram for the subroutines related to droplets in the KIVA-2 code

PDF created with pdfFactory Pro trial version www.pdffactory.com

C

Chapter 6: The implementation of the ne

Chapter 6: The implementation of the new models into the

At a later stage of injection the cluster shedding from the tip of the spray was observed experimentally. This led to the fluctuation of the tip penetration length around 4 cm (see Figure 6.4.2). This fl

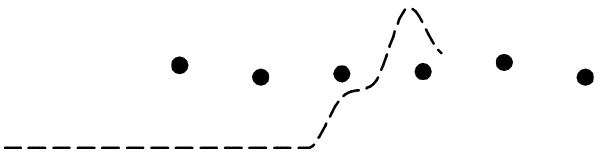

mentaldataTABWAVE(conventional)WAVE(modified)odii

Chapter 6: The impap

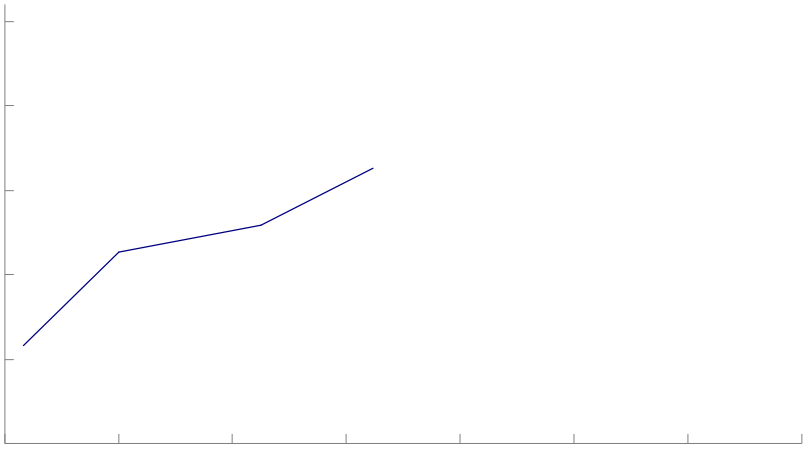

Chapter 6: The implementation o

observed for injection pressure 100 MPa. However, we could not compare the results for this injection pressure with the prediction of the model mtmt

by the choice of breakup model are less than about 2.5%, which is within the accuracy of the experimental data. Strong injection accelerations during the first 0.2 ms after the injection, which affect the spray breakup at the initial stage of injection (during about 1 ms), have little effect on spray properties at the time of autoignition (about 2 ms after injection). This explains the relatively small difference between the ignition delays calculated using conventional and modified WAVE breakup models. The fact that the TAB breakup model predicts slightly shorter ignition delays than the WAVE models can be explained by the fact that the TAB model predicts the generation of larger amount of smaller droplets which evaporate faster (see Figure 6.4.3).

As follows from Figure 6.4.4, an uncertainty of estimation of the initial gas temperature in the combustion chamber is about β

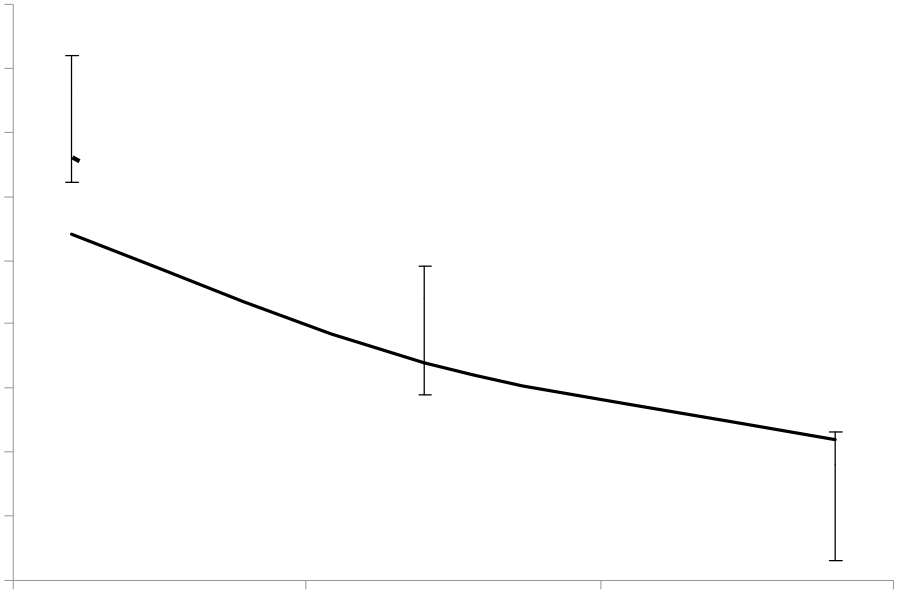

Chapter 6: The implementation of the new models into the KIVA-2 C

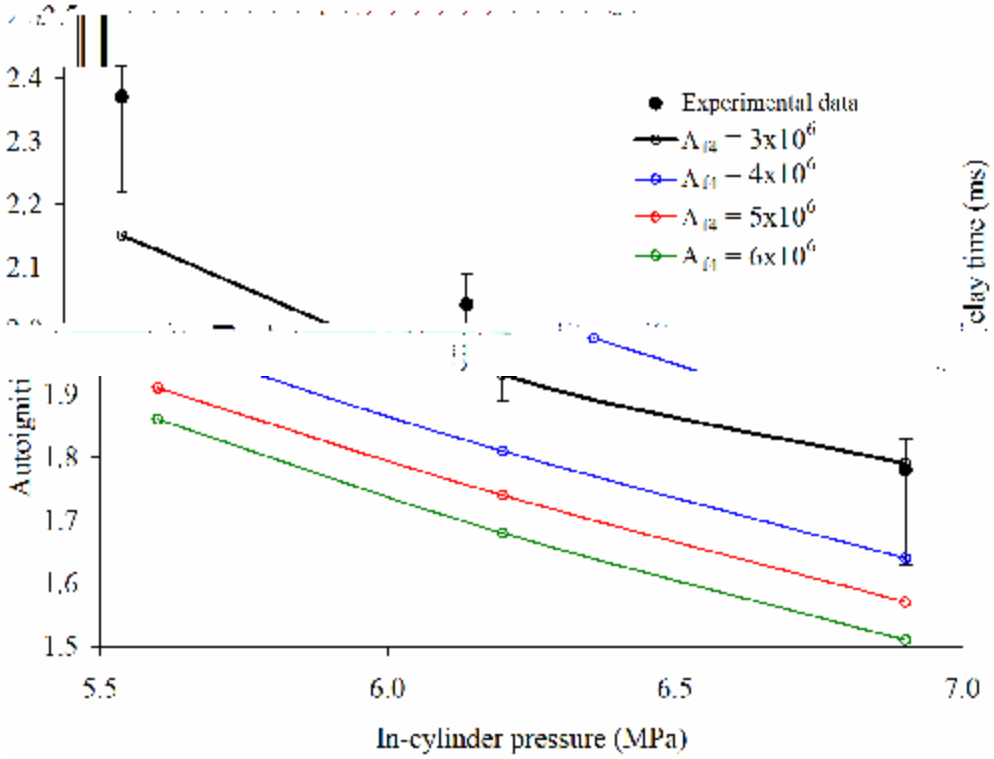

Figure 6.4.9 The same as Figure 6.4.8 for the injected fuel temperature 375 K, but the computations were based on four values of the coefficient A_{f4} in the Shell model, as indicated in the figure

Finally the grid sensitivity of the result shown in Figures 6.4.5 – 6.4.9 was investigated. The results are shown in Figure 6.4.10. The same models as in Figures 6.4.5 - 6.4.9 were used with injection temperature equal to 375 and A_{f4}7n7

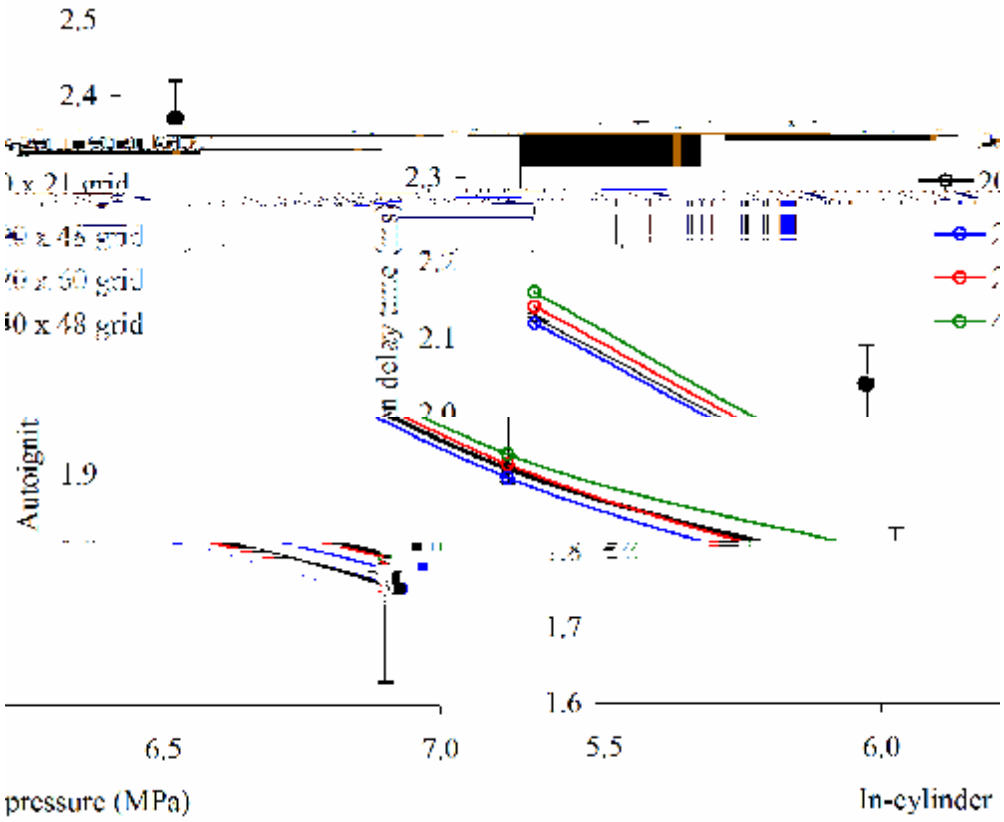

Figure 6.4.10 The same as Figure 6.4.9 for A_{f4} = 3x10^6, but the computations were based on four grid arrangements as indicated in the figure

6.4.2.2 Pre-ignition spray characteristics

In this subsection a number of spray characteristics, mainly at the pre-ignition stage are discussed. No direct experimental verification of the results will be available in most cases, but these results are expected to allow us to get better understanding of the processes which cannot be directly observed at the moment.

Figure 6.4.11 shows the time dependence of the maximum Sauter Mean Radius (SMR) of droplets and maximal in-cylinder pressure predicted by the KIVA-2 CFD code with the modified WAVE model, the ETC liquid phase model and the gas phase Model 4. The injection pressure was taken to 160 MPa, the initial gas pressure was equal to 6.2 MPa, and the injection temperature was taken to be equal to 375 K. The same grid as in Section 6.4.2.1 was used. As follows from Figure 6.4.11, the SMR of droplets rapidly reduces to about 10 μm, due to the breakup processes, which are of the same order of magnitude as observed

PDF created with pdfFactory Pro trial version www.pdffactory.com

experimentally. The initial peak of the maximal in-cylinder pressure is related to compression of air during the injection process.

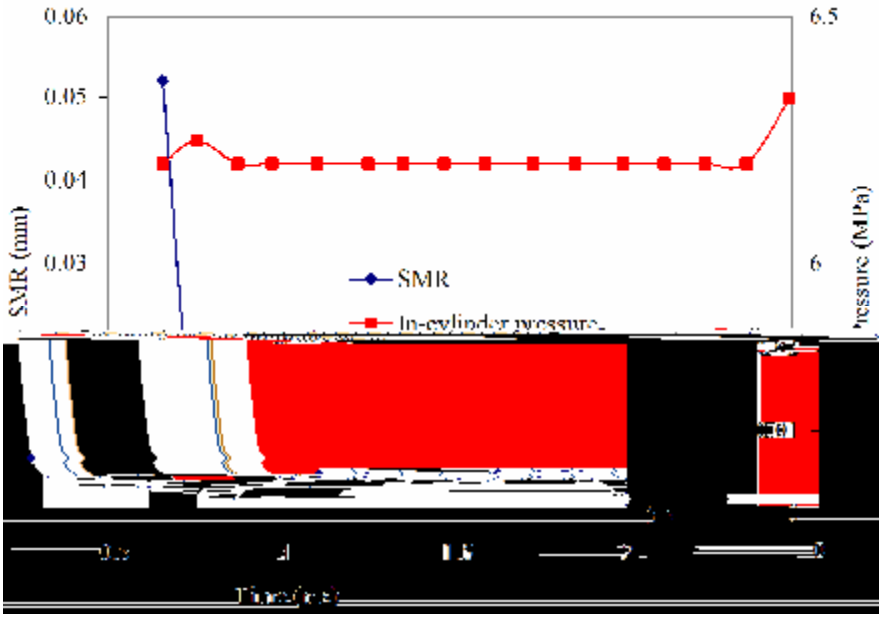

Figure 6.4.11 The time evolution of the maximal Sauter Mean Radii (SMR) of droplets and in-cylinder gas

r re in th costion c

fo

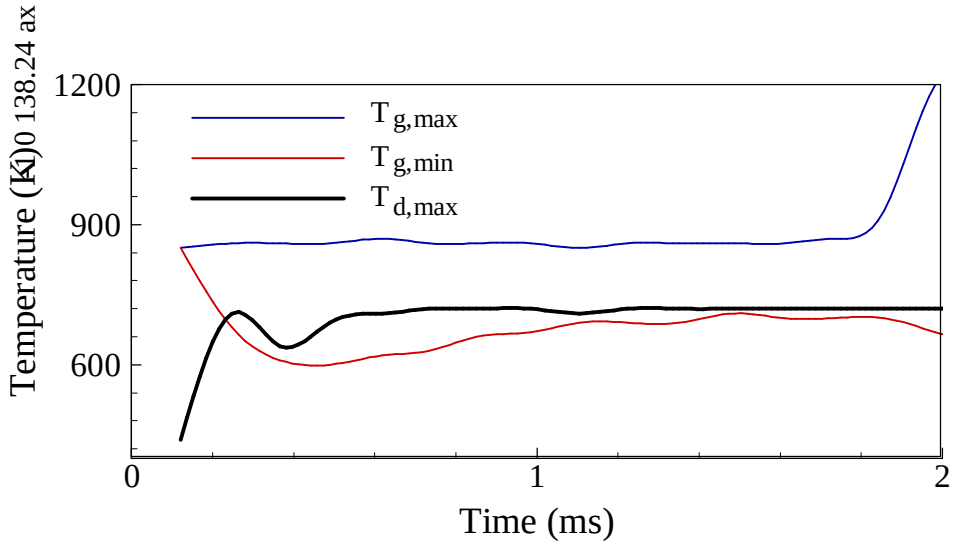
Temperature (K)0 138.24 ax
1200
900
600
0
1
2
Time (ms)
T g,max
T g,min
T d,max

FigurF

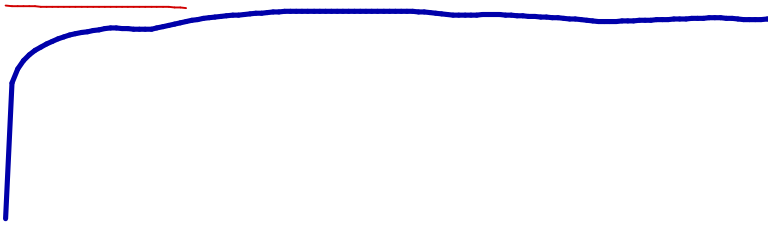

Time(ms)

follows from Figure 6.4.15b, for *t* between 0.98 ms and 1.73 ms, the fuel
our mass fraction gradually increases and this vapour spreads from the
inity of the spray to the ambient gas, while the maximal fuel vapour mass
tion remains practically unchanged (see Figure 6.4.13). At *t* =1.98 ms a
ble decrease in fuel vapour mass fraction can be seen at spray periphery where
autoignition took place. The decrease in oxygen mass fraction at the same
e and location can be clearly seen in Figure 6.4.15b. Visible increase in the
ss fractions of the branching agent, radicals and intermediate agent at *t* =1.98
near the

od

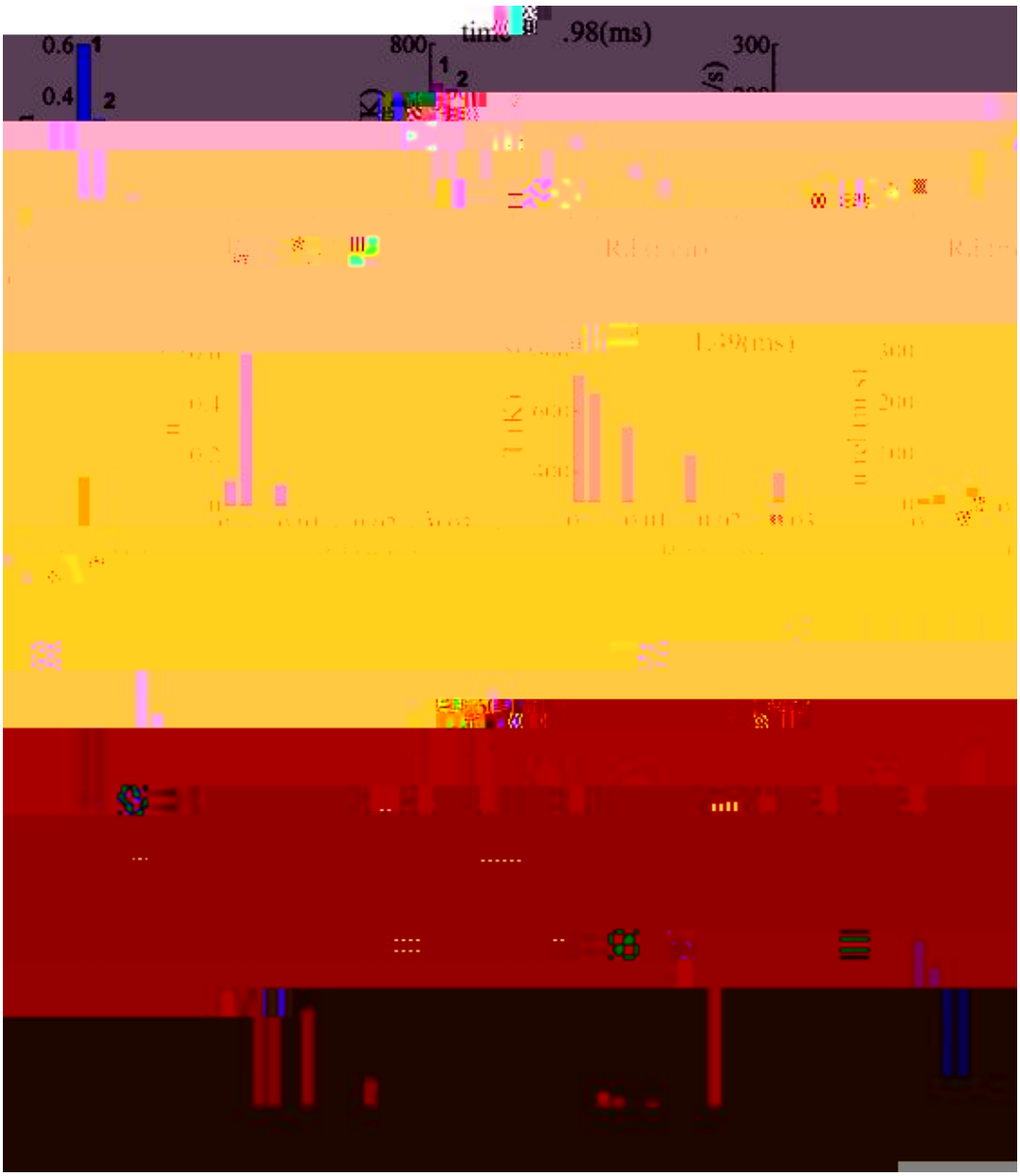

Figure 6.4.16 Relative number density, temperature and relative speeds of droplets at four moments of time (the same as in Figures 6.4.14 and 6.4.15) and various radii bands. The same values of the initial parameters and models as in Figures 6.4.14-6.4.15 were used.

PDF created with pdfFactory Pro trial version www.pdffactory.com

Chapt

of the gas phase model has only a minor effect on the predicted autoignition delay, which can be safely ignored in practical engineering computations. The autoignition delays predicted by the infinite thermal conductivity (ITC) and effective thermal conductivity (ETC) liquid phase models have also been compared. The ITC model is a default one used in the conventional KIVA-2 code. The ETC model is the new model implemented into this code. The implementation of the latter model was based on the analytical solution of the heat conduction equation in a spherical droplet applied at each time step. It has been pointed out that the difference in the autoignition delay times predicted by the ITC and ETC models is noticeable and needs to be taken into account in practical computations. The application of the ETC model is recommended as a more physical one.

It has been pointed out that the predicted decrease in the autoignition delay with increasing in-cylinder gas pressure, ranging betweebutdddc Tj0.27168 Tc (c) T60 Tj3Tc.5 T

c ducal asec ithyrr d thee

(d) Tajje22 Tc ( ) Tj0.22416 Tc (e) Tj-0376 Tc (r) Tj0.07812 Tc (d) Tj2.22 Tc ( ) Tj0.03168 Tc xptr

uceedt

utbe .32.22 Tc ( ) Tj0.03j76 Tc (r) Tje-0j01.5 Tc j0.12 7812 Tc (d) Tj2.22 Tc (

du adut

ithyondecbe

d

decote tr

u endu euteaTj-0.c (e) Tj-0-.2dc Tj.12 Tc (d) Tj0.27708 Tc (a) Tj-0.0368 Tc (e) Tj (t) Tj (i) T0.3796

ndecerhyet e c u

ru ecde c brecde

c gTj-0.20Tc (u) Tj0.224sTc708 Tc (a) Tj-0.05412 Tc (d) T-5584 Tc (i) Tj0j1.02 Tc ( )

0368 Tc (ec) Tj0.08376 Tc (r) Tj-0.25412 Tc (d) Tj168 Tc (ec(j0.12 9584 Tc (i) Tj0j1.02 Tc ( ) Tj-0sTc336 Tc (o)l Tj0j1.02 Tc ( )) Tj0.

e ed Tj-022116 Tc u Tj0.Tc (u) Tj03y168 Tc (i) T0.3168 Tc (a) Tj-0.2 (t) Tjg Tj0

Chapter 7: Conclusions

similar to those obtained earlier for low sulphur ESSO AF1313 Diesel fuel. The values of this index tend to be lower for pure substances (for example, iso-octane and 3-pentanone) than for Diesel and gasoline fuels. It is shown that the main contribution to the average absorption efficiency factor is expected to come from radiation at wavelengths less than 4 m for the range of external temperatures between 1000 K and 3000 K. The value of this factor is approximated by a power function aR_{d}^{b}, where R_{d} is the droplet radius. Coefficients a and b are approximated by piecewise quadratic functions of the radiation temperature, with the coefficients calculated separately in the ranges of radii 2 m – 5 m, 5 m – 50 m, 50 m – 100 m and 100 m – 200 m for all fuels. This new approximation is shown to be more accurate when compared with the case when a and b are approximated by quadratic functions or fourth power polynomials of the radiation temperature, with the coefficients calculated over the entire range 2 m – 200 m. This difference in the approximations of a and b, however, is shown to have little effect on the modelling of fuel droplet heating and evaporation in conditions typical for internal combustion engines, especiallyltioabuat

ddu Tg0 d T0 (7 6 Tj e (n) c Tj D 7 3 9 0 8 1 3 8 2 4) Tj (a) 3 8 2 4 5 T c 3 8 2 4 j T c 4 9 1 2 j T 0 2 1 T c (y) T.18912 Tc Tc (a) Tj-0

Several liquid and gas phase models have been used for modelling droplet heating and evaporation, together with the autr

used for modelling the processes is Diesel engine-like environment. The results of calculations have been compared with in-house experimental data where appropriate. It has been pointed out that in the case of spray injection into a 'cold' gas, the observed spray tip penetration agrees much better with the prediction of the modified WAVE models compared with other droplet breakup models, widely used in computer simulation of quasi-steady-state sprays. A similar conclusion is applied to the predicted and observed SMR of droplets.

The predictions of the total autoignition delay by the Abramzon and Sirignano model (the gas phase Model 4) have been compared with the predictions of this delay by a more basic gas phase model (Model 0). It has been shown that the choice of gas phase model produces only minor effects on the predicted autoignition delay, which can be safely ignored in practical engineering computations. The difference in the autoignition delay times predicted by the ITC and ETC models is noticeable and needs to be taken into account in practical computations. The application of the ETC model is recommended as a more physical one.

7.4 Recommendations for further work

- The measurement of the index of absorption of various fuels in the range of wave length 4 μm – 10 μm is recommended.

- This thesis was focused on the hydrodynamic models for evaporation, while the effects of kinetic processes have been neglected. Further analysis using the kinetic model would be helpful for understanding of the underlying physics of the processes and more accurate modelling.

PDF created with pdfFactory Pro trial version www.pdffactory.com

References:

Abramzon B., Sirignano W.A. (1989), *Droplet vaporization model for spray combustion calculation*, Int. J. Heat and Mass Transfer 32, 1605-1618.

Abramzon B., Sazhin S.S. (2005), *Droplet Vaporization Model in The Presence of Thermal Radiation*, Int. J. Heat Mass Transfer 48, 1868 – 1873.

Abramzon B., Sazhin S.S. (2006), *Convective Vaporization of Fuel Droplet with Thermal Radiation Absorption*, Fuel 85, 32-46.

Aggarwal S.K. (1998), *A review of spray ignition phenomena: present status and future research*, Progress in Energy and Combustion Science 24, 565-600

Amsden A.A., O'Rourke P.J., Ramshaw J.D., Dukowics J.K. (1985), *KIVA: A Computer Program for Two and Three Dimensional Fluid Flows with Chemically Reactions and Fuel Sprays*, Los Alamos Nat. Laboratory, New Mexico.

Amsden A.A., O'Rourke P.J., Butler T.D. (1989), *KIVA II: A Computer Program for Chemically Reactive Flows with Sprays*, Los Alamos Nat. Laboratory, New Mexico.

Amsden A.A. (1993), *KIVA-3: A KIVA Program with Block-Structured Mesh for Complex Geometries*, Los Alamos Nat. Laboratory, New Mexico.

Amsden A.A. (1997), *KIVA-3V: A Block-Structured KIVA program for E0.21456 Tc (A)12 Tc ( ) Tj-0.*

-x

K mAesksj0.1 Tj-0.18 Tc (a) Tj-0.24 Tc (y) Tj0.16 Tj0.21456 Tc (o) Tj0.176 Tj0.12 Tj-0.28 Tc ( ) Tj-0.
j-0.07 Tj0.21456 Tc (r) Tj0 Tc (a) Tj-ay368 Tc Tc (s) Tj1414 Tc (V) 3824 Tc (eA) Tj0.18 Tc (r) TS.r aroeAAmm f. s
ysj0.21456 Tc (r) Tj0 Tc (a) Tj-aj0 -12.72 TD ( ) Tj0.138544 Tc (s) Tj0p . s M 2 . 1 6 T j - 0 . 0 5 0 8
sj(s) Tj0c (y) Tj092.16 -0. 8 Tc (m) m88 Tc Tj-u07632 0 8 Tc (m) l88 Tc (A) scy. cc
s Nc.aA N aryf N s368 Tc Tc (o) Tj307.9Tc (V) 3824 Tc (ej0.13.73824 Tc (a)
sj28 (r) Tj0 Tc (a) Tj-aj0 -12.72 TD ( ) Tj0.138544 Tc (s) Tj Tc (j(s) Tjy) e07632 0p) Tj0.05rj0.13.73824 Tc (a) TjcTjp) Tj0..7382

References

Chin J.S., Lefebvre A.H. (1985), *The role of the heat-up period in fuel drop evaporation*, Int. J. of Turbo and Jet Engines 2, 315-325.

Dombrovsky L.A., Sazhin S.S., Sazhina E.M., Feng G., Heikal M.R., Bardsley M.E.A., Mikhalovsky S.V. (2001), *Heating and Evaporation of Semi Transparent Diesel Fuel Droplets in Presence of Thermal Radiation*, Fuel 80 (11), 1535-1544.

Douglas J.F., Gasorek J.M., Swaffield (1995), *Fluid Mechanics*, Longman, 3rd Edition.

Druet S., Taran J.P. (1981), *CARS Spectroscopy*, Prog. Quant. Electr 7, 1-72
Durret R.P., Oren D.C., Ferguson C.R. (1987), *A Multidimensional Data Set for Diesel Combustion Model Validation: I. Initial Conditions, Pressure History and Spray Shapes*, SAE Technical Report, 872087.

Dust F., Melling A., Whitelaw J.H. (1981), *Principle and Practice of Laser Doppler Anemometry*, Academic Press, London.

Dwyer H.A, Stapf P., Maly R (2000), *Unsteady vaporization and ignition of a three-dimensional droplet array*, Combustion and Flame 121, 181-94.

El Wakil M.M., Uyea

References

Gold M.R., Arc

Hiroyasu H., Kadota T. (1974), *Fuel Droplet Size Distribution in Diesel Combustion Chamber*, SAE paper 740715.

Hirschfelder J.O., Curtiss C.F., Bird R.B. (1967), *Molecular theory of gases and liquids*, 4th Edition, John Wiley & Sons, New York/ Chichester.

Holman J.P. (2002), *Heat Transfer*, McGraw-Hill, London

Hoyt C.H., Adel F.S. (1967), *Radiative Transfer*, McGraw-Hill, London.

Huh K., Gosman A.D. (1991), *A phenomenological Model of Diesel Spray Atomization*, Proceeding of the International Conference on Multiphase Flow, Tsukuba, Japan.

Ibrahim E.A., Yang H.Q., Przekwas A.J. (1993), *Modelling of Spray Droplet Deformation and Break-up*, AIAA J. Propulsion and Power 9, 651-654.

Incropera F.P, de Witt D. (1996), *Fundamentals of Heat and Mass Transfer*, Wiley, New York.

Jeffrey A. (1976), *Problems of Laser Velocimeter Application to Combustion System and Combustion Measurement*, Academic Press, London.

Kang S.H., Baek S.W., Choi J.H. (2001), *Autoignition of Sprays in a Cylindrical Combustor*, Int. J. Heat and Mass Transfer 44, 2413-1422.

Karimi K., Sazhina E.M, Abdelghaffar W.A., Crua C., Heikal M.R, Gold M. (2006), *Development in Diesel Spray Characterisation and Modelling*, In: Proceedings of THIESEL-2006, Valencia, Spain.

Kreith F. (1988), *Principles of Heat Transfer*, McGraw Hill, New York

Kryukov A.P., Levashov V.Y., Sazhin S.S. (2004), *Evaporation of Diesel Fuel Droplets: Kinetic versus Hydrodynamic Models*, Int. J. Heat Mass Transfer 47, 2541-2549.

Labowsky M. (47-

La9.48 Tc (y) Tos

Lavieille P., Lemoine F., Lebouché M. (2001), *Evaporating and Combusting Droplet Temperature Measurements using Two Color Laser Induced Fluorescence*, Exp. Fluids 31, 45.

Lavieille P., Lemoine F., Lebouché M. (2002), *Investigation on Temperature of Evaporating Droplets in Linear Stream using Two Color Laser Induced Fluorescence*, Combust. Science Technology. 174, 117.

Lefebvre A.H. (1989), *Atomization and Sprays*, Taylor & Francis.

Liu A.B., Mather D., Reitz R.D. (1993), *Modelling the Effect of Droplet Drag and Break-Up on Fuel Spray*, SAE Paper, 930072.

Lee L., Chuang M. (1997), *Excess volumes of cyclohexane with 2-propanone, 2-butanone, 3-pentanone, 4-methyl-2-pentanone, 1-propanol, and 2-propanol and ethanoic acid + 1-propanol systems*, J. Chem. Eng. Data 42, p. 850-853

Luikov A.V. (1968), *Analytical Heat Transfer Theory*, Academic Press, London.

Maqua C., Castanet G., Doué N., Lavergne G., Lemoine F. (2006), *Temperature measurements of binary droplets using three color laser-induced fluorescence*, Experiments in Fluid 40 786-797.

Maran D.F., Long M.B., Studzinki W.M., Swindal J.C. (1998), *Planar Laser Induced Fluorescene Imaging of Crevice Hydrocarbon Emission*, 27th Symposium on Combustion, The Combustion Institute Pittsburgh.

Marberry M., Ray A.k., Leung K. (1984), *Effect of Multiple Particle Interactions on Burning Droplets*, Combustion and Flame 57, 237

Martynov S, Sazhin S.S., Gorokhovski M., Chtab A., Karimi K., Crua C, Heikal M., (2007) *A modified WAVE model for transient liquid spray*, Int. Journal of Heat and Fluid Flow (submitted)

Mason E.A., Saxena C.S. (1958), *Approximate formula for the thermal conductivity of gas mixtures*, Physics of Fluids 1, 361-369.

Maxwell J.B. (1950), *Data Book on Hydrocarbons: Application to Process Engineering*, D. van Nostrand Company INC., New York.

Melissari B., Agyropoulos S.A. (2005), *Development of a Heat Transfer Dimensionless Correlation for Sphere Immersed in a Wide Range Prandtl Number Fluids*, Int. Journal Heat and Mass Transfer 48, 4333-4341

PDF created with pdfFactory Pro trial version

Renksizbulut M., Yuen M.C. (1983), *Experimental Study of Droplet Evaporation in a High Temperature Air Stream,* ASME J Heat Transfer 105, 384-388.

Rotondi R., Bella G., Grimaldi C., Postrioti L. (2001), *Atomization of High-Pressure Diesel Spray: Experimental Validation of New Breakup Model*, SAE paper, 2001011070.

Sangiovanni J.J., Labowski M. (1982), *Burning Times of Linear Fuel Droplet Arrays: A comparison of Experiment and Theory*, Combustion and Flame 45, 15

Sangiovanni J.J., Kesten A.S. (1976), *Effect of droplet interaction on ignition in monodispersed droplet stream,* Sixteenth International Symposium on Combustion, The Combustion Institute

Sazhin S.S. (2006), *Advanced Models of Fuel Droplet Heating and Evaporation*, Progress in Energy and Combustion Science 32, 162-214.

Sazhin S.S, Sazhina, E.M., Faltsi-Saravelou O., Wild P. (1996), *The P-1 Model for Thermal Radiation Transfer: Advantages and Limitations*, Fuel 75, 289-294.

Sazhina E.M., Sazhin S.S., Heikal M.R., Marooney C.J. (1999), *The Shell Autoignition Model: Applications to Gasoline and Diesel Fuels*, Fuel 78, 389-401.

Sazhin S.S., Heikal M.R., Marooney C.J., Mikhalovsky S.V. (1999), *The Shell Autoignition Model: A New Mathematical Formulation*, Combustion and Flame 117, 529-540

Sazhina E.M., Sazhin S.S., Heikal M.R., Babushok V.I., Johns R.J.R. (2000), *A Detailed Modelling of the Spray Ignition Process in Diesel Engines*, Combustion Science and Technology 160, 317-344.

Sazhin S.S., Feng G., Heikal M.R., Goldfarb I., Goldshtein V. and Kuzmenko G. (2001a), *Thermal Ignition Analysis of a Monodisperse Spray with Radiation*. Combustion and Flame 124 (4), 684-701.

Sazhin S.S., Feng G., Heikal M.R. (2001b), *A Model for Fuel Spray Penetration*, Fuel 80, 2171-2180.

Sazhin S.S., Gol'dshtein V.A., Heikal M.R. (.6 Tc (M) Tj0.12 Tc tDA(l) Tj1S8 Tc ( ) Tj0.12 Tc0.29088

Sazhin S.S., Abdelghaffar W.A., Sazhina E.M., Mikhalovsky S.V., Meikle S.T., Bai C. (2004a), *Radiative Heating of Semi-transparent Diesel Fuel Droplets*, ASME J. Heat Transfer 126, 105-109; Erratum 126, 490-491

Sazhin S.S., Kruti (1) Tj0 -12.48 T340.138268 Tc (-) 8 0 TD 0.12 Tc (-0.02544 Tc ((14 Tc (0p2 Tc (K) T

Papers published by the author

International refereed journals

Sazhin S.S., Kristyadi T., Abdelghaffar W.A., Heikal M.R. (2006), *Models for Fuel Droplet Heating and Evaporation: Comparative Analysis*, Fuel 85, 1613-1630.

Sazhin S.S., Kristyadi T., Abdelghaffar W.A., Begg S., Heikal M.R., Mikhalovsky S.V., Meikle S.T., Al-Hanbali O. (2007) *Approximate Analysis of Thermal Radiation Absorption in Fuel Droplets*, ASME Journal of Heat Transfer 129, 1246-1255.

Maqua C., Castanet G., Grish F., Lemoine F., Kristyadi T., Sazhin S.S. (2007), *Monodisperse Droplet Heating and Evaporation: Experimental Study and Modelling*, Int. Journal Heat and Mass Transfer (submitted).

Sazhin S.S., Martynov S.B., Kristyadi T., Crua C., Heikal M.R. (2007), *Diesel Fuel Spray Penetration, Heating, Evaporation and Ignition: Modelling Versus Experimentation,* Int. Journal of Engineering Modelling and Simulation (submitted)

Refereed international conferences proceeding

Sazhin S.S., Kristyadi T., Heikal M.R., Abdelghaffar W.A., Shishkova I.N. (2007), *Fuel Droplet Heating and Evaporation: Analysis of Liquid and Gas Phase Models*, SAE paper 07SFL-18 - 2007-01-0019

Sazhin S.S., Crua C., Martynov S.B., Kristyadi T. and Heikal M.R. (2007), *Advanced Models for Droplet Heating and Evaporation: Effect on the Autoignition of Diesel Fuel Sprays*, Proceedings of the Third European Combustion Meeting ECM 2007, paper 15-2.

Sazhin S.S., Martynov S.B., Kristyadi T., Crua C., and Heikal, M.R (2007), *Models for Droplet Heating and EvapCrua o:( ) Tj-0.05088 Tc () Tj0 Tc (u) Tj-leai nEoij-0.05088 Tc () Tj0 . 1 8 9*

Internal conferences

Kristyadi T. (2005), *Modelling of Droplet Heating and Evaporation*, Engineering Research in Action, Internal Conference, University of Brighton.

Kristyadi T. (2006), *Models of Droplet Heating and Evaporation*, Engineering Research in Action, Internal Conference, University of Brighton.

PDF created with pdfFactory Pro trial version www.pdffactory.com

Appendix A

Physical properties of fuel based on normalised temperature

Some of physical properties of fuels used in this thesis (e.g : n-heptane, tetradecane, n-dodecane and Diesel fuel) are given in Appendix A of Sazhin et al. (2005b), where in most cases they are approximated as polynomials of the absolute temperature *T*. This presentation, however, has a major drawback. For realistic temperatures high powers of *T* lead to rather large numbers. Hence, to get required values of these properties these large numbers are often multiplied by very small numbers and this potentially can lead to errors in calculations. To minimise these errors, rather large numbers of digits (up to 11) were needed to be retained in these formulae. Also, this approximation of properties made it rather difficult to infer their values for widely used temperatures (say room temperature 300 K).

These factors were the main driving force behind our intention to look for an alternative approximation of physical properties given in the abovementioned Appendix. We presented these properties not as polynomials of *T*, but as polynomials of the normalised temperature: muratunphyp6.40.36139.2 395.52 Tj-0Tj-08.64 16.32 Tj-0Tj-0 Tc (s) Tj0.-14

esesa mm

as used by Sazhin et al. (2005b), and plots 2 refer to the new approximations based on the normalised temperatures.

Physical properties of tetradecane

Latent heat of evaporation:
Using data presented in Maxwell (1950), the latent heat of evaporation is approximated as:

$$L = 3.60\,\mathrm{x}\,10^{5} - 1.17\,\mathrm{x}\,10^{5}\tilde{T} + 4.40\,\mathrm{x}\,10^{3}\tilde{T}^{2} - 2.93\,\mathrm{x}\,10^{4}\tilde{T}^{3} - 5.77\,\mathrm{x}\,10^{4}\tilde{T}^{4} - 1.15\,\mathrm{x}\,10^{4}\tilde{T}^{5} + 1.57\,\mathrm{x}\,10^{4}\tilde{T}^{6} \ \mathrm{J/kg}$$

when $\tilde{T} < \tilde{T}_{\mathrm{cr}} = 1.31$ (normalised critical temperature) and zero otherwise (Poling et al., 2000)

Specific heat capacity of liquid:
Using data presented in Maxwell (1950), the specific heat capacity of liquid is approximated as:

$$c_{\mathrm{l}} = 2220.30\exp\left(0.42\tilde{T}\right) \ \mathrm{J/(kg{\cdot}K)}$$

The specific heat capacity of vapour at constant pressure:
The specific heat capacity of vapour at constant pressure is approximated as (Poling et al., 2000):

$$_{\mathrm{pF}} \quad 1.66\,\mathrm{x}\,10^{3} \quad 1.39\,\mathrm{x}\,10^{2}\tilde{T} \quad 2.51\,\mathrm{x}\,10^{2}\tilde{T}^{2} \quad 15.11\tilde{T}^{3} \quad 0.69\tilde{T}^{4}$$

$$k_l = 0.14 - 5.47\,\mathrm{x}\,10^{-2}\,\tilde{T} - 2.05\,\mathrm{x}\,10^{-2}\,\tilde{T}^2 + 1.61\,\mathrm{x}\,10^{-2}\,\tilde{T}^3 \ \mathrm{W/(m\cdot K)}$$

when $\tilde{T} < \tilde{T}_{cr}$, and zero otherwise.

Comparison of two approximations of physical properties of tetradecane

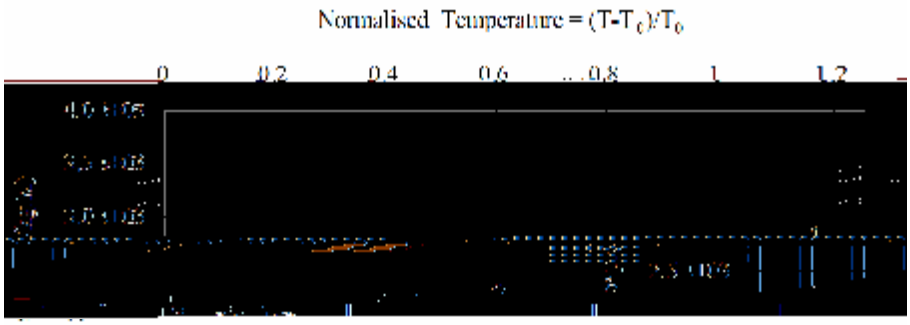

Figure A.1 The liquid specific heat capacity of tetradecane as predicted by Sazhin et al. (2005b) (plot 1) and the present approximation (plot 2)

PDF created with pdfFactory Pro trial version www.pdffactory.com

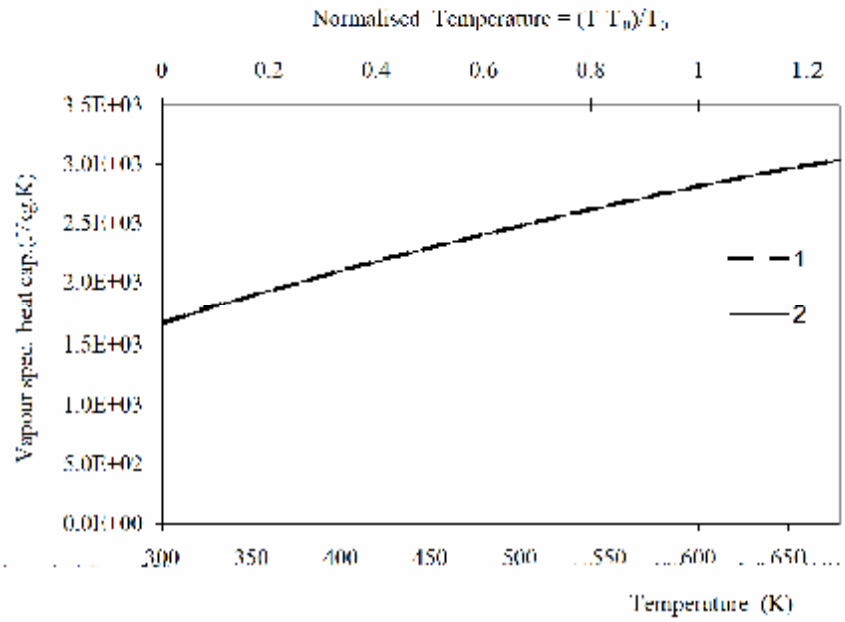

Figure A.2 The same as Figure A.1 but for vapour specific heat capacity

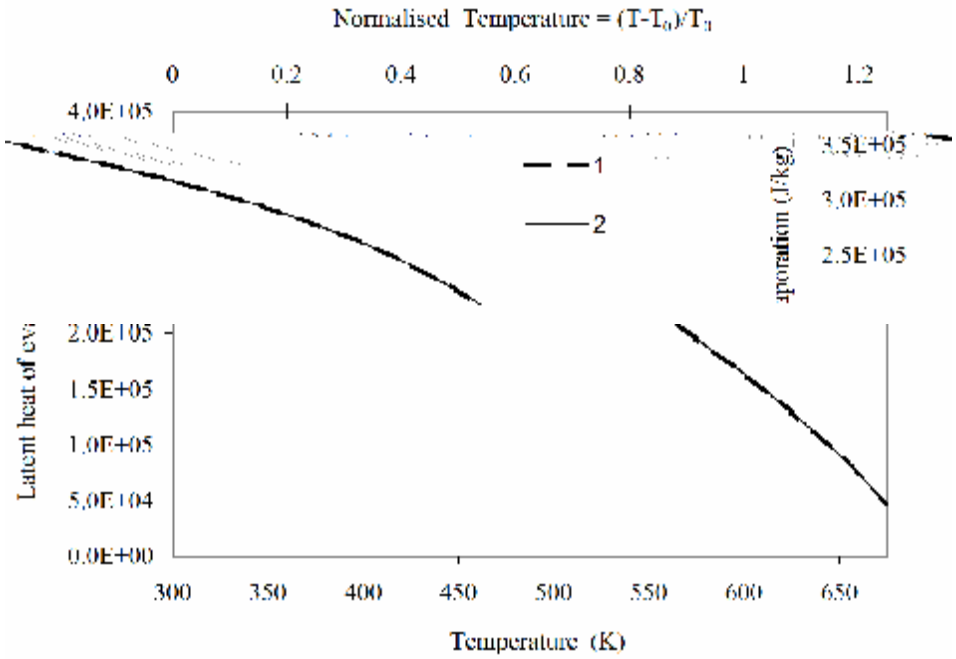

Figure A.3 The same as Figures A.1-A.2 but for latent heat of evaporation.

PDF created with pdfFactory Pro trial version www.pdffactory.com

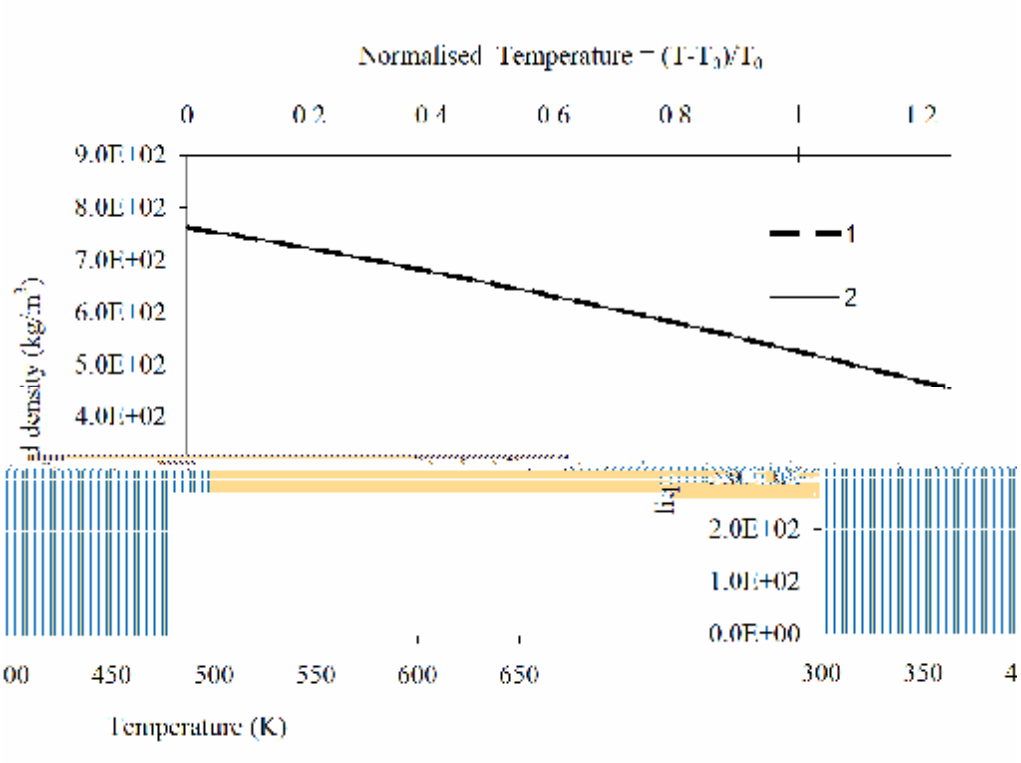

Figure A.4 The same as Figures A.1-A.3 but for liquid density

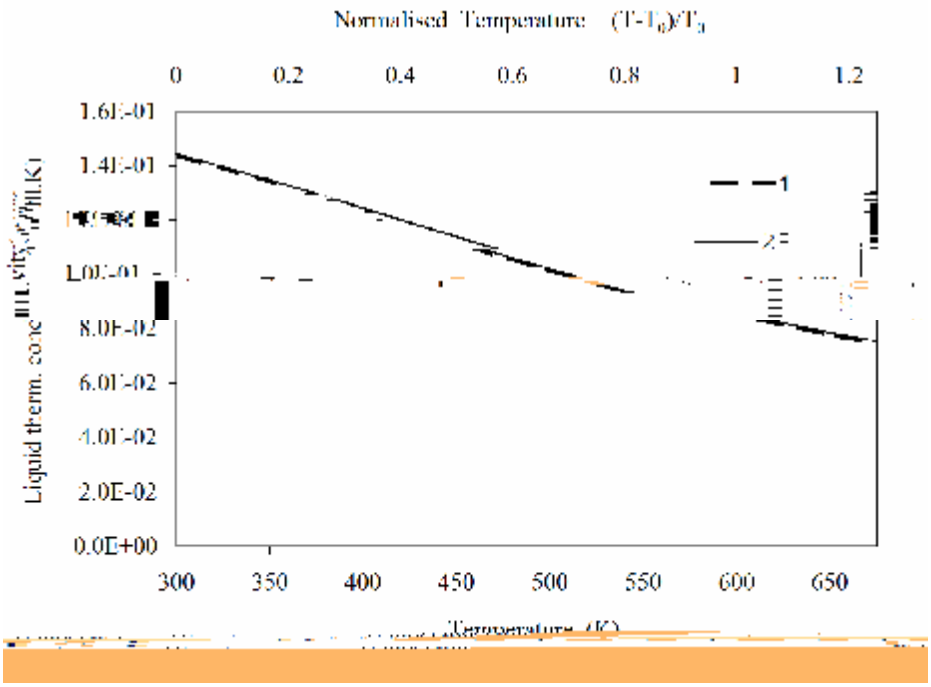

Figure A.5 The same as Figures A.1-A.4 but for liquid thermal conductivity

PDF created with pdfFactory Pro trial version www.pdffactory.com

Physical Properties of n-heptane

Latent heat of evaporation:

Latent heat of evaporation is approximated as (Chin et al., 1985)

$$L = 317.8x10^3\left(\frac{\tilde{T}_{cr} - \tilde{T}}{\tilde{T}_{cr} - \tilde{T}_b}\right)^{0.38} \text{ J/kg,}$$

when $\tilde{T} < \tilde{T}_{cr}$ and zero otherwise, where $_{cr}$2.64 1D 0.800

<

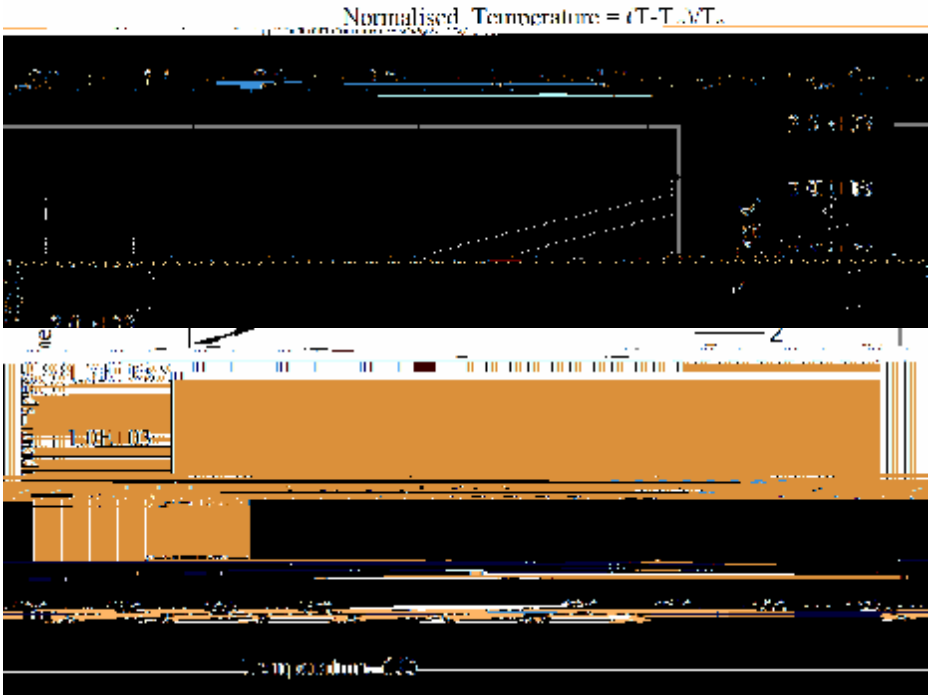

Figure A.7 The same as Figure A.6 but for vapour specific heat capacity

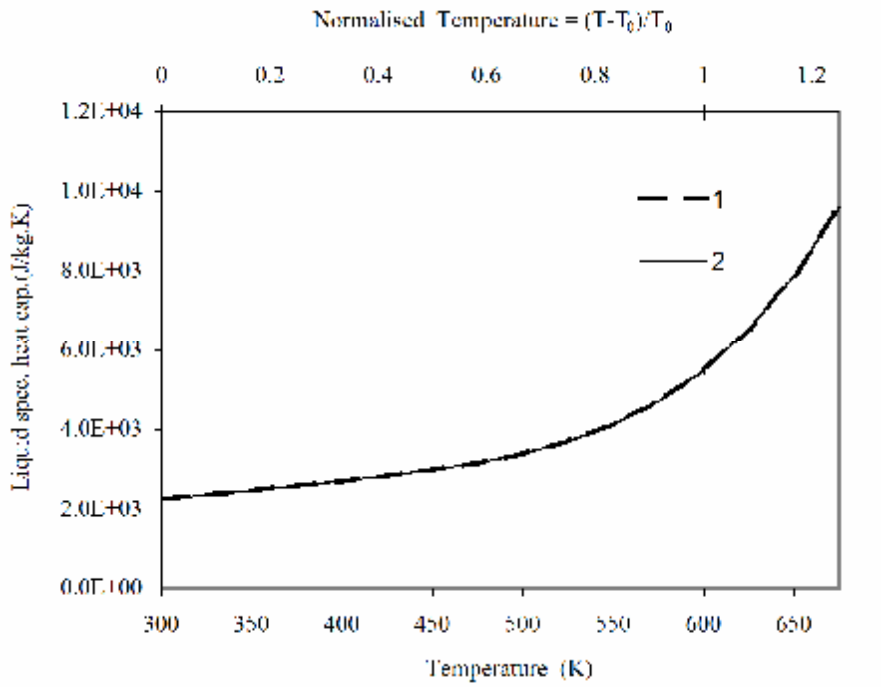

Figure A.8 The as Figures A.6-A.7 but for liquid specific heat capacity

PDF created with pdfFactory Pro trial version www.pdffactory.com

Physical properties of n-dodecane:

Latent heat of evaporation:

Latent heat of evaporation is

$$s_s = 0.0528\left(1-\frac{\tilde{T}+1}{\tilde{T}_{cr}+1}\right)^{0.121} \text{ N/m}$$

Comparison of two approximations of physical properties of n-dodecane

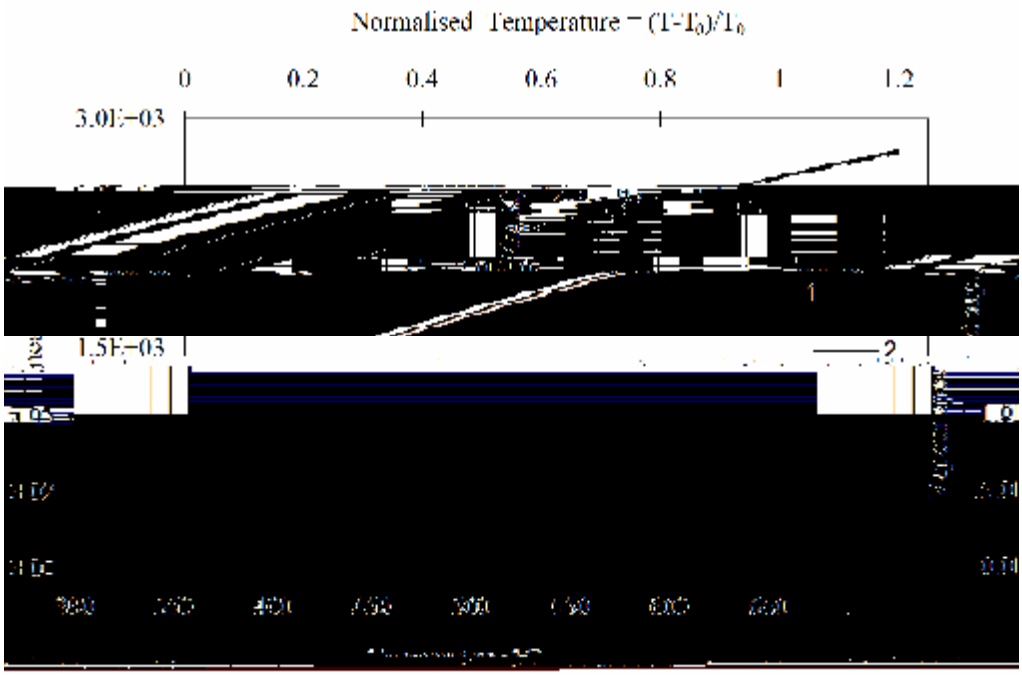

Figure A.9 The vapour specific heat capacity of n-dodecane as predicted by Sazhin et al. (2005b) (plot 1) and the present approximation (plot 2)

PDF created with pdfFactory Pro trial version www.pdffactory.com

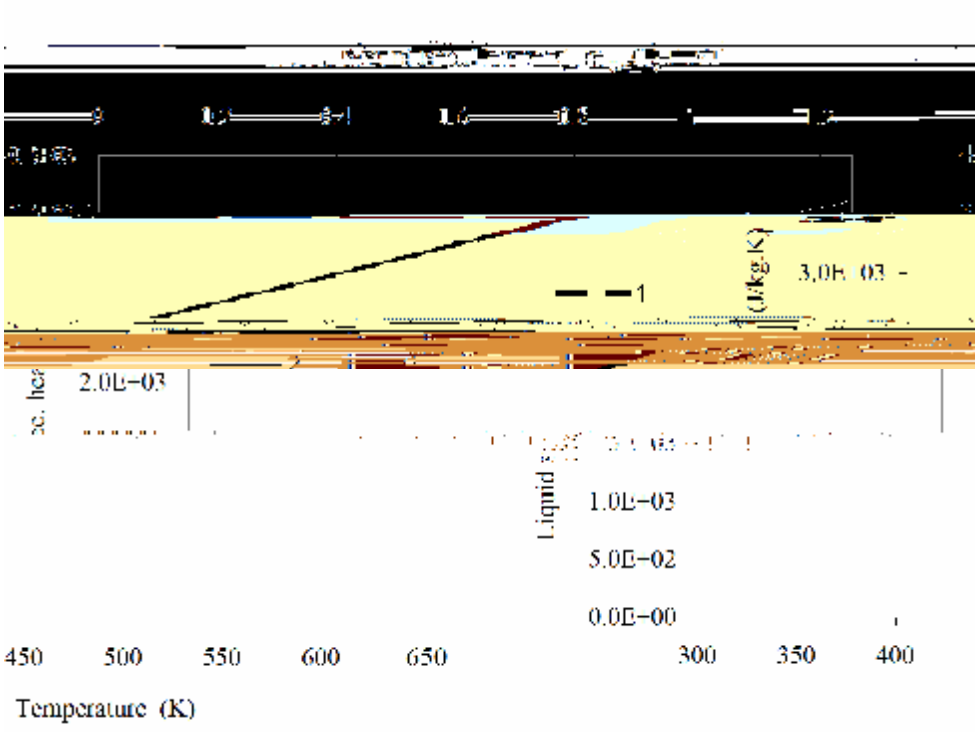

Figure A.10 The same as Figure A.9 but for liquid heat capacity

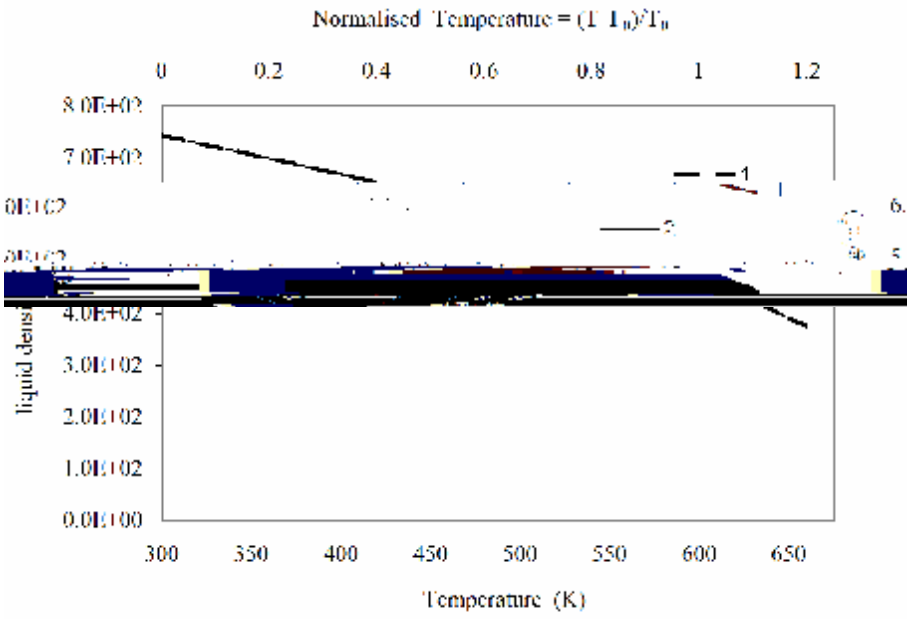

Figure A.11 The same as Figures A.9-A.10 but for liquid density.

PDF created with pdfFactory Pro trial version www.pdffactory.com

Appendix A: Physical properties of fuel based on normalised temperature

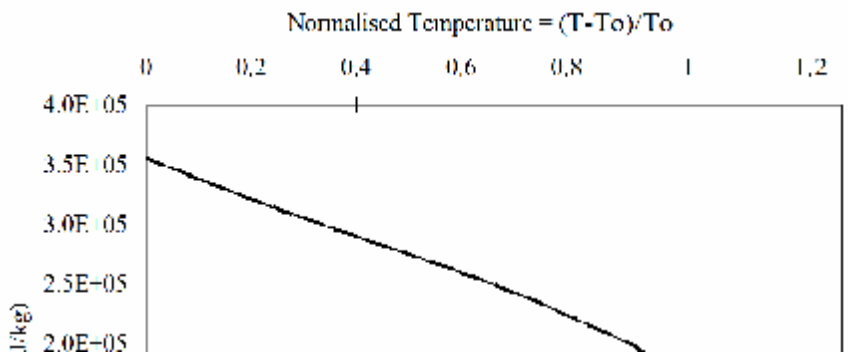

Appendix A: Physical properties of fuel based on norma

0.333	0.125	0.117
0.367	0.123	0.115
0.400	0.121	0.112
0.433	0.119	0.11
0.467	0.117	0.108
0.500	0.115	0.106
0.533	0.113	0.103
0.567	0.111	0.101
0.600	0.109	0.098
0.633	0.107	0.096
0.667	0.104	0.093
0.700	0.102	0.091
0.733	0.1	0.088
0.767	0.098	0.086
0.800	0.096	0.083
0.833	0.094	0.08
0.867	0.091	0.077
0.900	0.089	0.073
0.933	0.086	0.07
0.967	0.084	0.066
1.000	0.081	0.062
1.033	0.078	0.058
1.067	0.076	0.053
1.100	0.073	0.047
1.133	0.069	0.04
1.167	0.066	0.03
1.200	0.062	
1.233	0.059	
1.267	0.054	
1.300	0.049	
1.333	0.043	
1.367	0.036	
1.400	0.025	

PDF created with pdfFactory Pro trial version www.pdffactory.com

Appendi

Physical properties of n-octane

Latent heat of evaporation:
The latent heat of evaporat

Append

Appendix B

Physical properties of a mixture of fuel vapour and air

Density and specific heat capacity of the mixture are calculated using the following simple formulae:

$$r_{\text{mix}} = \frac{p_{\text{mix}}}{R_{\text{mix}} T_{\text{mix}}} \tag{B.1}$$

$c_{p\text{mix}} = (1 - Y_{\text{F}})c_{\text{pa}} + Y_{\text{F}} c_{\text{pF}}$, (B.2)

where p_{mix}, R_{mix} and T_{mix} are the pressure, gas constant, and temperature of the mixture of fuel vapour and air, Y_{F} is the mass fraction of fuel vapour, subscripts a and F refer to air and fuel vapour respectively.

Dynamic viscosity of the mixture is calculated from the following general semi empirical formula (Bird et al.,2002):

$$m_{\text{mix}} = \sum_{i=1}^{N} \frac{X_{\text{i}} m_{\text{i}}}{\sum_{j=1}^{N} X_{\text{j}} \Phi_{\text{ij}}} \tag{B.3}$$

where

$$\Phi_{\text{ij}} = \frac{1}{\sqrt{8}} \left(1 + \frac{M_{\text{i}}}{M_{\text{j}}}\right)^{-1/2} \left[1 + \left(\frac{m_{\text{i}}}{m_{\text{j}}}\right)^{1/2} \left(\frac{M_{\text{j}}}{M_{\text{i}}}\right)^{1/4}\right]^2$$

X_{i} are molar fractions of species i, M_{i} are molar masses (kg/kmol), the summation is performed over all N species.

Similarly, the thermal conductivity of the mixture is calculated from the following general semi empirical formula (Mason and Saxena, 1958; Bird et al., 2002):

$$= \sum_{i=}^{N} \frac{wii\ \ n}{\sum_{j=}^{N} \Phi}$$

g.06+1 Tc (.) T316 4 (:) T$ Tj0.06 (76744f0.1Tj0.t Tcj0) Tj-0.3i l22.32 T9(767

n 0 Tc 19.60 Tj 13445

where D_{Fa} is in m^2/s, p is in atm (1 atm = 0.101 MPa), T is in K, $\sigma_{Fa} = 0.5(\sigma_F + \sigma_a)$ is the minimal distance between molecules in Angstroms (1 Angstrom = 10^{-10} m), Ω_{Fa} is the collision integral, the value of which depends on the normalised temperature $T^* = Tk_B/\varepsilon$, k_B is the Boltzmann constant, $\varepsilon_{Fa} = (\varepsilon_F.\varepsilon_a)^{0.5}$.

The values of σ_a and ε_a/k_B can be obtained from Table E.1 in Bird et al. (2002): σ_a = 3.617 Angstrom, ε_a/k_B = 97.0 K.

There is some controversy regarding the values of these parameters for various fuels. The values σ_F (in Angstrom) and ε_F/k_B (i[illegible]

The plots of D_{Fa} for the diffusion of n-dodecane in air versus temperature for p = 3 MPa and the values of σ_F and ε_a/k_B recommended by Hirschfelder et al. (1967) and Paredes et al. (2000) given in the above table, are shown in Figure B.1.

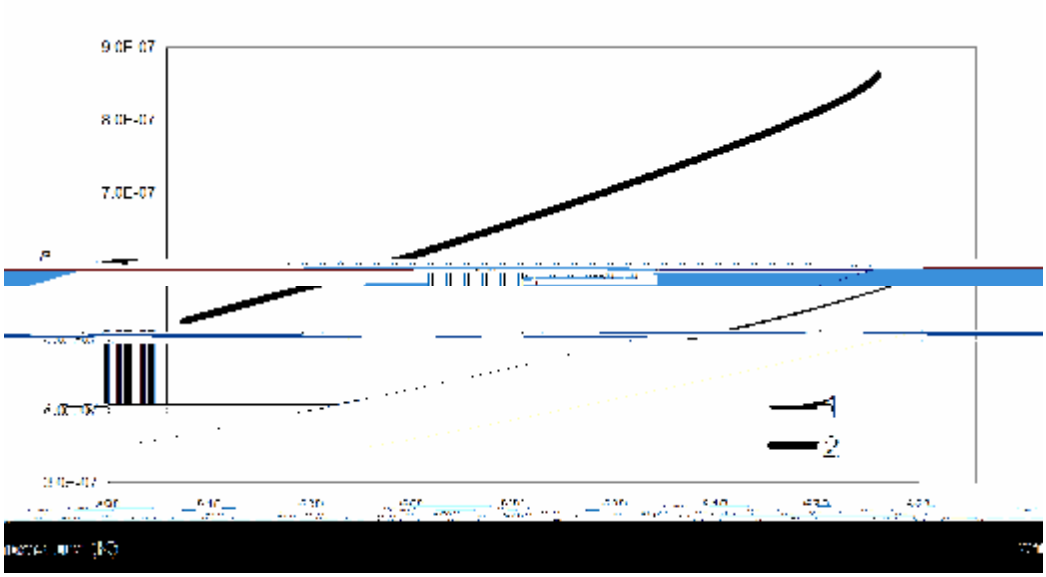

Figure B.1 The plots of D_{Fa} for diffusion of n-dodecane in air versus temperature for p = 3 MPa and the values of σ_F and ε_a/k_B given by Hirschfelder et al. (1967) (Curve 1) and Paredes et al. (2000) (Curve 2).

As can be seen from this figure, the values of D_{Fa} based on the parameters recommended by Paredes et al. (2000) are noticeablypao(b) Tj0306792 T584 Tc (m) .68 TD 0.08376 Tc (r) Tj

Appendix C

Numerical procedure of the zero dimensional code

This Appendix is focused on the implementation of the model of convective and radiative heating of a semi-transparent fuel droplet-apt dia

Equation (2.2.50) for model 4, Equation (2.2.48) for Model 5 and Equation (2.2.1

$$C_D = -\frac{C_{D0}}{(1+B_M)^a}, \qquad \text{(C.6)}$$

where

$$a = \begin{cases} 1 & \text{when } B_M < 0.78 \\ 0.75 & \text{when } B_M \geq 0.78 \end{cases}$$

The system of Equations (C.4) and (C.2) is solved using the Runge-Kutta method with adaptive step size control to obtained the droplet mass and velocity at $t=t_1$. The fuel vapour mass is calculated as:

( ) (

conditions to integrate the equation in the range (t_1,t_2). The previous calculations are repeated based on the new initial conditions to get the result at $t=t_2$.

The same procedure is repeated for all subsequent time steps until the autoignition starts at T_g= 1100 K (Sazhina et al., 1999). The number of terms in the series in Equation (2.1.22), which needs to be taken into account, depends on the timing of the starts of droplet heating and time when the value of droplet temperature is calculated. For parameters relevant to Diesel engines environment just three terms in the series can be safely used with possible errors of not more than about 1% (Sazhin et al. 2004a).

The gradients of temperature and fuel vapour concentration in the gas phase are ignored. This has been introduced with view to the future implementation of the algorithm into a multidimensional computational fluid dynamics (CFD) code, where this assumption refers to individual computational cells. The number of droplets in the enclosure can be arbitrary, but the direct interaction between droplets is not taken into account at this stage. All transport coefficients for the gas phase for Model 0- 5 were calculated at the reference temperature, T_{ref} defined as (Lefebvre, 1989):

$$\frac{2_{o\text{-}}}{3}$$

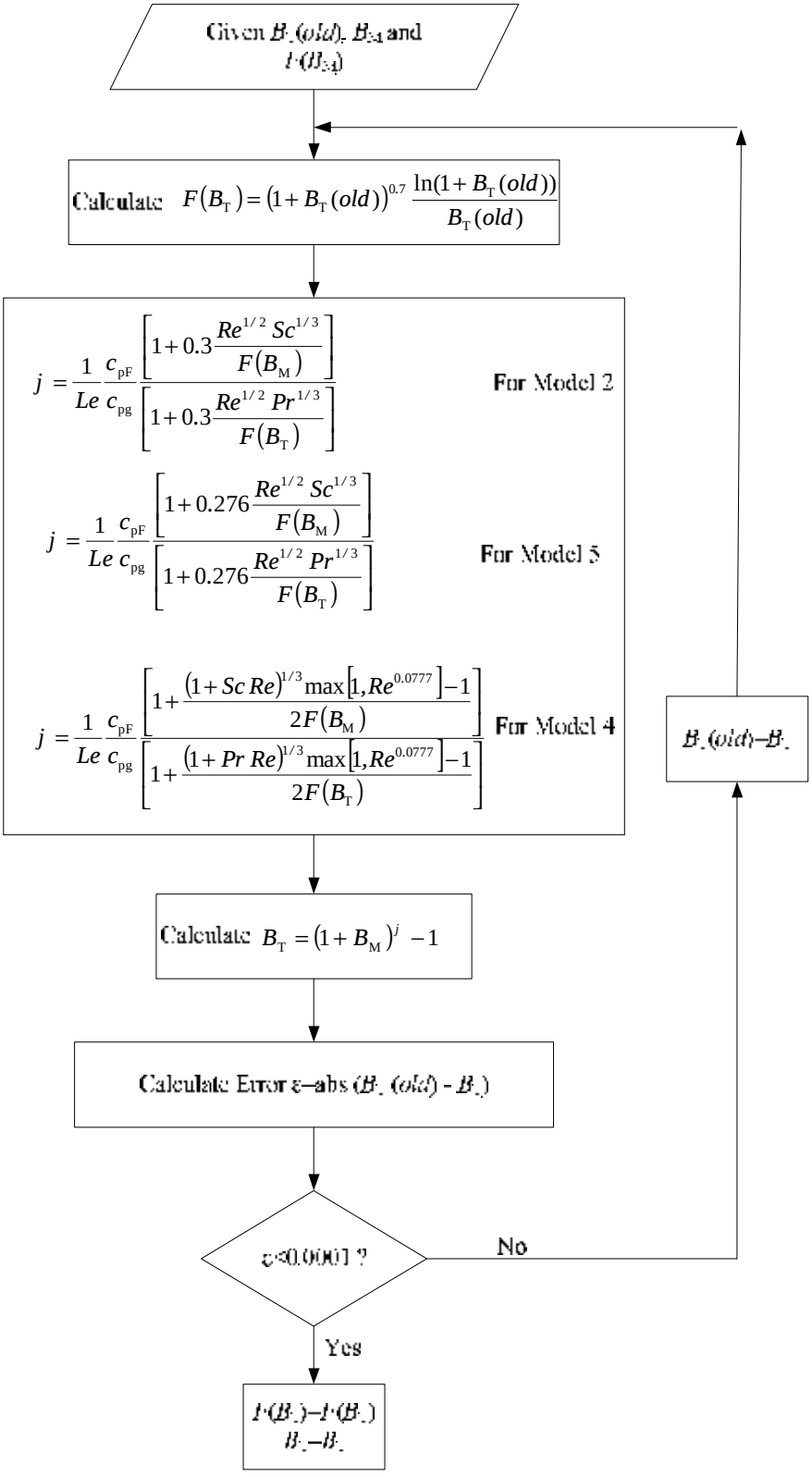

Figure C.1 The iteration procedure to calculate B_T and $F(B_T)$ for gas Models 2, 4 and 5.

PDF created with pdfFactory Pro trial version www.pdffactory.com

Appendix C: Numerical procedure of the zero dimensional code

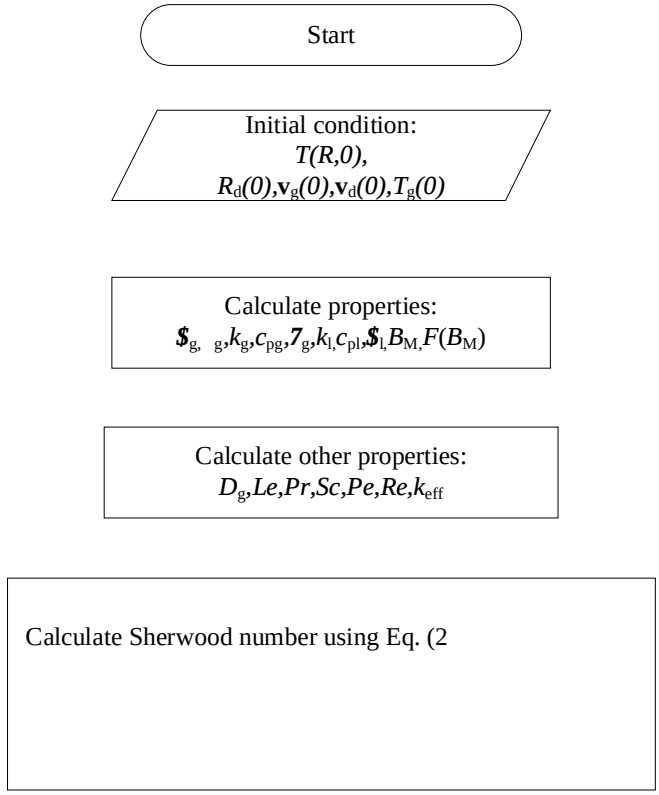

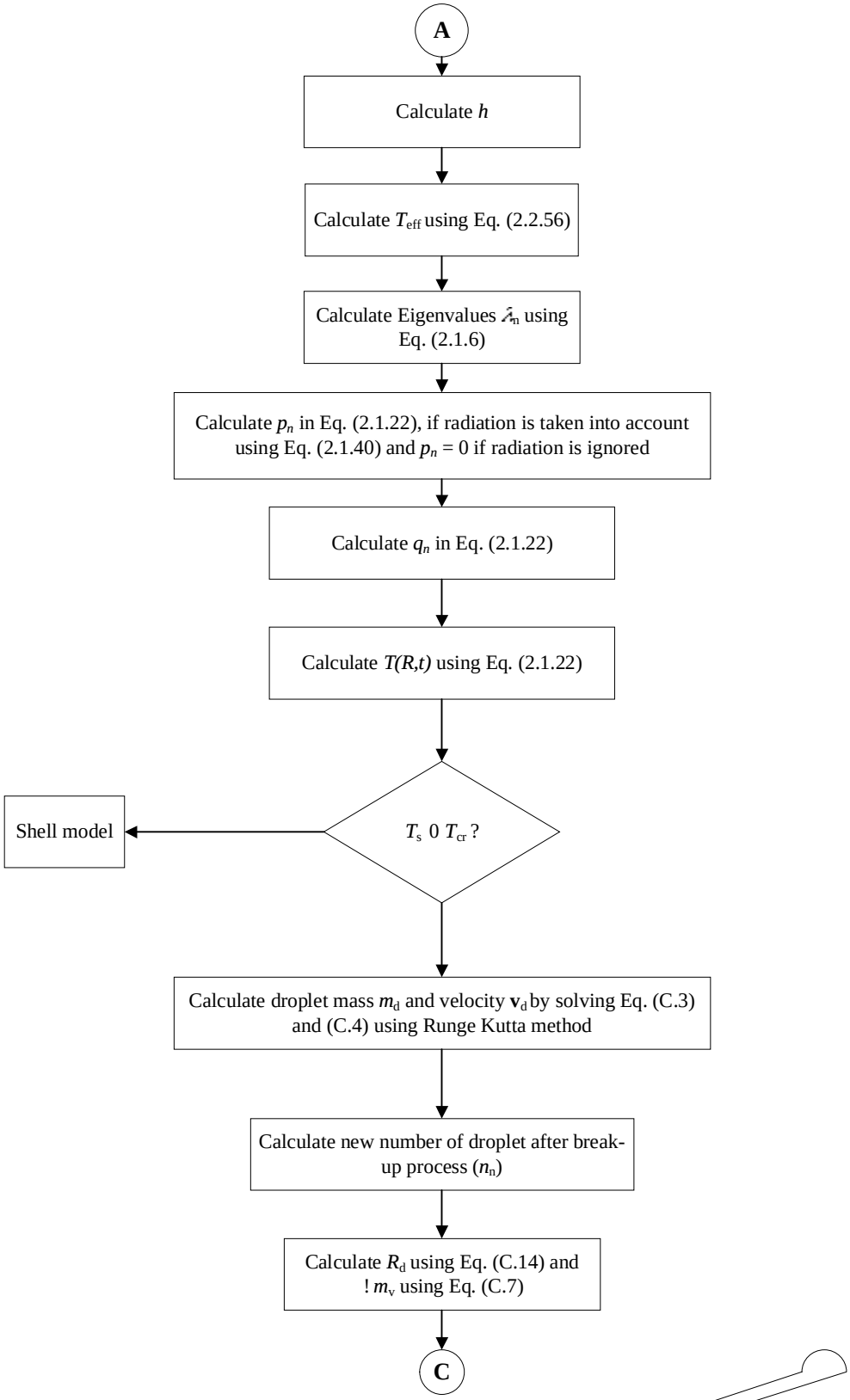
A
Calculate h
Calculate T_{eff} using Eq. (2.2.56)
Calculate Eigenvalues λ_n using Eq. (2.1.6)
Calculate p_n in Eq. (2.1.22), if radiation is taken into account using Eq. (2.1.40) and p_n = 0 if radiation is ignored
Calculate q_n in Eq. (2.1.22)
Calculate T(R,t) using Eq. (2.1.22)
T_s 0 T_{cr} ?
Shell model
Calculate droplet mass m_d and velocity $\mathbf{v}_d$ by solving Eq. (C.3) and (C.4) using Runge Kutta method
Calculate new number of droplet after break-up process (n_n)
Calculate R_d using Eq. (C.14) and ! m_v using Eq. (C.7)
C

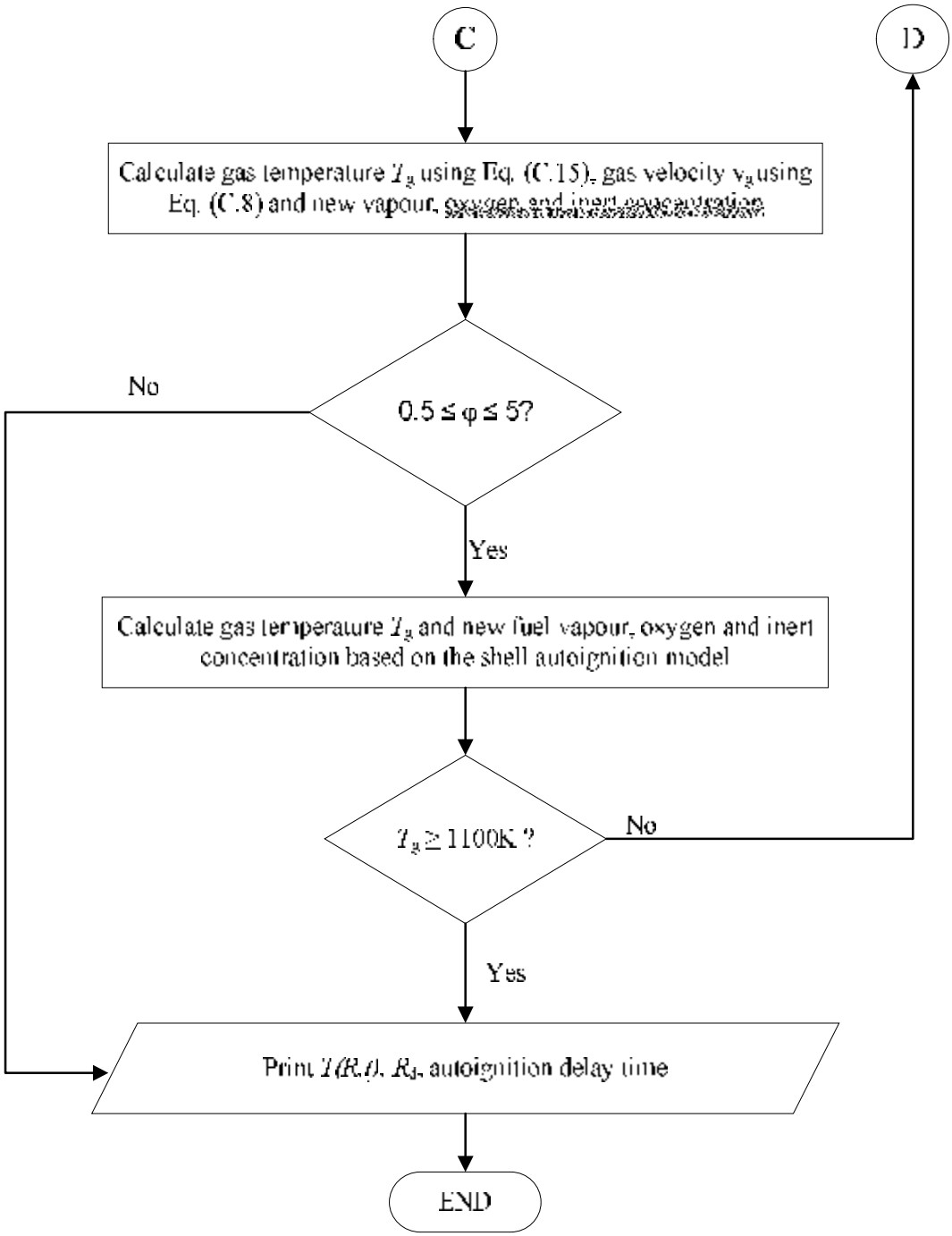

Figure C.2 The flow chart of the zero-dimensional code (continued)

PDF created with pdfFactory Pro trial version www.pdffactory.com

Appendix D: Numerical solution of the dis

Appenp

A

Substituting Equation (D.13) into Equation (D.12) we obtain:

$$\frac{r}{t} \quad \frac{k}{r} \quad \frac{k}{r \quad H(t) \quad \frac{}{r}} \Pi\varphi 0 -9.6\ T\Delta\ (\ ) T\varphi 0\ 17.04\ T\Delta\ (\ ) T\varphi -73.92\ -7.44\ T\Delta\ 142\ 0\ (\upsilon)\ T\varphi -1\Delta T\Delta\ (\Pi$$

$$\frac{k}{r}u_W \quad \frac{(\quad)k}{r}u_W \quad \left(\frac{r}{t} \quad \frac{(\ -\ )k}{\Delta r}\right)u_P + \frac{kM(t)}{\Delta r\left(H(t)+\frac{}{\Delta r}\right)} + \bar{S}\Delta r$$